Observed and modeled MOC related flow into the Caribbean Sea and the North Atlantic Ocean

Kerstin Kirchner

Universität Bremen, 2007

Observed and modeled MOC related flow into the Caribbean Sea and the North Atlantic Ocean

vom Fachbereich für Physik und Elektrotechnik
der Universität Bremen

zur Erlangung des akademischen Grades eines

Doktor der Naturwissenschaften (Dr. rer. nat)

genehmigte Dissertation

von

Dipl. Oz. Kerstin Kirchner

aus Hamburg

1. Gutachterin:	Prof. Dr. rer. nat. Monika Rhein
2. Gutachter:	Prof. Dr. rer. nat. Claus W. Böning
Eingereicht am:	24.09.2007
Tag des Promotionskolloquiums:	19.11.2007

Abstract

The transport of South Atlantic Water (SAW) into the northern hemisphere is investigated in this work. This flow represents the warm upper branch of the Meridional Overturning Circulation (MOC) and thus has a direct influence on the global heat budget. This part of the MOC is difficult to observe since the wind driven subtropical gyres and the complex equatorial current system interact with the SAW flow. The area near the Lesser Antilles is one of the sparse locations suitable to directly observe the principal part of the net SAW flow. Three different mechanisms are known which are responsible for the import of South Atlantic Water into the North Atlantic: (i) transport by a surface current which follows the South American coast, (ii) transport by rings that travel northwards along the coast, and (iii) transport by so-called Subtropical Cells in the interior Atlantic Ocean. The first two processes will be investigated directly in the present study, but conclusions can be drawn from presented results on the third mechanism.

A variety of data sources is used: direct hydrographic and velocity observations from ship surveys, profiles from Argo floats and data from a high-resolution ocean model. The $\frac{1}{12}^\circ$ FLAME model provides a resolution which is capable of comprising the complex topographic conditions at the Lesser Antilles. A climatological run is used as well as a run with variable wind and heat forcing. The SAW fractions are estimated by an isopycnal mixing approach, which yields the percentages of South Atlantic Water in the investigated area. The analysis was applied to the observational data and adopted to the model data as well, since the results should remain comparable.

Total transports and inflow from SAW into the Caribbean through the Lesser Antilles Passages are calculated from CTD and ADCP data and compared to results of the $\frac{1}{12}^\circ$ FLAME model. The model and the observations show high consistency in the strength of the mean total inflow and its range of variability as well as in the general distribution of water from South Atlantic origin. The model run with variable forcing slightly overestimates the SAW inflow into the Caribbean. During several ship cruises large rings were observed in the North Atlantic at 16°N. The ring propagation is investigated in FLAME and the complex interaction of the rings with the Lesser Antilles discussed. The spreading of SAW into the North Atlantic is analyzed using a data set of hydrographic ship measurements and Argo float data.

The mean SAW transport into the Caribbean as derived from observational data is estimated to be 9.3 Sv. The climatological run with FLAME yields a similar annual mean transport of 8.6 Sv, while FLAME_INTER exhibits slightly stronger inflow, with 10.7 Sv in the mean. When the rings observed at 16°N are taken into account the total SAW transport investigated in the present study sums up to 15.3 Sv. Since the upper layer MOC transport crossing the equator is estimated to be in the order of 16-18 Sv, the remaining SAW transport by the subtropical cells in the interior Atlantic is less than 3 Sv.

Zusammenfassung

In dieser Arbeit wird der Transport und die Ausbreitung von Südatlantikwasser in die nördliche Hemisphäre untersucht. Diese Strömungen sind Teil der globalen ozeanischen Umwälzbewegung (MOC) und spielen eine entscheidende Rolle für den nordwärtigen Wärmetransport im Atlantik. Die oberflächennahen Anteile der MOC im tropischen Atlantik sind schwer zu untersuchen, da das komplexe zonale Strömungssystem am Äquator und die windgetrieben Subtropenwirbel den MOC-Transport überlagern. Eines der wenigen geeigneten Gebiete, in denen man den Eintrag von Südatlantikwasser direkt bestimmen kann, ist die Region um die Kleinen Antillen, östlich der Karbik. Das Südatlantikwasser wird durch drei unterschiedliche Mechanismen in den Nordatlantik importiert: entweder durch eine Oberflächenströmung entlang der Südamerikanischen Küste, oder durch große Wirbel, die ebenfalls entlang der Küste nach Norden wandern, oder durch sogenannte Subtropische Zellen im inneren Atlantischen Ozean. In dieser Arbeit werden die ersten beiden Transportwege direkt untersucht. Die vorliegenden Ergebnisse erlauben jedoch Rückschlüsse auf den dritten Transportmechanismus.

Daten aus direkten hydrographischen Messungen sowie Strömungsmessungen während verschiedener Schiffsreisen werden mit Vertikalprofilen von Argo-Bojen sowie Daten eines hochaufgelösten Ozean-Modells kombiniert. Das $\frac{1}{12}^\circ$ FLAME Modell verfügt über eine Auflösung, die eine Darstellung der Topographie der kleinen Antillen ermöglicht. Zur Verfügung stehen zwei Modellläufe, ein klimatologischer Lauf und ein Lauf mit variablem Antrieb im Windfeld und den Wärmeflüssen. Der relative Anteil der Wassermassen aus dem Nord- und Südatlantik wird durch eine isopyknische Wassermassenanalyse bestimmt, die die Anteile an Südatlantikwasser im Untersuchungsgebiet liefert. Die Analyse wurde quasi unverändert auch auf die Modelldaten angewendet, um eine möglichst gute Vergleichbarkeit der Ergebnisse zu erreichen.

Die Gesamttransporte in die Karibik wurden aus Daten von Schiffsmessungen (CTD und ADCP) und dem Modell ermittelt, ebenso der Transport von Südatlantikwasser. Ein Vergleich von Modell- und Messergebnissen zeigt, dass das Modell die Stärke und Variabilität des Karibikeinstroms gut darstellt. Auch die Verteilung von Südatlantikwasser im Modell stimmt gut mit den Beobachtungen überein. Der Modelllauf mit variablem Antrieb zeigt ein wenig höhere Südatlantikwassertransporte. Die Ausbreitung und Wechselwirkung der Wirbel mit den Inseln der Kleinen Antillen wird im Modell untersucht. Für eine Untersuchung der weiträumigen Ausbreitung von Südatlantikwasser wird ein Datensatz aus Argo-Profilen und hydrographischen Schiffsmessungen erstellt. Während der Schiffsreisen wurden auf einem Schnitt im Atlantik bei 16°N grosse antizyklonale Wirbel entdeckt und in dieser Arbeit quantifiziert.

Der mittlere Transport von Südatlantikwasser in die Karibik beträgt 9.3 Sv in den Beobachtungen. Der klimatologische Lauf in FLAME ergibt einen ähnlichen Einstrom von 8.6 Sv. Der Lauf mit variablem Antrieb dagegen zeigt mit 10.7 Sv einen stärkeren Einstrom durch die Kleinen Antillen. Berücksichtigt man nun auch die bei 16°N vermessenen Wirbel, so beträgt der gesamte beobachtete Transport von Südatlantikwasser 15.3 Sv im westlichen Nordatlantik. Da der gesamte warme Zweig der MOC Zirkulation etwa 16-18 Sv beträgt, ist der fehlende Teil, der über den inneren Transportweg durch die Subtropischen Zellen erfolgt, kleiner als 3 Sv.

Contents

1 Introduction

The Meridional Overturning Circulation (MOC) describes the oceanic meridional flow field which transports large amounts of heat into the North Atlantic (Rahmstorf, 2006). In Figure 1.1 a schematic of the global MOC (sometimes denoted as the 'oceanic conveyor belt') is depicted. A well-known and broadly simplified picture of the Atlantic MOC consists of warm, shallow flow, which is northward in the whole Atlantic. Upper ocean waters from the South Atlantic cross the equator into the northern hemisphere. Preconditioning of the water column combined with air-sea interaction favors the occurrence of deep convection in a few very limited regions of the North Atlantic (see Figure 1.1). As a result of wintertime deep convection happening in the western subpolar North Atlantic surface waters are transformed to intermediate waters. These join the dense overflows which originate from the Nordic Seas and cross the Greenland-Scotland Ridge. This compound of water masses constitutes North Atlantic Deep Water (NADW) which is exported from the subpolar North Atlantic. The southward flow of NADW represents the lower limb of the 'conveyor' (Broecker, 1991). The meridional stream function in the Atlantic is shown in Figure 1.2*a*. Below the NADW cell bottom water is present which is formed in small amounts near Antarctica. It slides into the Atlantic from the south and is slowly entrained on its way northward into the NADW layer.

The occurrence of winter-time deep convection is an outstanding feature of the western subpolar North Atlantic. In contrast, surface waters of the North Pacific are too fresh and winterly buoyancy losses at the sea surface hence too small to allow for deep convection to occur there. Other types of dense water formation occur only along the Antarctic continent, but are governed by different physical processes: brine rejection and interaction with shelf ice produces the dense water there.

The Atlantic is not only outstanding concerning the deep water formation, but also with respect to the shallow, warm component of the MOC: the meridional heat transport is northward in the whole basin. The net movement of heat in the tropics is directed away from the equator in the world ocean (cf. Figure 1.2*b*), but directed northward in the South Atlantic. The Atlantic heat transport is therefore considered 'abnormal' (following Stommel, 1980). The export of North Atlantic Deep Water within the overturning circulation from the subpolar North Atlantic is estimated to be in the range of 13-18 Sv (e.g. Dickson and Brown, 1994; Ganachaud and Wunsch, 2000). Only a small amount is compensated by Antarctic Bottom Water. The important part in closing the balance assumes the upper ocean warm water. At 24°N, the northward flow above the North Atlantic Deep Water is 16 ± 2 Sv, which results in 1.3 PW ($1PW = 10^{15}\ W$) northward heat transport (Ganachaud and Wunsch, 2000). As the Atlantic cannot obtain that much heat

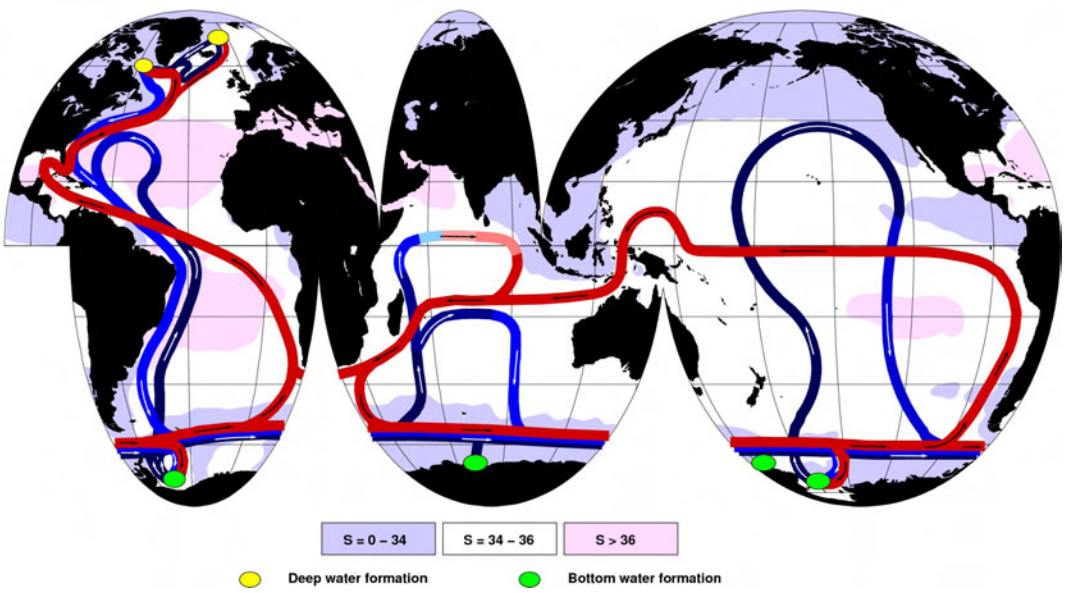

Figure 1.1: Schematic of the global thermohaline circulation from Kieke (2005). Warm currents of the upper ocean in red colors, cold deep currents in blue. Shaded in blue and red are areas of low and high surface salinity, the white regions represent a moderate value.

alone, heat (and fresh water as well) is transported from the Pacific and Indian Oceans into the South Atlantic.

In the Atlantic, the meridional heat transport is closely related to the strength of the overturning circulation. Model studies suggest that an increase of 2 Sv in the overturning results in 0.1 PW increase in heat transport (Böning et al., 1996). The Atlantic MOC reacts sensitive to changes in the freshwater forcing and other disturbances. For example, a modified MOC was found for glacial times (Figure 1.2*b*). It may even come to a near shut down of the MOC as was the case during the Heinrich event 17,500 years ago or during the Younger Dryas cold event (McManus et al., 2004). The importance of the strength of the meridional heat transport in the North Atlantic for the climate of the adjoining countries is obvious, especially the conditions in Europe depend on the sea surface temperature in the North Atlantic (Duplessy, 1999). The connection between climate variability and changes in the Atlantic thermohaline circulation is evident from both paleoclimate records and coupled models (e.g. Clark et al., 2002). Thus, the detailed understanding and monitoring of the Atlantic meridional overturning is an important issue in the oceanographic research. However, observing the shallow branch of the Meridional Overturning Circulation directly is difficult in the North Atlantic. The MOC interacts with the Gulf Stream system and provides additional volume and heat for the North Atlantic Subtropical Gyre, but the MOC portion of the transport can hardly be detected.

An important connection between the northern subtropical gyre and the equatorial gyre represents the South Atlantic Water (SAW) flow into the North Atlantic and the Caribbean Sea. The conventional Sverdrup theory predicts a uniform inflow through the Lesser Antilles island arc and an outflow at the southern Caribbean. A model study by Johns et al. (2002) actually demonstrated this circulation, when the model was purely

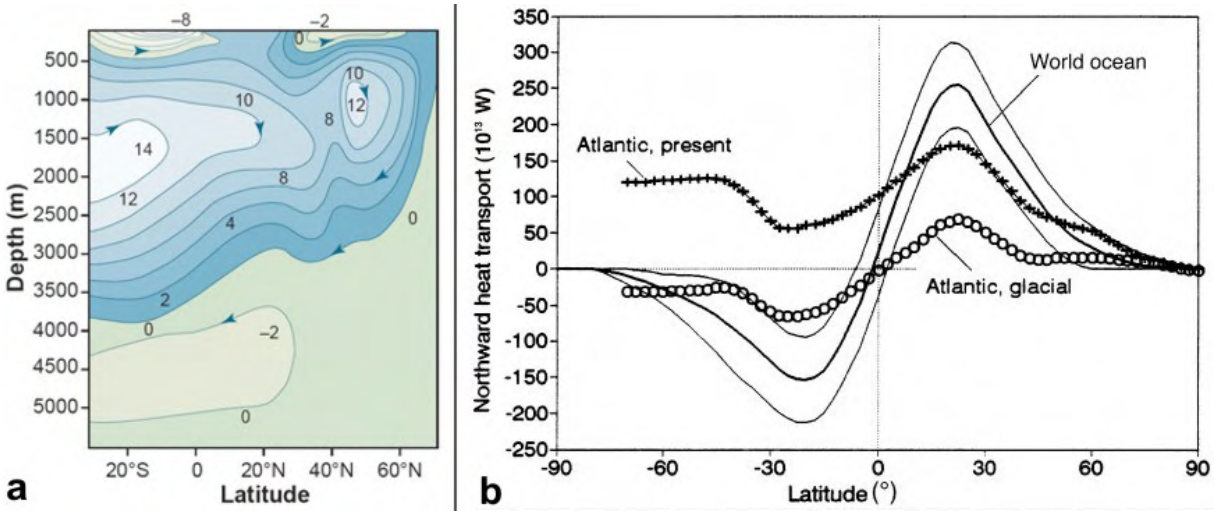

Figure 1.2: a: Stream function of meridional overturning in the Atlantic, from Wunsch (2002). b: Estimates of the annual heat transport in the world ocean (with error bounds) and the Atlantic (present and glacial) from Berger and Wefer (1996).

wind-forced: The Florida Current transport, which contains the northern outflow out of the Caribbean Sea, was reduced to 21 Sv (which is roughly 10 Sv less than the observed transport), the tropical-subtropical gyre boundary was located at 15°N and outflow occurred through the southernmost Caribbean passage (Grenada Passage). The SAW transport from the equator to the Lesser Antilles and into the Caribbean Sea occurs despite a different projection from the Sverdrup theory. Thus, the MOC has clearly large impact on the currents in this area as the Florida Current transport is much higher and inflow into the Caribbean is known to be strong in the southern passages. Wilson and Johns (1997) found more than 8 Sv entering the Caribbean south of St. Vincent, an island located close to the southern end of the island arc.

The region between the equatorial and subtropical gyres, where the interhemispheric exchange occurs, is one of the sparse locations suitable to directly measure the net South Atlantic Water flow into the North Atlantic and the Caribbean Sea: the small passages between the Lesser Antilles can be observed within reasonable ship time and only one additional survey in the Atlantic is necessary (the 16°N section is used) to obtain the total western boundary transport. In this region, the water masses from the North and South Atlantic can be distinguished by their different hydrographic features. The direct pathway along the western boundary for the upper ocean MOC return flow is the main focus of this work.

SAW is not only transported along the western boundary to the Caribbean Sea; exchange between the hemispheres also occurs in the central Atlantic. Shallow meridional overturning cells, so-called Subtropical/Tropical Cells (STCs), connect the subtropics and tropics through complex processes. The locations of the Atlantic STCs are indicated in Figure 1.3 from Zhang et al. (2003). During winter water is subducted in the subtropics; this water is transported towards the equator, where it is upwelled to the surface. Surface water is advected back to the subtropics by poleward Ekman transport, which closes the

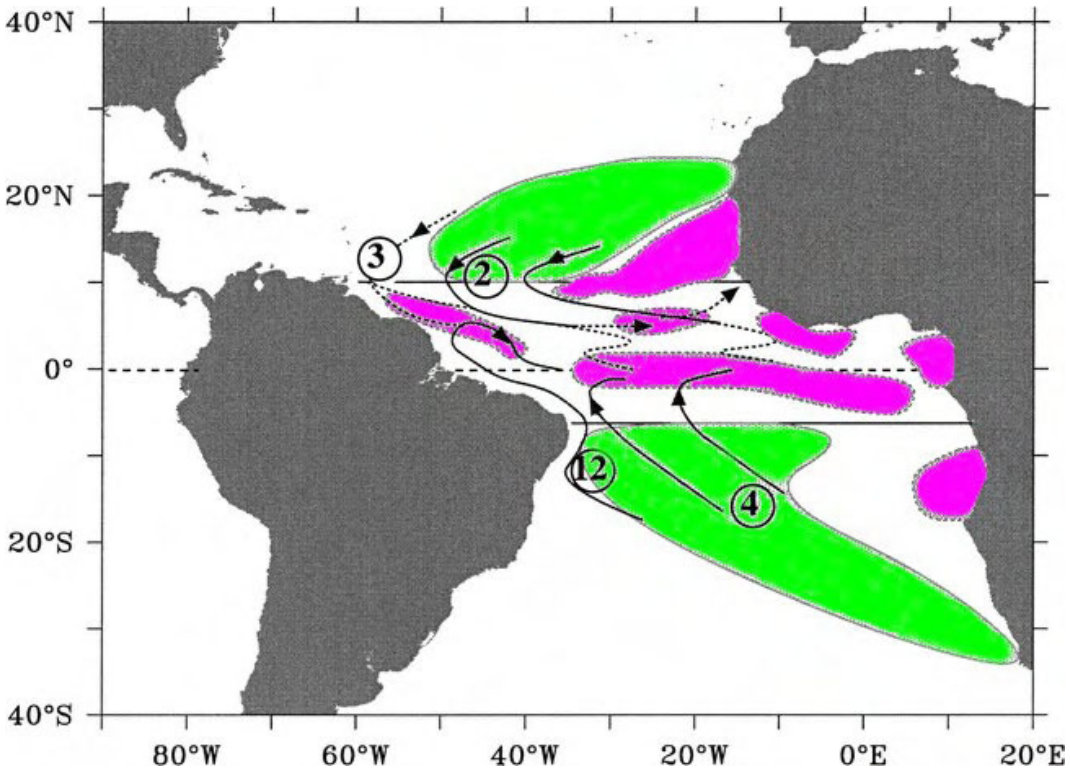

Figure 1.3: Schematic of the pathways and transports (Sv) of equatorward pycnocline flow from Zhang et al. (2003). Green: subduction areas and potential pathways towards the equator; pink: upwelling regions.

cell (e.g. Snowden and Molinari, 2003). The upwelled water is subject to air-sea heat and salt exchange, and the distinct SAW properties vanish in the South Atlantic STC. The STCs interact with the zonal currents of the equatorial current system, and particles, which are subducted in the South Atlantic, may take therefore a very complex route (Halliwell et al., 2003 give examples). Some part of the MOC transport takes the STC pathway in the central Atlantic. This SAW is transformed and modified on its way into the northern hemisphere; the typical South Atlantic characteristics in temperature and salinity are lost.

The connection between the equatorial Atlantic and the Caribbean Sea, and the transport pathways of SAW, have been topics of research for some time. A steady coastal current along the Brazilian shelf has been assumed to transport SAW continuously to the Caribbean as indicated by tracer patterns (Lux et al., 2001). The existence of this current has always been questionable since available data on the shelf is sparse as only few measurements were carried out there. Recent results from moorings strongly neglect this coastal current (Baklouti et al., 2007). Instead, the transport is obtained by large eddies, propagating northward along the western boundary. These rings conserve the unique SAW features and reach the Lesser Antilles with nearly pure SAW in the core. Assumably, interaction with the island topography can trap the rings. Consequently, they decay while released SAW enters the Caribbean (Fratantoni and Richardson, 2006). The strength of the transport into the Caribbean Sea (total transport as well as SAW transport only) and its continuity is one of the important questions for understanding

the MOC flow in the region and one of the major topics addressed in this work. The transport through the passages along the island arc is investigated, distinguished for the water masses in the vertical layers, and the locations of the strongest inflow are identified. Whether the inflow follows a seasonal cycle or is subject to smaller frequency variability is another topic of this research. The question, how far north SAW can be identified by temperature and salinity properties, is also addressed.

The distribution of SAW near the Lesser Antilles and in the western tropical North Atlantic is investigated by a collection of historical and recent data, obtained from measurements derived by ship cruises and by profiling floats. A high-resolution ocean model is used for further investigations, and the respective results are compared to the observations.

Concerning the rings, which transport SAW northward, many questions are still unanswered. While their generation and propagation towards the Caribbean has been observed several times (cf. Chapter 2), their demise is poorly understood. Some rings get trapped at the Lesser Antilles, but some presumably remain in the Atlantic. The rings remaining in the Atlantic are examined at the latitude of Guadeloupe, east of the Lesser Antilles. Important aims of this work refer to investigating the structure of the rings this far north and quantifying the northward transport of different water masses by rings.

The results of this study provide a detailed view on the large-scale SAW distribution in the western tropical/subtropical North Atlantic. The relative importance of the Caribbean pathway vs. the Atlantic pathway along the western boundary is evaluated. The impact of the inner Atlantic pathway on the MOC transport (via the STCs and the equatorial current system) is then reasoned out.

This work is structured as follows: an introduction to the tropical currents and water masses, their origins and fates, follows in the next Chapter. Chapter 3 gives an overview on the observational data used in this study, as well as the model description. The model output has been used for comparison with the measurements, since the measurements are sparse in some areas. The methods explained in Chapter 3 were applied to both data sets, the observational data as well as the modeled data. In Chapter 4, the Caribbean inflow region is examined in detail, while Chapter 5 focuses on the Atlantic pathway. The question of pathways and fate of North Brazil Current Rings is addressed there. The overall picture of the South Atlantic Water spreading into the North Atlantic is given in Chapter 6. In the discussion and outlook (Chapter 7), an evaluation of the warm branch of the MOC is presented and the dominating features and processes are discussed. Topics for further investigations are pointed out.

2 The Tropical Atlantic: Currents and Water Masses

In this chapter an overview of the topography in the area of investigation is given, and the upper ocean currents are introduced. The water mass properties at the Lesser Antilles emerge from a mixture of northern and southern origin waters. The different water masses of the tropical Atlantic from both hemispheres are introduced and their origins discussed. Density layers are defined according to the water mass properties, dividing the warm surface waters from the central waters and intermediate waters. The denotation South Atlantic Water (SAW) is used as a generic term for all southern water masses from the surface down to the border of the deep water (approx. 1100 m).

2.1 Topographic Setting

The tropical Atlantic covers the low-latitude region between 23.5°N and 23.5°S. At the equator the Atlantic extends from 10°E to 45°W, that is, the tropical Atlantic has a dimension of approx. 6000 km in width. North of 10°N the Atlantic is connected via an Island chain to the Caribbean Sea (also named American Mediterranean). The small islands east and south of Puerto Rico form the eastern border of the Caribbean and are called the Lesser Antilles Islands. The Greater Antilles are comprised of Cuba, Jamaica, Hispaniola, and Puerto Rico, and form the northern border of the Caribbean Sea. To the northwest, the Caribbean is connected to the Gulf of Mexico, to the west and south it is bonded by the continent of America, that is Mexico and Central America (Belize, Guatemala, Honduras, Nicaragua, Costa Rica, Panama) as well as Columbia and Venezuela.

Geographical overviews of the region addressed in this work (the western tropical Atlantic and the eastern Caribbean Sea) are given in Figure 2.1 and Figure 2.2. In general, the passages between the Lesser Antilles are narrow but deep: 1000 m are reached from St. Vincent to Guadeloupe Passage; and through Anegada Passage, even deep water exchange is possible. An exception is the area between Antigua Passage and Anegada Passage, where the Virgin Islands are located (cf. Fig 2.2). Here, the sill is everywhere shallower than 200 m. Grenada Passage was not investigated directly, but a section from Tobago to St. Vincent covers this passage. The topography between St. Vincent and Grenada is complex, with the small islands called 'Grenadines' forming several small passages. Thus valuable ship time was saved by this approach. At the eastern side of the Lesser Antilles, the Atlantic slopes steeply and deepens to more than 3000 m.

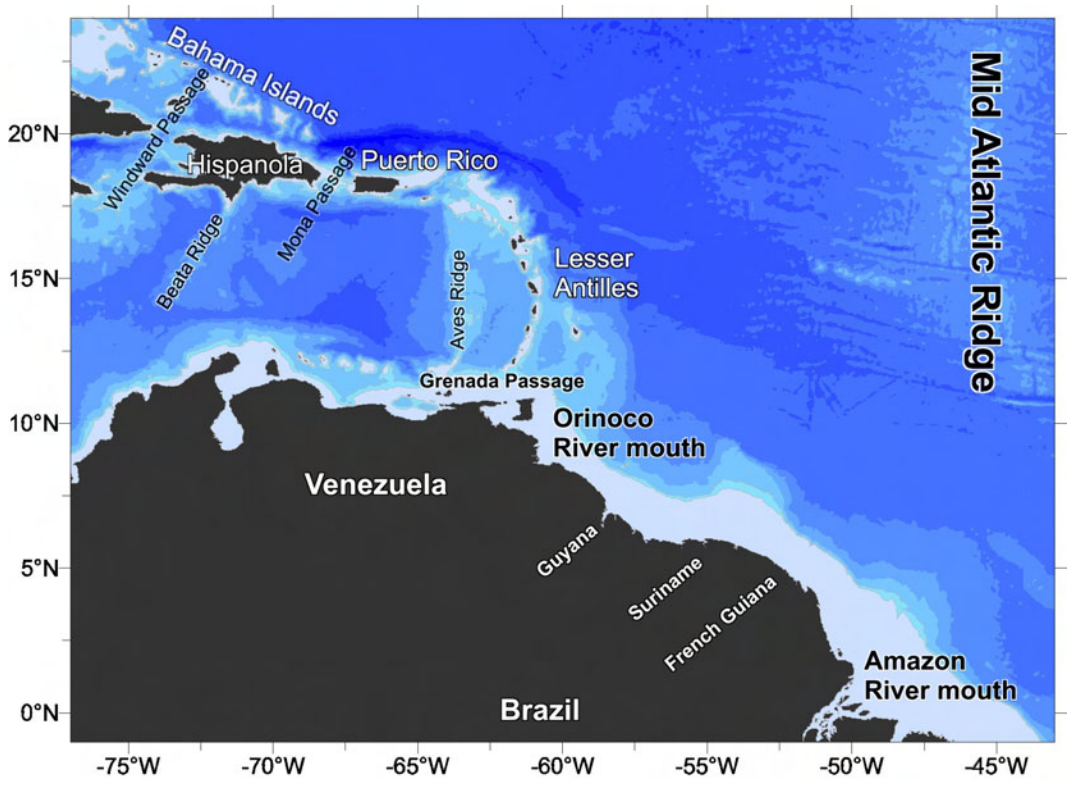

Figure 2.1: Topography of the western tropical North Atlantic and the eastern Caribbean Sea. The lightest blue color marks the shallow shelf area with depths less than 200 m.

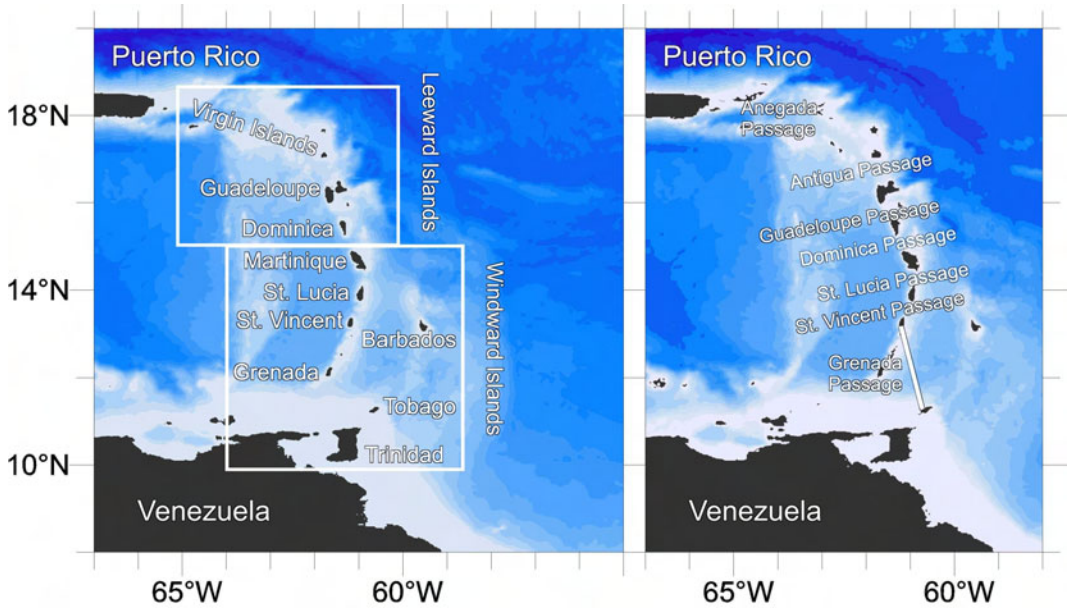

Figure 2.2: Topography of the Lesser Antilles Island Arc. The lightest blue color marks again the shallow topography with a depth less than 200 m.

2.2 Major currents in the western tropical North Atlantic

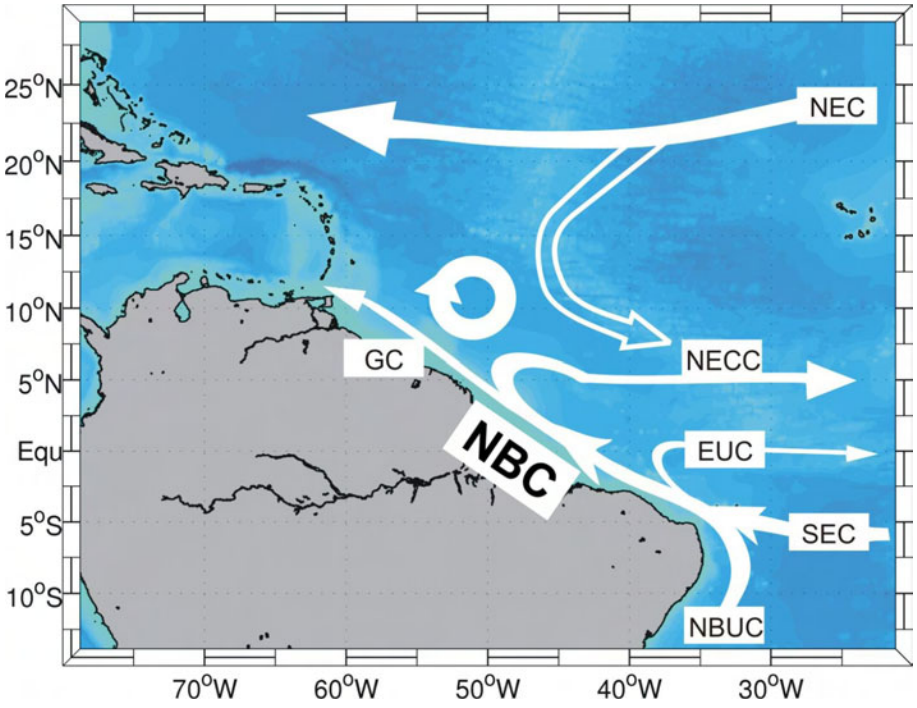

Figure 2.3: Upper ocean currents in the western tropical Atlantic. NEC: North Equatorial Current; GC: Guyana Current; NECC: North Equatorial Countercurrent; EUC: Equatorial Undercurrent; SEC: South Equatorial Current; NBUC: North Brazil Undercurrent.

A schematic overview of the currents in the tropical western Atlantic is given in Figure 2.3. The most prominent upper ocean current for the meridional and cross-hemispheric exchange is the North Brazil Current (NBC), flowing northward across the equator at the western boundary. The NBC arises from the combination of the subsurface North Brazil Undercurrent (NBUC) with the South Equatorial Current (SEC) (Schott et al., 1998). Parts of the NBC are lost at the equator, where the Equatorial Undercurrent (EUC) is formed in the thermocline layer. The NBC retroflects eastward from the Brazilian coast near 6°–7°N into the North Equatorial Countercurrent (NECC), and large quantities of its waters recirculate within the equatorial current system. The eastward tropical currents (NECC, EUC) show some North Atlantic influence as well. As a part of the subtropical gyre the North Equatorial Current (NEC) transports upper ocean waters south-westward and directly supplies water both to the NECC and the Caribbean Sea (Snowden and Molinari, 2003). A detailed description of the equatorial currents and the NBC can be found in Stramma and Schott (1999) and Schott et al. (1998).

At the NBC retrofection large anticyclonic rings are shed. This so-called NBC-Rings move north-westward towards the Lesser Antilles (e.g. Fratantoni and Glickson, 2002) and carry SAW within them. The retroflection of the NBC is at its maximum from July-December and weak in March and April, but the ring pinch-off occurs all year round (Goni and Johns, 2003; Garraffo et al., 2003). One of the first detailed descriptions of the ring shedding from the NBC retroflection was given by Johns et al. (1990). Three types

of rings exist: shallow and surface intensified rings, deep and surface intensified rings, deep and subsurface intensified rings. The surface intensified types can be recognized by satellites (Didden and Schott, 1993; Hu et al., 2004). In Garzoli et al. (2003) the ring shedding from November 1998 to June 2000 is described. The authors report 11 rings in this period, which had a mean diameter of 390 km and a propagation speed of 12.4 km/day.

2.3 Water masses in the tropical Atlantic

The water masses relevant for this study form the water column from the surface to about 1200 m (the density $\sigma_\theta = 27.6\ kgm^{-3}$). The characterization of the water masses and their limiting densities are chosen according to the regime in the western tropical North Atlantic, following the description by Stramma and Schott (1999). The upper layers are part of the warm watersphere, which extends between the two polar fronts at 45°S and 60°N in the surface Atlantic Ocean. The border to the coldwatersphere lies at the 8-10°C isotherms. The upper water masses originating in the South Atlantic are all influenced by the Agulhas Current leakage around the southern tip of Africa. The transport, which occurs mainly in Agulhas Rings, includes intermediate, central and surface waters from the Indian Ocean (Lutjeharms, 1996).

The water masses are introduced following their depth: starting at the surface, the first layer is Tropical Surface Water (TSW), followed by Salinity Maximum Water (SMW) just underneath. The third layer is formed by Central Water (CW). Intermediate Water (IW) is the deepest layer considered in this work. An overview of the vertical position of each water mass is given in Table 2.1. Their most characteristic attribute is stated in the last column. More details follow in the next sections. Every layer has sources in both hemispheres and a mixture of this sources formes the water in the western tropical North Atlantic. Within the NBC all southern types of the water masses described below enter the northern hemisphere (eg. Stramma et al., 2005).

water mass	σ_θ range	depth	comment
TSW	$\sigma_\theta < 24.5\ kgm^{-3}$	surface to 80 m	Amazon discharge influence
SMW	$25.4 - 26.3\ kgm^{-3}$	80 m to 200 m	S maximum
CW	$26.3 - 27.1\ kgm^{-3}$	200 m to 500 m	linear T/S relationship
IW	$27.1 - 27.8\ kgm^{-3}$	500 m to 1100 m	S minimum

Table 2.1: Water mass classification in density range and approximate depth. The comments contain the major characteristics of the water masses.

Tropical Surface Water - TSW

The TSW consists of water lighter than $\sigma_\theta < 24.5\ kgm^{-3}$, and occupies the upper 50 m to 80 m of the tropical Atlantic. Large amounts of South Atlantic TSW enter the North Atlantic with the NBC. TSW is modified by the atmosphere and river input, especially the Amazon River outflow near the equator. The fluxes modifying the TSW are unknown for high resolution requirements. Gridded freely available datasets, like the NCEP/NCAR reanalysis project (Kalnay et al., 1996), give the surface fluxes from the ocean to the atmosphere on a 2.5°x2.5° grid. Since this spatial resolution is far from sufficient to be used in a small region as the Caribbean, assumptions have to be made on the South Atlantic influence on TSW. The exact position of the transition region to North Atlantic surface water is unknown, only the Amazon river plume can be traced relatively easily (see Hellweger and Gordon, 2002). But where the salinity minimum of the plume has dispersed (near Guadeloupe, the mean surface salinity is >35), there is no chance of tracking the South Atlantic surface water. While several studies indicate a strong influence of Amazon River discharge even in the area of Barbados (Hellweger and Gordon, 2002; Kelly et al., 2000), a connection to the northern passages (Anegada, Antigua) is unknown. Dessier and Donguy (1994) analysed historical surface salinity data and found a maximum Amazon outflow patch in June, extending to 20°N, but one has to be careful with the salinity observations, since the Orinoco outflow, which lies on the northern hemisphere (8°N, cf. Fig. 2.1), has some contribution as well. Publications showing the chlorophyll-a distribution from satellite data (e.g. Signorini et al., 1999), indicate Amazon and Orinoco influence in all the Caribbean Sea, but not at the northern Atlantic side (e.g. north of Puerto Rico). Since there is evidence of strong southern TSW transport to the Lesser Antilles, the TSW is assumed to be of South Atlantic origin south of Guadeloupe, but not further north.

Salinity Maximum Water - SMW

The SMW is embedded in the density rage $\sigma_\theta = 25.4 - 26.3\ kgm^{-3}$ and consists of three different types in the tropical Atlantic (one northern type, two southern types). In both hemispheres this highly saline water mass is formed by the excess of evaporation over precipitation in the subtropics. Near the equatorial region, where the intertropical convergence zone and river outflow lead to a large input of fresh water, subduction of this high salinity water to a subsurface layer occurs. The salinity maximum in the South Atlantic develops near 15°-20°S at the ocean surface and extends subsurface both northward and southward (Mémery et al., 2000). At 20°S a surface salinity of even 37.5 can be observed. North of 10-7°S the surface salinity is rapidly decreased to < 36. The South Atlantic SMW is transported westward with the SEC off the formation region. When reaching the American cost, it spreads in both directions (northward and southward) with the boundary currents. The northern branch in the NBUC dilutes the salinity maximum to 36.7 on the density surface $\sigma_\theta = 25.0\ kgm^{-3}$ at the equator (Mémery et al., 2000). The

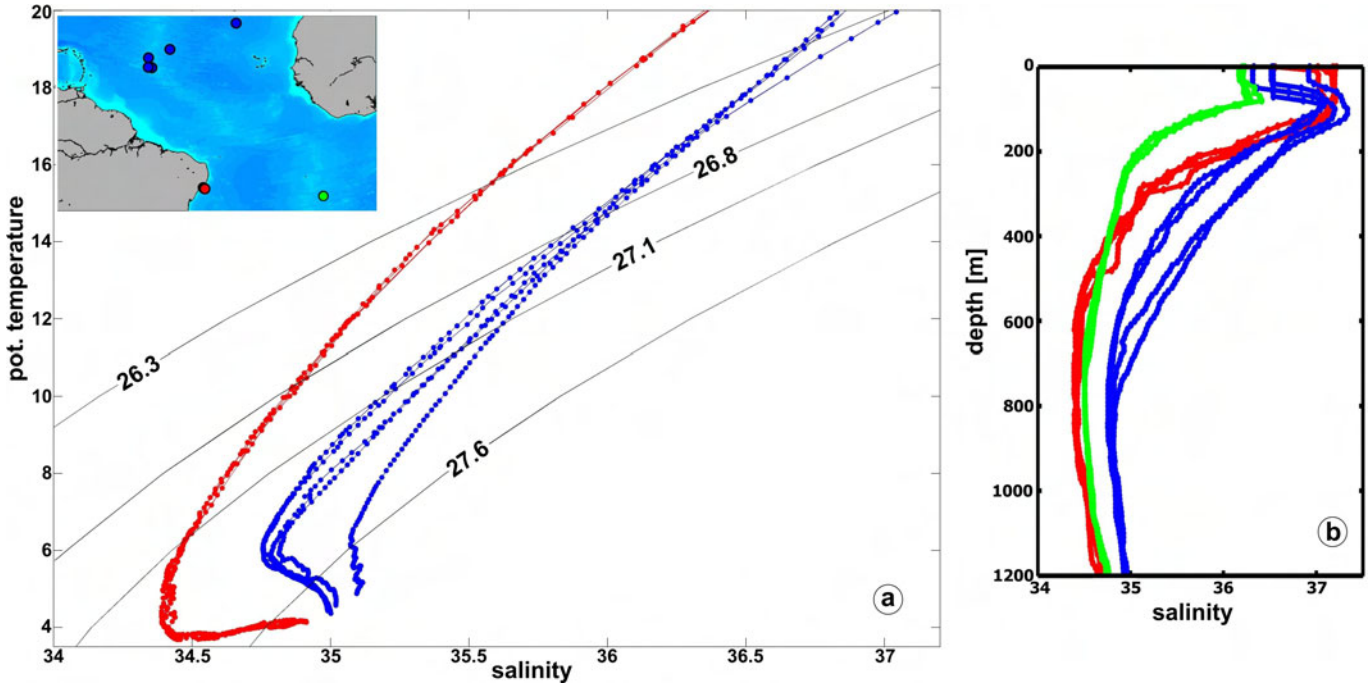

Figure 2.4: a: Examples for temperature and salinity relationships from the North and South Atlantic in 200-1100 m depth (CW and IW), with locations. b: Corresponding salinity profiles, the southern fresher SMW source has been added (green). The profile locations are indicated on the map in a.

South Atlantic provides another source in this density range, which is noticeably fresher (Wilson et al., 1994). From the eastern Atlantic, this water mass is brought to the western boundary with the equatorial branch of the SEC. When crossing the equator, the SMW layer within the NBC consists of both southern sources.

The northern salinity maximum lies in the density range bounded by the 25.6 kgm^{-3} to 26.3 kgm^{-3} isopycnals (Snowden and Molinari, 2003). The salinity in this layer exceeds above 37 in the formation region in the North Atlantic subtropics. Near the Lesser Antilles the salinity in northern SMW is still higher than in southern SMW and the maximum lies deeper than its southern counterpart. At the density $\sigma_\theta = 26.25\ kgm^{-3}$ the southern SMW reaches a salinity of 36.2, while the salinity in the northern SMW is as high as 36.9 (measured south of the Lesser Antilles, from Bourles et al. (1999)). Examples of salinity profiles for the three types of SMW are given in Figure 2.4 b.

Central Water - CW

The CW occupies the density range of $\sigma_\theta = 26.3\ kgm^{-3}$ and $\sigma_\theta = 27.1\ kgm^{-3}$, which corresponds to a temperature range of 20°-5°C. The salinity is decreasing from 36.0 at 20°C to 34.3 at the border to the deeper intermediate water. Occasionally, the CW water is further subdivided into an upper and a lower layer (UCW and LCW) by the isopycnal $\sigma_\theta = 26.8\ kgm^{-3}$. The Central Waters are characterized by an almost linear T-S relationship, as illustrated in Figure 2.4. South of approx. 15°N, the South Atlantic Central Water (SACW) dominates this layer. The front is stretched to 20°N at the

eastern boundary, where it is particulary strong. The behavior is different near the western boundary, where the front gets indistinct, as the horizontal gradients vanish due to mixing within the North Equatorial Current (Klein and Tomczak, 1994). As the northern and southern Central Waters cover the same density range, exchange of water parcels across the front, which is not seen in the density field, is easy. The origin of SACW lies at the Subtropical Convergence, where this water is formed by subduction, as all Central Waters are in the southern hemisphere. In the tropical South Atlantic, a mixture of this freshly subducted SACW with Indian Central Water (brought into the South Atlantic by Agulhas Rings) is found. In the South Atlantic the main thermocline is included in the SACW. The northern hemispheric counterpart shows a linear T-S relationship as well, but at higher salinities. North Atlantic Central Water (NACW) is formed in the Sargasso Sea during winter, as well as north of Madeira. Waters from the Arctic and Labrador Seas also contribute to the NACW layer.

Intermediate Water - IW

The deepest water mass considered here is the IW. This layer is dominated by inflow from the south. The Antarctic Intermediate Water (AAIW) covers the density range $\sigma_\theta = 27.1 - 27.7\ kgm^{-3}$ in the tropical Atlantic. This bordering isopycnals will be used, following earlier water mass definitions in this region (e.g. Stramma and England, 1999). The sources for AAIW lie in the surface waters of the Circumpolar Current: The Pacific inflow through Drake Passage is modified in the southwestern Atlantic in the Falkland Current Loop, forming Atlantic AAIW (Talley, 1996). From the east via the Agulhas Current leakage, some Indian saltier AAIW contributes to this layer as well (e.g. Lutjeharms, 1996, Giulivi and Gordon, 2006). The AAIW density increases on its way north, however it remains nearly uniform between 20°S and 20°N.

North of the equator, the AAIW still dominates the intermediate layer down to 1100 m. The AAIW salinity minimum can be traced best at the western boundary, into the Caribbean Sea and in the Florida current as well. Up to 24°N the AAIW is still recognizable by a minimum in salinity, but traces of AAIW can be followed as far as nearly 60°N by silica analysis (Tsuchiya, 1989). The influence of AAIW and the transition region to North Atlantic intermediate waters, which are composed of Mediterranean Outflow Water, Subarctic Intermediate Water and Labrador Sea Water, thus lies farther north than the SACW/NACW influence (Arhan et al., 1994). The AAIW is characterized just south of the equator by a salinity minimum of 34.5 at the density $\sigma_\theta = 27.3\ kgm^{-3}$, which is found at 700-800 m (see Figure 2.4. The outcropping latitude of this density lies at 50°S during winter (and south of Greenland in the North Atlantic). In the tropical western North Atlantic the low salinity AAIW layer covers the depth range from 700 m to 1100 m. In terms of potential temperature, the AAIW acquires the range 6.0-4.2°C.

3 Data and Methods

The investigation of the Meridional Overturning Circulation in the Atlantic Ocean is part of the international CLIVAR (Climate Variability and Predictability) program. An improvement in understanding and describing the processes of climate and climate variability, as well as the extension of climate records, is one of the main objectives in the program. A part of the German contribution to the CLIVAR program were six ship cruises in the tropical Atlantic, carried out by the University of Bremen. The investigation was focused on the shallow upper branch of the Atlantic MOC, which crosses the equator and partly enters the Caribbean Sea. The South Atlantic inflow can be separated from the northern waters by temperature and salinity properties, which were obtained during the cruises. An isopycnal mixing approach provides the SAW portion at the locations, where the hydrographic measurements were performed. Historical observed profile data from the HydroBase project and Argo float data complement the information about the SAW distribution obtained by the ship cruises. The data coverage in the western tropical Atlantic is nevertheless sparse; and a high resolution ocean model is used to compensate this lack of data. The model gives an excellent spatial and temporal resolution, and is used to study the mechanisms of the upper ocean flow and its variability. In this chapter an overview of the observations and measurements during the ship cruises are given; and the collected data set from historical observations and Argo floats is introduced. The model is presented in detail and the water mass analysis for identifying the SAW is explained as well.

3.1 Ship cruises

Four repeats of hydrographic measurements in the Lesser Antilles passages and six at 16°N (from Guadeloupe eastward) were performed by the University of Bremen, operating from different research vessels. Table 3.1 gives an overview of the cruises and in Figure 3.1 the hydrographic stations are illustrated. The cruises date from December 2000 to September 2005. The cruise track was partly different in each survey. Especially the 16°N section, starting at Guadeloupe, ended every time at another longitude. While several repeats exist for the passages south of Guadeloupe and at 16°N eastward, measurements in the two northern passages (Antigua and Anegada) were only operated once. In April 2003 the 16°N section was reduced to only 60°W, since ship time was short during that cruise. This extent is not sufficient to resolve NBC rings, this single observation is therefore not used in the following. Except for one cruise (S 152 in December 2000) all data were collected between April and September, results from the cruises are thus grouped in the summer season.

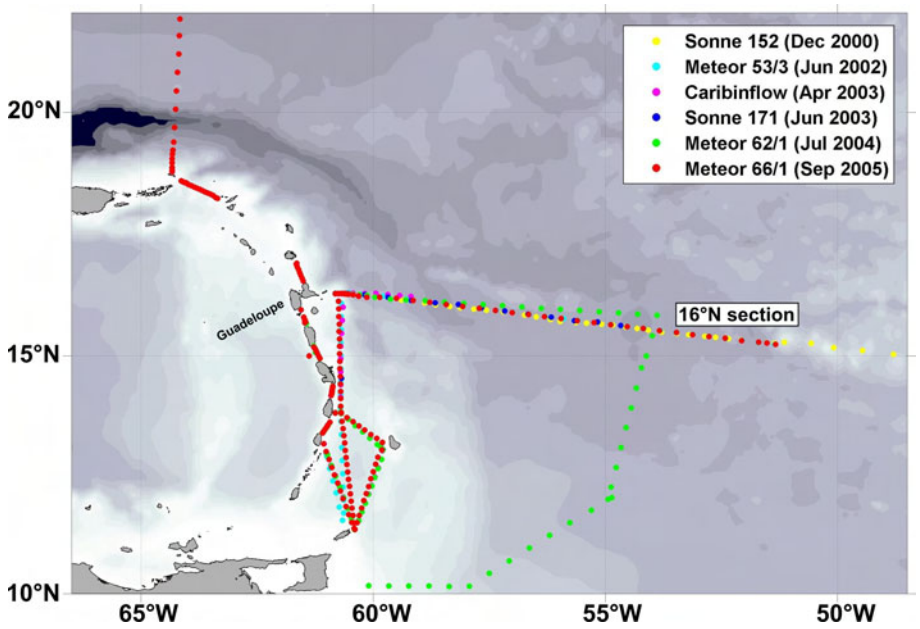

Figure 3.1: Stations during the ship cruises in the western tropical Atlantic. Note that the dots for more recent cruises overlay the older ones. The passages south of Guadeloupe have been frequented four times, the 16°N section five times.

cruise	vessel	date	passages	16°N eastern end
S 152	RV Sonne	December 2000	no	48°W
M 53/3	RV Meteor	June 2002	yes	51°W
Caribinflow	RV Atalante	April 2003	yes	60°W
S 171	RV Sonne	June 2003	no	54°W
M 62/1	RV Meteor	July 2004	yes	53°W
M 66/1	RV Meteor	September 2005	yes	51°W

Table 3.1: Ship cruises in the western tropical Atlantic during 2000-2005. The 16°N section had different extensions during all cruises, starting at Guadeloupe to the longitude given above. During cruise M 66/1 Anegada and Antigua Passage were attended in addition to the other passages.

CTD data

During each cruise CTD measurements (conductivity, temperature and depth) were carried out with a Seabird Electronics (SBE) 911plus instrument. From the temperature and conductivity profiles, the salinity was assessed. The conductivity sensor was calibrated by water samples taken from 10L Niskin bottles, which were operated by a 22 bottle SeaBird carousel. About five water samples were taken for every profile for calibration purpose, and the respective salinity was measured by means of a Guildline Autosal salinometer (types 8400A and 8400B were used). Further details can be found in the cruise reports, available on http://www.ifm.uni-hamburg.de/~wwwls/cruise2.html. The CTD accuracy for all cruises was 0.002-0.003°C for temperature and 0.002-0.003 for salinity. The calibrated and controlled raw-data were interpolated on 10 m steps.

The CTD stations were performed with high resolution in the passages, that is a geographical distance of only 1-2 nm (nautical miles) between the casts. At 16°N near Guadeloupe the resolution was 2-15 nm, increasing to 20-40 nm further east.

ADCP data

Different types of ADCP instruments (Acoustic Doppler Current Profiler) were installed on the research vessels, either into the well of the ship, or mounted into the ships hull (called vm-ADCP, vm for 'vessel mounted'). Important capabilities of different ADCP devices are their working frequencies and bin lengths. The working frequency of an ADCP assigns the penetration depth of the sinal and therefore the measuring range of the instrument. ADCPs break up the current profiles into depth cells, which are called bins. The bin length denotes to the size of a depth cell. The average velocity for each bin is measured by the ADCP. An overview over the instruments is given in Table 3.2. On RV Sonne, where only one instrument was available, the range of the vm-ADCP was 500-800 m. On RV Atalante and RV Meteor, the high-frequency vm-ADCP was used with a smaller bin length, which gave high vertical resolution near the surface. The other instrument completed the profile down to 700-1400 m, depending on the instrument and on the weather conditions. Hourly averaged horizontal velocities were associated with an error of 0.05 ms^{-1} for all cruises (Rhein et al., 2005). Attached to the CTD/water sampling system, additional ADCPs, so-called lowered ADCPs (LADCPs), were operated. During three cruises (S152, M53/3, S171) a 150 kHz narrow band ADCP was used. The range of this instrument was 300 m at best and decreased occasionally to 100 m at large depths. The error was estimated to be in the range of 0.05 ms^{-1} for individual measurements. During the other cruises (Caribinflow, M62/1, M66/1) two RDI 3000 kHz Workhorse Monitor instruments were operated. The two instruments were arranged as a master and slave synchronized system. The system worked with a 1 ping/s rate and a bin length of 10 m. The package achieved a range from 100 to 300 m and obtained very high accuracy, even in weak current conditions (error less than 0.02 ms^{-1}).

vessel	ADCP	frequency	bin length
RV Sonne	Ocean Surveyor	75 kHz	16 m
RV Meteor	Ocean Surveyor	75 kHz	8 m
RV Meteor	Ocean Surveyor	38 kHz	32 m
RV Atalante	narrow band ADCP	75 kHz	16 m
RV Atalante	narrow band ADCP	300 kHz	4 m

Table 3.2: vm-ADCP devices, mounted on the three research vessels.

At the stations where both ADCP types were perfoming measurements the LADCP data showed good agreement with the vm-ADCP data (pers. com. M. Walter). The LADCP data was used to complete profiles in the few cases, where the range of the vm-ADCPs was not sufficient to reach 1200 m depth.

3.2 Other data sources

Argo floats

In the Argo program numerous free-drifting profiling floats that measure the temperature and salinity of the upper 2000 m of the ocean, were deployed since 2000 in the World Ocean (see http://www.argo.ucsd.edu for detailed information). The aim of the Argo program is to accomplish 3000 such profiling floats in the word ocean. After the deployment by ships or aircraft the floats work autonomically for approx. 4-5 years (until the battery breaks down). Every float has a fixed parking depth, to which the float descends. After ten days, the float sinks to 2000 m and then ascends to the sea surface. Temperature and conductivity profiles are measured on the way up and finally send to the data center by satellite connection. The float then sinks again to its prescribed parking depth and a new cycle starts. The accuracy requirements of Argo for the float measurements are 0.005°C for temperature and 0.01 for salinity (which is obtained through the conductivity and temperature data). The floats are calibrated by the manufacturer before deployment and are expected to give good measurements over their lifetime. Oka and Ando (2004) re-calibrated the temperature and conductivity sensors of three Argo profiling floats, which were recovered after operating for four to nine months. Their results indicate that the floats basically showed no significant drift (however, one of the floats had an operational error).

When using the Argo data, an extensive quality control is needed. The raw data holds still many faults. Some floats have been shown to report the salinity and temperature data at wrong depths (Schiermeier, 2007), profiles from these floats must be completely expelled until a revision is published. All profiles were quality controlled carefully, so that only plausible profiles became part of this analysis.

When a float reaches the surface, the profile data is delivered within 24; the quality control procedures on the real-time data provided by the Data Centers (eg. http://www.coriolis.eu.org/cdc/argo.htm) are thus limited and automatic. The date and the locations (latitude, longitude) should be tested for sensible data, the range of temperature and salinity values limited to -2.5°C-40°C and 0.0-41.0 PSU and flaws in the profiles flagged as bad data. A detailed manual of the desired quality control is provided by the Argo Data Management Team (available on http://www.jamstec.go.jp/ARGORC/docs_top.html). Unfortunately, not all profiles are checked by this concept and especially the older profiles remain untested in the data set. Hence the profiles used here were checked by a specially developed check. The quality control firstly filtered all profiles, which were marked as erroneous by the Data Centers. In a second step, all spikes in the data were erased. Additionally, explicitly absurd data for the upper tropical Atlantic was removed, that is: salinities above 41 or below 15, or temperatures exceeding 30°C. A check for density increasing with depth was also performed and density inversions erased. The third and last quality control included a statistical approach: the data were divided into regional boxes, containing 10°-20° in latitude and

longitude. A mean profile was calculated for every box and single profiles, varying more than the doubled standard deviation from the mean, were removed. By this approach the data were filtered thoroughly; but the possibility of remaining systematic errors, like sensor drift, can not be ruled out.

Hydrobase

The HydroBase data set is a collection of observed temperature and salinity data, and thus a tool for climatological analysis of oceanographic properties (Curry, 2001; http://www.whoi.edu/science/PO/hydrobase). In addition to the cruises carried out by the University of Bremen, older historical data from ship cruises in the western tropical Atlantic were extracted from Hydrobase. The data coverage is still sparse and all the observed profiles remain snapshots, some months are highly under represented. An analysis of variability on the timescale of years or decades must remain for future investigations.

3.3 The 1/12° FLAME Model

The sparse observational data can only adumbrate the flow across and along the Lesser Antilles Island arc. To complement the understanding of the currents and water mass spreading in the area, an ocean general circulation model is used. The high-resolution FLAME model (Family of Linked Atlantic Model Experiments, FLAME; Dengg et al., 1999) has been developed at IFM-GEOMAR in Kiel for studying the wind-driven and thermohaline circulation in the Atlantic Ocean and meets the demands necessary for this study. FLAME is based on the Modular Ocean Model code (MOM2.1; Pacanowski, 1995, solving the primitive equations, but several refinements were applied to the configuration (e.g. Eden and Böning, 2002).

The simulation considered here uses a horizontal grid of $\frac{1}{12}^\circ$ and 45 vertical levels, for a domain from 70°N to 18°S in the Atlantic (cf. Eden and Böning, 2002; Böning et al., 2006). The model is forced with monthly-mean wind stresses and heat fluxes based on a climatology of the European Centre for Medium Range Forecasts (ECMWF) analysis following Böning et al. (1996) and the DYNAMO study (Willebrand et al., 2001). Sea surface salinity, as well as the hydrographic conditions at the closed northern, and the inflow through the open southern boundaries are damped towards climatological values. The model bathymetry was not fine tuned for the purpose of this study and thus lacks some detail in the area of the Antilles passages (e.g., missing some of the deep parts); all passages are nevertheless represented in the model (see Chapter 4). The model has been integrated for 15 years with climatological forcing; the last year of this run is referred to as FLAME_CLIM. The following 15-year run included interannual variability and is named FLAME_INTER in the following.

The model provides velocity, temperature and salinity on the defined depth levels. The velocity grid points are displaced slightly from the temperature/salinity grid points

(Arakawa B grid). The topography is shallower and passages between islands are narrower in the velocity grid than in the temperature and salinity grid. When temperature and salinity information was needed at the velocity positions, the four surrounding points were interpolated to obtain the data at the needed position. The interpolation was always done this way (T- and S-data interpolated on u- and v-points), so that on land points artificial flow was avoided.

The FLAME model used has a much finer resolution than previous studies (Fratantoni et al., 2000, Johns et al., 2002), namely $\frac{1}{12}^\circ$ vs. $\frac{1}{3}^\circ$ and 45 vs. 6 vertical layers. These coarser models represent the narrow passages with one single gridpoint, while FLAME has at least three in velocity and more in temperature and salinity with adequate vertical resolution, too. The Lesser Antilles are represented as shallow ocean points and are still about 35 m deep. When estimating the inflow through the Lesser Antilles in the model, every gridpoint on the way from Tobago to Puerto Rico was considered, so that the passages merge into each other (see Chapter 4). Grenada Passage was substituted by a section going from Tobago to St. Vincent, analog to the cruise track (cf. Chapter 2).

3.4 Tides

In the small passages from St. Vincent to Guadeloupe the tides were investigated. For a time period of 3-24 h the inflow through every passage was measured repeatedly, so that the tidal cycles were resolved (the time needed for one passage crossing was only 70 min to 2.5 hours, depending on the width of the passage). The tides were removed by averaging over multiple ADCP repeats during each cruise. For example, during April 2003 transport variability for one tidal phase from 1.6 Sv to 8.8 Sv was observed in St. Vincent Passage. The effect of the tides in St. Lucia Passage was found to be of comparable order, but less crucial in the northern passages (Dominica, Guadeloupe). Grenada Passage was approximated by a section from Tobago to St. Vincent (cf. 2.2). The section took about 20 h to complete (including the CTD measurements). Only one cast was performed during each cruise, thus no tide correction was possible for this section. Antigua and Anegada Passage were only visited during M 66/1 in September 2005. The tides were removed by the same method as before: multiple ADCP casts were averaged. The velocity field in Anegada Passage was strongly influenced by tides during that cruise.

3.5 Transport calculations

Transports are obtained from the vm-ADCP data (complemented by LADCP profiles, if necessary), which were interpolated on a regular grid, corresponding to the CTD data. The vertical resolution in the velocity data was adjusted to 10 m steps as in the hydrographic data (see above). The horizontal grid resolution was 7.5 nm in Grenada Passage, 0.4 nm in the passages from St. Vincent to Guadeloupe and 0.7 nm in Antigua and Anegada Passage. Volume transports directed into the Caribbean Sea through the Lesser

Antilles Passages were derived by integrating the velocity fields over the passages. The error from the data interpolation was negligible. The current was found to be at maximum in the upper layers, thus weak currents at depth and a fine data resolution minimized the error from missing bottom triangles, which were therefore neglected. On the 16°N section near Guadeloupe the data was interpolated on grid points with 15 nm distance. East of Guadeloupe the topography rapidly deepens and the ocean bottom was presumably of no importance for the shallow flow considered here.

3.6 Water mass analysis

The applied water mass analysis uses an isopycnal mixing approach. In the analysis salinity and temperature data are used as constrains. With this information, only two sources can be distinguished. One source represents the northern waters, the other is located in the southern hemisphere (Rhein et al., 2005). For defining the sources, profiles from historical data in the North and South Atlantic were chosen. The hydrographic properties of the source waters are shown in Figure 3.2 (red: observations; blue: model). The northern source consists of profiles from 24.5°N, east of 60°W for water denser than 26.3 kgm^{-3} and from 16°N/55°W for water above $\sigma_\theta = 26.3\ kgm^{-3}$ (locations 1 and 2 in the map of Fig. 3.2). The shift to 16°N was necessary for the SMW, as this water mass is partly formed south of 24°N (Zhang et al., 2003). The south Atlantic sources (locations 4 and 3) are defined at the western boundary at 10°S/35°W for $\sigma_\theta > 26.3\ kgm^{-3}$ and further east for the SMW layer ($24.5\ kgm^{-3} < \sigma_\theta < 26.3\ kgm^{-3}$). In this choice, the fresher eastern SMW source (cf. Chapter 2) is used in the analysis, as the salty South Atlantic source is indistinguishable from the northern type (Fig 3.2). Missing in the analysis is thus the salty South Atlantic SMW source, as well as the surface water above $\sigma_\theta = 26.3\ kgm^{-3}$, which is modified by the atmosphere and river input and considered to be fully of southern hemispheric origin south of 16°N (see Chapter 2).

The source profiles for the model T/S analysis were extracted from the climatological run at nearly identical positions (10°S/35°W, 3°S/23°W: southern source and 18°N/55°W, 24°N/50°W: northern source). The model simulates the observed water masses very accurately and the same separating isopycnals are used as water mass boundaries as in the observational analysis.

The T/S analysis is used to calculate the portion of south Atlantic water in water sample (measured or modeled). The source profiles are considered representatives of the pure northern and southern waters (Fig. 3.2). The analysis calculates the fraction of each source component necessary to obtain the properties of the given water sample. The result is the SAW fraction in percent.

The choice of the source waters lead to errors of ±3-6% due to temperature and salinity uncertainties. The influence of diapycnal mixing was calculated by varying the density of both source water masses. The resulting uncertainty in the SAW fractions were ±5-10%

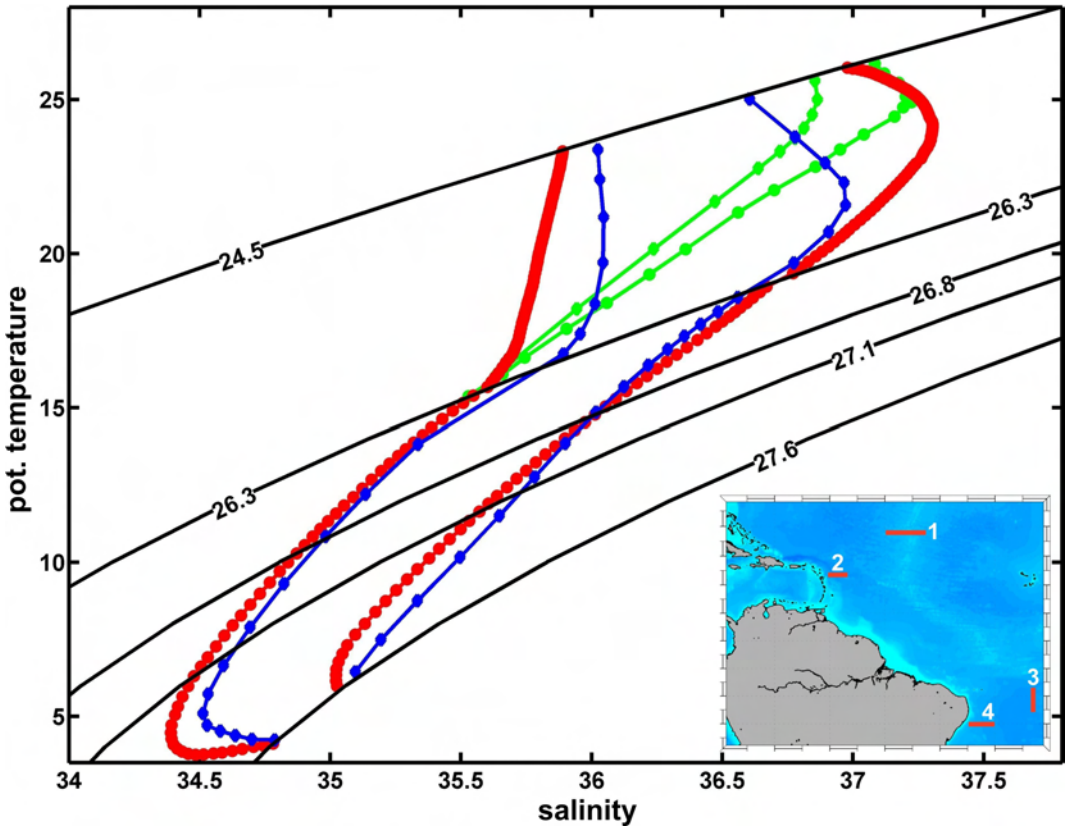

Figure 3.2: Source water profiles used for the T/S analysis. The red profiles represent the observational sources and the blue profiles were extracted from the model. The shorter green lines show the salty South Atlantic source. The small map illustrates the locations, where the source waters were chosen. 1: northern source with $\sigma_\theta > 26.3\ kgm^{-3}$; 2: northern source with $\sigma_\theta < 26.3\ kgm^{-3}$; 3: southern source with $\sigma_\theta < 26.3\ kgm^{-3}$; 4: southern source with $\sigma_\theta > 26.3\ kgm^{-3}$

(see Rhein et al., 2005). The overall uncertainty of SAW fractions obtained by this method was thus estimated to be ±12% in the IW layer and of ±6% in the CW layers. The error in the SMW is clearly higher, due to the neglected western South Atlantic source.

A combination of the transport calculations with the SAW portions leads to SAW transports into the Caribbean. The SAW transports were derived by multiplying the passage velocity with the corresponding SAW fraction at each grid point, and then integration over the passage.

4 The Caribbean inflow through the Lesser Antilles

A branch of the shallow meridional overturning in the Atlantic enters the Caribbean Sea through the narrow passages between the Lesser Antilles. This flow continues into the Gulf of Mexico and leaves the Caribbean through Florida Strait and becomes part of the Gulf Stream. In this Chapter the transports through the passages obtained from observations are investigated and compared to model results. Since only a part of the inflow can be connected to the MOC, namely the South Atlantic Water portion, this fraction is estimated and discussed. The variability of the inflow is discussed shortly. The new results are evaluated in the context of previous work. Parts of this Chapter (concerning the observational results and the climatological run in FLAME) were already published in Kirchner et al. (2007).

4.1 Observed inflow

Current velocities were obtained during ship cruises carried out in the Lesser Antilles Passages since 1991, from which transports into the Caribbean were calculated (Chapter 3). In Figure 4.1 all transports, which were inferred by those measurements, are presented. The transports are normally directed into the Caribbean. The transports are plotted versus the month of observation, independent of the year. They represent snapshots of the inflow. Triangles mark the estimates provided by Johns et al. (2002), while the circles represent results inferred from the cruises carried out by the University of Bremen. The dashed line is the mean value, which is given in Table 4.1 and discussed below (together with the modeled mean). The transport at the shallow section ($<$ 200 m depth) between Antigua and Anegada passage was negligible (0.04 Sv) during the survey in September 2005. As no more data from this shallow region was available, it was disregarded for the observational results.

The wide range of variability is the most eye-catching feature in Figure 4.1. In the case of Grenada Passage (a) the minimum transport ever recognized (May) is directly followed by the maximum in the subsequent month (June). Even in the same month of observation, the calculated transports vary in a range of several Sverdrup: For example, the two estimates of the inflow through St. Vincent Passage (b) in April diverge nearly 6 Sv. The transports are strongest through Grenada Passage and weakest through Guadeloupe Passage, whereas the other passages vary between. Infrequently a net outflow is found, except for Grenada and Antigua Passage, but the mean remains decidedly positive (that is inflow) in all passages. Nonetheless only six to fifteen surveys were operated in these passages, and unfortunately the observations do not cover every month.

More data is needed to get solid conclusions on the mechanisms causing the observed variability, particularly a seasonal cycle is not discovered. The range of the observed inflow implies nevertheless a strong impact of mesoscale effects; an explanation might be found in NBC rings interacting with the island topography, which may be responsible for the varying situations in different years.

Since only six measurements were carried out in Anegada and Antigua Passage (see Fig. 4.1 *f* and *g*), it was refrained from presenting the total inflow into the Caribbean versus the month of observation. For the passages south of Guadeloupe (Fig. 4.1 *a*-*e*) the data coverage is improved. Rhein et al. (2005) found for the inflow through these passages the maximum transport in June and the minimum in April/May. The cruise from September 2005 fits into the known transport range in fall, but still no measurements were performed in spring (January-March). The lack of data make it difficult to infer a seasonal cycle for the inflow from the observations.

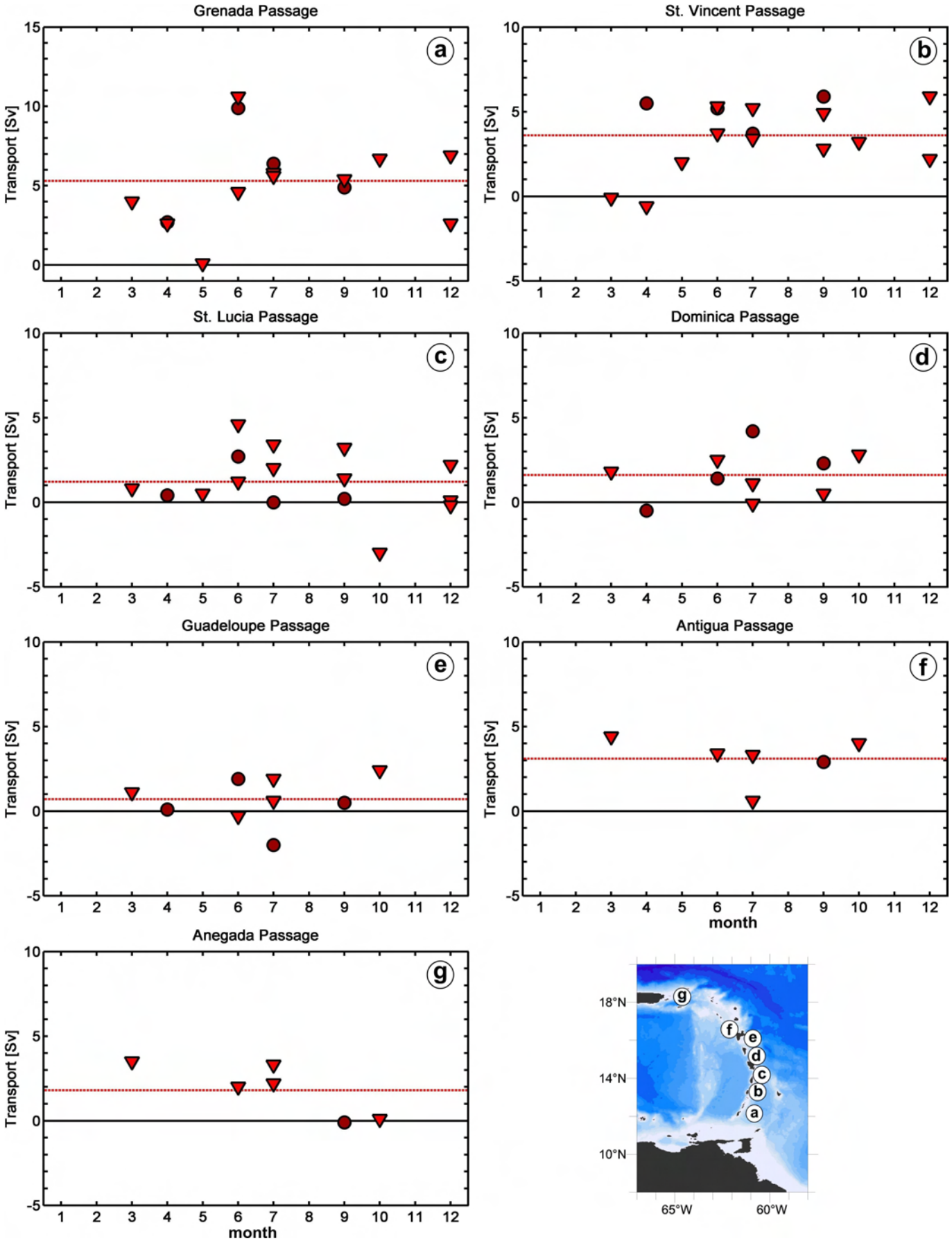

Figure 4.1: Transports (in Sv) through the Lesser Antilles Passages, derived from velocity observations. The transports are plotted against the month of observation. Triangles: transports from Johns et al., 2002; circles: transports obtained from cruises carried out by the University of Bremen (see Chap. 3); dashed line: mean value. The small map illustrates the passage locations. Note the different scale for Grenada Passage.

4.2 Modeled inflow

The high resolution in FLAME provides four grid points in the smallest passage (St. Lucia Passage *c*), which is only one less than CTD stations carried out there. The other passages possess a higher resolution. Of course, the vertical resolution is much coarser in the model (cf. Chapter 3). In the FLAME_CLIM run, where only a mean wind field forcing was applied, the monthly mean velocity fields are analyzed. The runs with variable wind forcing (FLAME_INTER) includes high frequency variability such as eddies and waves. As the discussion in this section attends the mean inflow, the FLAME_INTER data was averaged: from a 15-year time series, the mean inflow for every month was calculated.

In Figure 4.2 the monthly mean transport for every passage is illustrated from both FLAME_CLIM (blue) and FLAME_INTER (black). The shading around the FLAME_INTER results marks the doubled standard deviation. The annual means are marked by the dotted lines and the observations from Fig. 4.1 are included again for comparison. The FLAME_CLIM run shows larger variability than FLAME_INTER, but stays mostly within the doubled standard deviation of the FLAME_INTER mean. As a typical example serves St. Lucia Passage (*c*): Here, the overall variability in FLAME_CLIM is 5 Sv, compared to 2 Sv in FLAME_INTER, and the FLAME_CLIM transports mostly stay within the shaded area around the FLAME_INTER transports. The mean transport through the two southernmost passages (Grenada and St. Vincent, *a* and *b*) is larger in FLAME_INTER, but in all other passages the FLAME_CLIM run exhibits stronger inflow. The agreement of both runs in the total inflow into the Caribbean through the passages from Anegada to Grenada is excellent (Fig. 4.2 *h*). The observed mean inflow is indicated by the thin red dashed line; the modeled transport is about 2 Sv higher (a detailed comparison follows in the next section).

A seasonal cycle in the model also can hardly be identified. While FLAME_CLIM finds a more or less ambiguous cycle in Grenada Passage (the interpretation strongly depends on the low inflow in October), the FLAME_INTER run clearly provides a high inflow season during May-July and a minimum season from October to December. This does not correspond to the seasonal cycle of the NBC retroflection, which is at its maximum in boreal fall (Garzoli et al., 2004). The only indisputable seasonal cycle in FLAME_CLIM occurs in Anegada Passage (Fig. 4.2 *g*), but this is totally absent in FLAME_INTER, i.e. the model runs dissent from each other on this topic. In the other passages smaller amplitudes occur (especially in FLAME_INTER) and both model runs do not support any cycle. For the total inflow through all passages both runs agree in a high transport season during early summer (May-July) and minimum inflow from November to February.

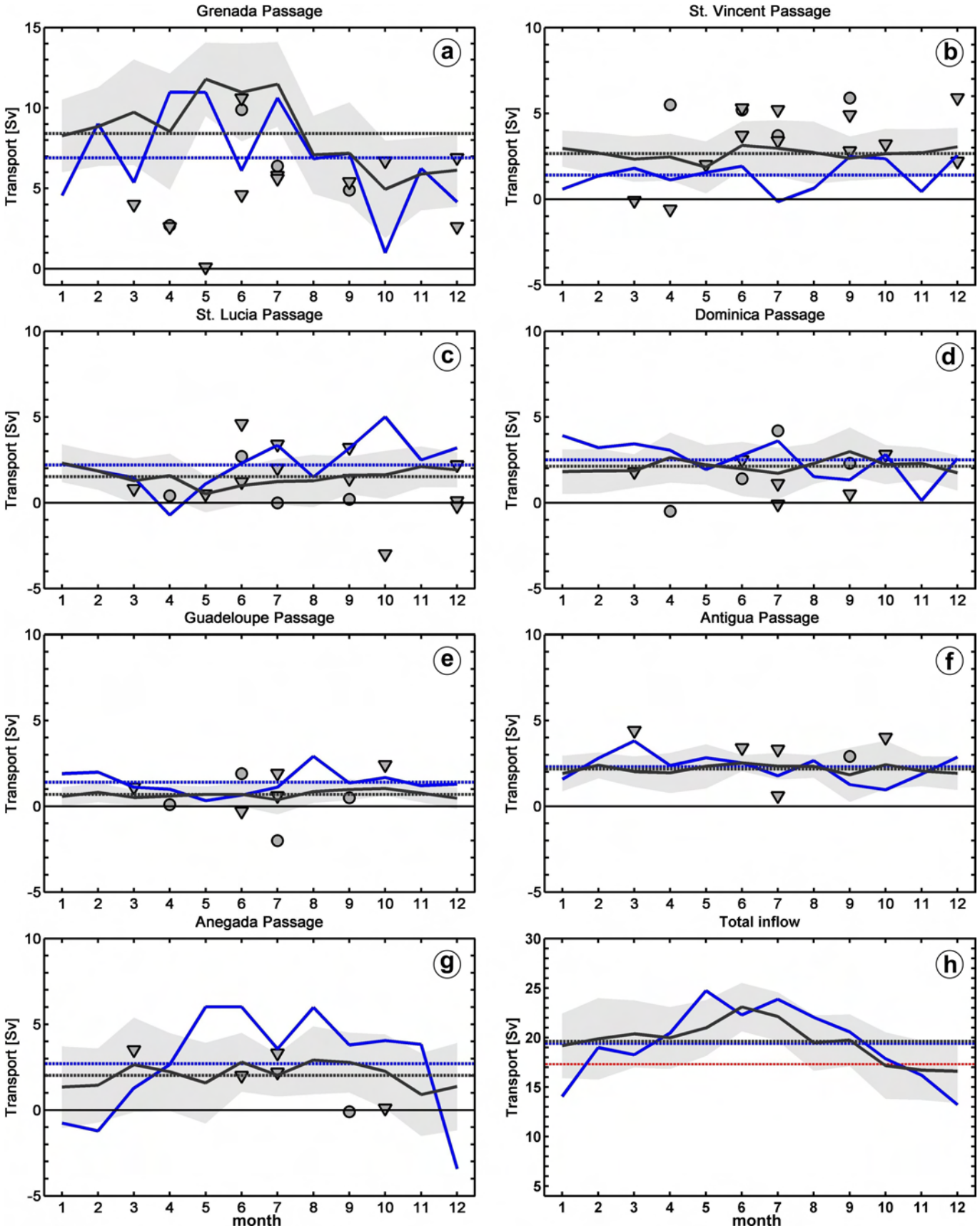

Figure 4.2: Monthly mean transports (in Sv) through the Lesser Antilles Passages, derived from the FLAME model. The transports are plotted against the month. Blue: monthly means from the climatological run (FLAME_CLIM); grey: monthly means from the 15-year time series in FLAME_INTER, the shading borders the doubled standard deviation; dashed lines: mean values. The grey markers repeat the transports from Figure 4.2. The thin red dashed line in the last subfigure (h) represents the mean observed total inflow from Table 4.1. Note the different scales for Grenada Passage (a) and the total inflow (h).

Total inflow: Observations vs. model

The mean transports through the Lesser Antilles Passages are given in Table 4.1 for the observations and both model runs. The standard deviations are large, sometimes larger than the mean itself (eg. Guadeloupe Passage in observations, Anegada Passage in FLAME). The large range of variability was evident as well in Figures 4.1 and 4.2. One should remember that observations in winter are sparse or even missing; and few repeats were carried out in some passages. Some disagreements between the results from observations and model may be due to this circumstances, as well as raise the standard deviation. The standard errors are always smaller than the means. The magnitude of the standard error strongly depends on the number of measurements/model values (n), hence the low error for the FLAME_INTER run (n=*180*), and contains no further physical information. Thus only the standard deviation is discussed further.

	observations	FLAME_CLIM	FLAME_INTER
Grenada	5.3 ±2.8 (0.8)	6.9 ±3.1 (0.9)	8.4 ±3.4 (0.3)
St. Vincent	3.6 ±2.0 (0.5)	1.4 ±0.9 (0.3)	2.7 ±1.4 (0.1)
St. Lucia	1.2 ±1.8 (0.5)	2.2 ±1.4 (0.4)	1.5 ±1.3 (0.1)
Dominica	1.6 ±1.4 (0.5)	2.5 ±1.1 (0.3)	2.1 ±1.3 (0.1)
Guadeloupe	0.7 ±1.4 (0.5)	1.4 ±0.7 (0.2)	0.7 ±0.6 (0.1)
Antigua	3.1 ±1.3 (0.6)	2.3 ±0.8 (0.2)	2.2 ±1.0 (0.1)
Anegada	1.8 ±1.5 (0.7)	2.7 ±3.1 (0.9)	2.0 ±2.2 (0.2)
total	17.3 ±4.8 (1.5)	19.4 ±4.9 (1.4)	19.6 ±4.8 (0.4)

Table 4.1: Mean inflow into the Caribbean (in Sv) through the Lesser Antilles passages with standard deviation and standard error in parenthesis. Observations vs. both model runs, all data presented in Figures 4.1 and 4.2 were used.

The mean model transports exceed the mean observed transports in all passages except St. Vincent and Antigua. The transports are strongest through Grenada Passage and weakest through Guadeloupe Passage in both model and observations. Both model runs exhibit noticeably larger transports through Grenada Passage than observed. This stronger inflow is partly compensated by smaller inflow through St. Vincent Passage. The differences occurring in these two passages might result from the somewhat simplified topography representation in the model; Grenada Passage throughflow is favored over St. Vincent Passage flow in the model. The total transport into the Caribbean Sea in the FLAME experiments match roughly the observed inflow. The model exhibits about 2 Sv stronger inflow than observed, but this lies within the standard deviation of nearly 5 Sv. Despite the differences in some details FLAME_CLIM and FLAME_INTER yield remarkably similar inflows (19.4 Sv ± 4.9 Sv vs. 19.6 Sv ± 4.8 Sv respectively, see Table 4.1). The climatological run can thus be considered representative of the model. Both model runs show a reasonable agreement with the observed inflow. Johns et al. (2002) found from observations a mean inflow through the Lesser Antilles passages of 18.4 Sv ± 4.7 Sv. This number is now renewed, as more ship cruises were carried out, which complement

the data set. Adding the new information, the inflow is slightly smaller at 17.3 Sv ± 4.8 Sv (Table 4.1). The model of Johns et al. (2002) with a $\frac{1}{3}^{\circ}$ resolution and 6 vertical layers showed an inflow of 21.7 Sv, while less inflow of 19.4 Sv to 19.6 Sv is found in FLAME, which is somewhat closer to the observations.

SAW fractions

The SAW fractions of the inflow were calculated by the temperature and salinity properties measured in the passages (the analysis was described in Chapter 3). Since the measurements used in Johns et al. (2002) were not available for further evaluations, the ship derived dataset is now reduced to the measurements done by the University of Bremen (Table 3.1).

Presented in Figure 4.3 is the SAW distribution versus depth from Tobago to Puerto Rico from observations and both model runs. The figure depicts the island arc from south to north, as indicated by the arrows on the small map. The horizontal scale of Anegada Passage is compressed by 50%. The top (*a*) gives the SAW distribution from September 2005 during the cruise M66/1; the other two (*b* and *c*) show the SAW distribution in the model. In Figure 4.3 *b* the annual mean from FLAME_CLIM is shown, while *c* gives the Mid-September 2005 distribution in FLAME_INTER (three day mean). The topography in Figure 4.3 *a* was derived from echosounder data, in *b* and *c* from the model grid. The model topography is smoother and exhibits less details. But as it is evident in the figure, all passages can be clearly identified.

The observed SAW distribution from September 2005 was taken here as a representative of all observations. The passages north of Guadeloupe were only surveyed during this one cruise. All observation agree in the general features (Rhein et al., 2005 and Kirchner et al., 2007) for the passages south of Guadeloupe, which are:

- SAW is dominant in the IW ($\sigma_\Theta = 27.1 - 27.6\ kgm^{-3}$) and LCW ($\sigma_\Theta = 26.8 - 27.1\ kgm^{-3}$) south of Guadeloupe
- SAW fractions are below 20% in SMW ($\sigma_\Theta = 24.5 - 26.3\ kgm^{-3}$) and UCW ($\sigma_\Theta = 26.3 - 26.8\ kgm^{-3}$) north of St. Vincent, but can show disturbances with higher SAW influence
- SAW fractions are highest in Grenada Passage, decreasing northwards

The one survey in Antigua Passages confirms the assumption that the SAW fractions decrease continuously when going further north, but the IW still shows high South Atlantic contribution. The SAW signal is significantly lower in the Anegada Passage, where even the mean SAW fraction in IW drops below 25%. Considering the entire passage, the mean SAW fractions observed in September 2005 are less than 15% in Anegada passage. The SAW influence increases when going southward to a portion of nearly 50% in Grenada passage. It is evident from Figure 4.3 *b* and *c*, that the SAW fractions in the model are higher in the IW, especially in FLAME_INTER, and lower in the UCW than observed.

The whole modeled SAW distribution is smoother, which is probably an effect of the averaging and the low vertical resolution (model vs. CTD data).

passage	observations	FLAME_CLIM	FLAME_INTER
Grenada	48% ± 16%	42% ± 2%	60% ± 6%
St. Vincent	44% ± 18%	41% ± 5%	58% ± 7%
St. Lucia	42% ± 16%	35% ± 4%	52% ± 7%
Dominica	31% ± 18%	26% ± 3%	36% ± 6%
Guadeloupe	28% ± 18%	16% ± 4%	24% ± 4%

Table 4.2: Mean South Atlantic Water fractions for $\sigma_\theta = 24.5 - 27.6\ kgm^{-3}$ for each passage, with standard deviation.

The mean SAW fractions for all passages, which were monitored repeatedly, are given in Table 4.2, with standard deviation. The high standard deviation for the SAW fractions obtained by observations is due to the limited number of measurements. Clearly, the influence of SAW decreases with higher latitudes, and the southern passages (Grenada, St. Vincent and St. Lucia) are expected to govern the SAW inflow. Divided by layers, the highest SAW fractions are found in the deeper layers, IW: 53%, LCW: 45% compared to UCW: 22%, SMW: 20%. The variation of this mean layer percentages during the four cruises are largest in the SMW layer: here, fractions between 17% and 35% occur. In the UCW layer the fractions are between 15%-27%, while in the layer below the variability decreases: the range is only 44%-53% in the LCW and 56%-59% in the IW.

Mean SAW fractions in Guadeloupe passage are only 16% in FLAME_CLIM and 24% in FLAME_INTER, which is both less than obtained from the observations, but within the standard deviation of the observed fractions. Antigua Passage differs as well (cf. Figure 4.3), the reason for this discrepancies is most likely the smoothed model topography, erasing the passages below approx. 450 m depth. The FLAME_CLIM fractions stays below the observed fractions in all passages, but the difference is less than 10% in the passages south of Martinique. In contrast, FLAME_INTER produces stronger SAW influence, the fractions are more than 10% higher than observed in St. Lucia, St. Vincent and Grenada Passage. This discrepancy is a consequence of the higher SAW fractions in IW and LCW in the model: 68% and 55% in FLAME_INTER vs. 53% and 45% observed. The climatological run agrees on high fractions in the IW (62%), but shows smaller fractions for the LCW: only 29%. The upper layers are thin and thus less important for the mean SAW fractions. During FLAME_INTER the model indicates 12% SAW in the UCW and 42% in the SMW (FLAME_CLIM gives UCW: 7%, SMW: 44%).

The low SAW fraction in UCW in the model are in good agreement with the older findings by Schmitz and Richardson (1991). The UCW layer used here corresponds roughly to their 12°-24°C water, in which the authors presume only 5% SAW in the Florida Current, as nearly all volume of this water mass is assumed to recirculate into the North Equatorial Undercurrent. This SAW loss by retroflection seems to be higher in the model (both experiments) than in the observations.

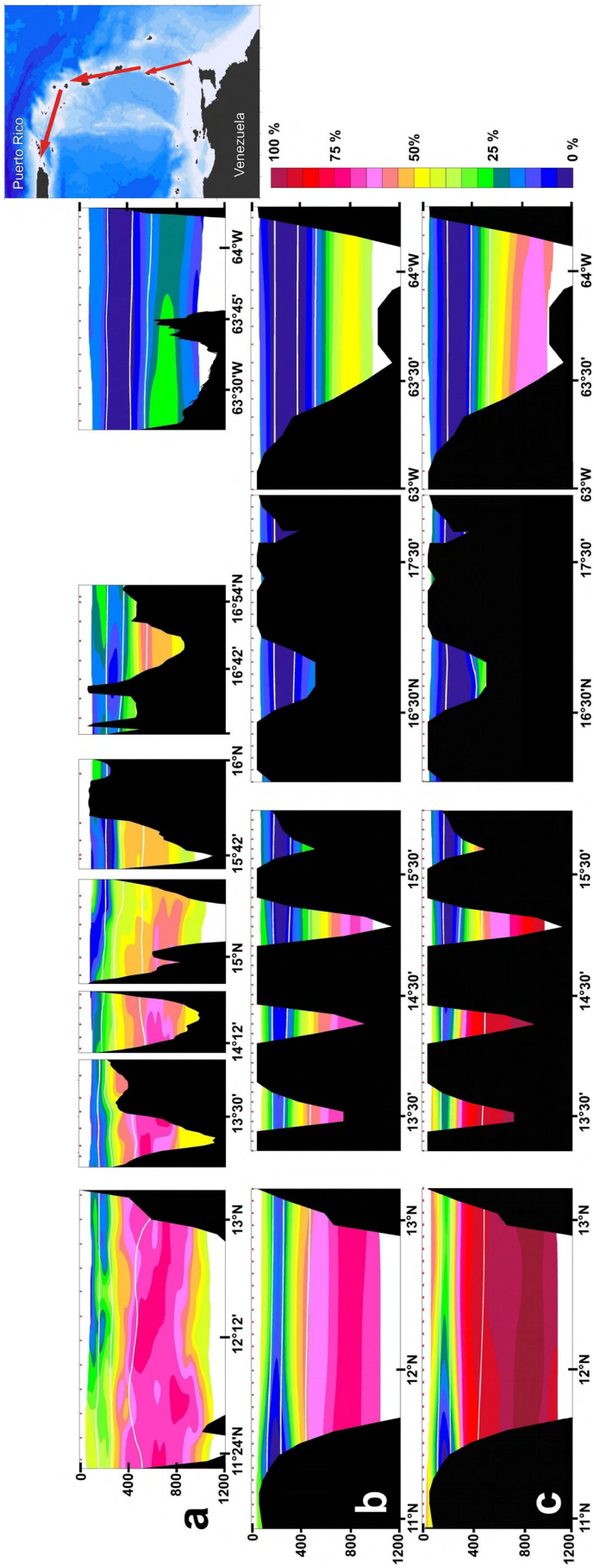

Figure 4.3: South Atlantic Water distribution (in %), shown from Tobago on the left going northward to Puerto Rico (cf. Figure 2.2). (a): SAW distribution, derived from observations in September 2000; (b): annual mean SAW distribution in FLAME_CLIM; and (c) in September 2005 in FLAME_INTER. The white isopycnals, separating the water masses, are 24.5 kgm^{-3}, 26.3 kgm^{-3}, 26.8 kgm^{-3}, 27.1 kgm^{-3}, 27.6 kgm^{-3}.

SAW transports

Relating the passage transports to SAW fractions yields SAW transports into the Caribbean. The calculated mean SAW transports through the passages south of Guadeloupe are summarized in Table 4.3 for the observations and in Tables 4.4 and 4.5 for the model. A detailed comparison of the observations with the FLAME_CLIM run for the summer month (April-September) was published in Kirchner et al. (2007), as all observations were carried out during this time of the year. In this study the agreement between the model and the observations were found to be convincing. The annual mean from the FLAME_CLIM model run is presented here. The complete 15-year time series was used to obtain the mean inflow in the FLAME_INTER run. South of Guadeloupe, the surface water lighter than $\sigma_\theta = 24.5\ kgm^{-3}$ was assumed to be of southern hemispheric origin entirely, while transports of water denser than $\sigma_\theta = 27.6\ kgm^{-3}$ were presumed to be purely from the North Atlantic (cf. Chapter 3).

The SAW transports through the northern passages Guadeloupe, Dominica and St. Lucia in the observations and the model are likewise low. The sum over this three passages for all layers is 1.3 Sv in the observations, 2.2 Sv in FLAME_CLIM and 1.7 Sv in FLAME_INTER. Although the modeled transports are slightly higher than the ones observed, the two southern passages, St. Vincent and Grenada, are most important in both model runs and observations.

The combined SAW flow through the two southern passages St. Vincent and Grenada is large (compared to the other passages) and of similar strength in the observations and FLAME_INTER (7.3 Sv vs. 8.5 Sv). FLAME_CLIM differs significantly, only 5.5 Sv are transported through the two passages in the annual mean. When only the summer months are considered (April-September, see Kirchner et al., 2007), the Grenada Passage SAW transport in FLAME_CLIM increases to 6.4 Sv (from 5.0 Sv annual mean), which together with St. Vincent passage results in 7.2 Sv, and matches almost exactly the observed inflow. The low Grenada inflow in the annual mean is a consequence of the weak inflow in October in FLAME_CLIM (cf Fig.4.2).

The most important difference between the observations and the model is the distribution of the inflow through the two southern passages: While St. Vincent and Grenada passages are of similar relevance in the observations, only a small proportion of the inflow occurs through St. Vincent passage in the model (both runs); Grenada passage is the key-gateway for the modeled inflow and especially the surface layers dominate the transport. The different model topography might be the reason for this finding.

The SAW transports, derived by observations, add up to a total inflow of 8.4 $\pm$ 2.4 Sv into the Caribbean south of Guadeloupe. FLAME_CLIM provides an SAW inflow of 7.6 $\pm$ 2.3 Sv in the annual mean and of 8.5 $\pm$ 1.7 Sv for the month April-September (Kirchner et al., 2007). In FLAME_INTER the total SAW transport into the Caribbean south of Guadeloupe sums up to 10.2 $\pm$ 1.6 Sv. The mean transports through St. Vincent and Grenada Passage are higher than in FLAME_CLIM. In this experiment, the transports in

summer are stronger than during the winter month as well. Thus, the included interannual variability in the forcing intensifies the SAW transport.

The apparent differences in the details between model and observations are perspicuous and not surprising. Since model experiments are still restricted in complexity by computer power, machine time and unknown input parameters. The outright agreement between the mean observed (total) SAW inflow and the modeled result for the same months is therefore formidable.

For Antigua and Anegada passages only a single ship survey with hydrographic data was available. The SAW inflow through these passages is small, zero in Anegada Passage and 0.6 Sv in Antigua Passage, when the surface flow is neglected (cf. Chapter 3). In the model, Antigua Passage yields 0.1 Sv SAW inflow and Anegada Passage 0.4 Sv inflow in the annual mean for FLAME_CLIM. Again, the transports from FLAME_INTER are higher, 0.2 Sv in Antigua and 0.7 Sv in Anegada Passage. The low transports through Antigua Passage in the model originated from the model topography: the passage is very shallow and does not contain any IW (the only water mass, where the SAW fractions are still high). Anegada Passage is in contrast wide and deep and the IW contributes to the inflow. These transports are nevertheless of minor impact for the total SAW inflow into the Caribbean, since the currents are weak in this layer and outflow occurs occasionally.

	observations		
	TSW + SMW	CW	IW
Grenada	2.1 ± 0.4 (0.2)	1.0 ± 0.6 (0.3)	0.6 ± 1.5 (0.7)
St. Vincent	2.8 ± 0.9 (0.5)	0.6 ± 0.3 (0.1)	0.2 ± 0.5 (0.3)
St. Lucia	0.8 ± 0.4 (0.2)	0.0 ± 0.2 (0.1)	-0.2 ± 0.3 (0.2)
Dominica	0.2 ± 1.1 (0.6)	0.2 ± 0.1 (0.1)	0.2 ± 0.4 (0.2)
Guadeloupe	0.1 ± 0.5 (0.3)	0.1 ± 0.2 (0.1)	-0.1 ± 0.1 (0.1)
total	6.0 ± 1.6 (0.4)	1.7 ± 0.7 (0.3)	0.7 ± 1.6 (0.9)

Table 4.3: Mean SAW inflow into the Caribbean (in Sv) through the passages south of Guadeloupe during our observations. The standard deviation is given, as well as the standard error in parenthesis. The columns refer to the water masses from the surface to $\sigma_\theta = 27.6\ kgm^{-3}$ (see Chapter 2). TSW: Tropical Surface Water, SMW: Salinity Maximum Water, CW: Central Water, IW: Intermediate Water. Differences to the total are due to rounding.

	FLAME_CLIM		
	TSW + SMW	CW	IW
Grenada	4.3 ± 2.0 (0.6)	0.5 ± 0.2 (0.1)	0.3 ± 0.2 (0.1)
St. Vincent	-0.1 ± 0.6 (0.2)	0.3 ± 0.1 (0.1)	0.3 ± 0.1 (0.1)
St. Lucia	0.1 ± 0.6 (0.2)	0.2 ± 0.1 (0.1)	0.7 ± 0.2 (0.1)
Dominica	0.4 ± 0.3 (0.1)	0.1 ± 0.1 (0.1)	0.2 ± 0.2 (0.2)
Guadeloupe	0.4 ± 0.5 (0.2)	0.1 ± 0.1 (0.1)	0.0 ± 0.0
total	5.1 ± 2.3 (1.0)	1.1 ± 0.3 (0.1)	1.4 ± 0.3 (0.1)

Table 4.4: Same as Table 4.3, but for the model run FLAME_CLIM (annual mean).

	FLAME_INTER		
	TSW + SMW	CW	IW
Grenada	5.3 ± 2.3 (0.2)	1.1 ± 0.7 (0.1)	0.4 ± 0.3 (0.1)
St. Vincent	0.3 ± 0.8 (0.1)	0.6 ± 0.3 (0.1)	0.8 ± 0.3 (0.1)
St. Lucia	0.0 ± 0.6 (0.1)	0.3 ± 0.3 (0.1)	0.4 ± 0.3 (0.1)
Dominica	0.1 ± 0.6 (0.1)	0.3 ± 0.2 (0.1)	0.4 ± 0.3 (0.1)
Guadeloupe	0.2 ± 0.4 (0.1)	0.0 ± 0.0 (0.1)	0.0 ± 0.0
total	5.9 ± 2.6 (1.2)	2.3 ± 0.8 (0.4)	2.0 ± 0.6 (0.3)

Table 4.5: Same as Table 4.3, but for the model run FLAME_INTER (15-year mean).

4.3 Inflow variability in Grenada Passage

It has been shown before, that Grenada Passage is the most important passage for the Caribbean SAW inflow (cf. Table 4.5). Since the observations are sparse, the FLAME model is used for an investigation of the inflow variability. A 15-year time series from Grenada Passage, obtained from the FLAME_INTER model run, is presented in Figure 4.4. The time series starts in 1990 and ends in 2005, used are the monthly mean transports. It is obvious, that the SAW transports follow the total transport closely, but is always less strong.

A discrete fourier transformation (DFT) of the transport through Grenada Passage shows that the spectral energy of the time series peaks at the frequency of 0.083 $month^{-1}$. That means, one cycle is performed during 12 month at this frequency, thus the seasonal cycle is represented. The power spectra for the total transport and the SAW transport are given in Figure 4.5. The spectral energy density peaks for the SAW time series at the same frequency (0.083 $month^{-1}$) as for the total transport time series, but offers less spectral energy. The power spectra show, that other frequencies are of no significance in the time series.

The impact of the seasonal cycle on the transport through Grenada Passage was evaluated by computing the harmonic constituents of the Fourier series. For the specified periods, which are the one year period (as the most important one obtained by the DFT) and the half year period besides, the amplitude and phase of the harmonic functions were calculated. In Figures 4.6 and 4.7 the harmonic functions are overlying the time series of Figure 4.4. In the one year seasonal cycle, the maximum inflow occurs in May and the minimum in November. The amplitude of the one-year oscillation is 2.7 Sv for the total inflow and 2.3 Sv for the SAW portion. The magnitude of the seasonal cycle agrees with the model study by Johns et al. (2002), where the authors have found a seasonal amplitude of 3 Sv in the Grenada Passage transport. However, the overall variability is noticeably higher in FLAME than in their low-resolution model and the seasonal cycle can only explain parts of the occurring transport variation. The half-year cycle peaks in January and July, minima occur in April and October. This period has an impact of less than 1 Sv and is thus as expected of only minor importance for the transport time series. Grenada Passage is as well influenced by shorter frequencies, on the time scales of 1-3 month.

Taking a closer look at the transports through Grenada Passage, variability on shorter time scales dominates and masks the seasonal signal. Figure 4.8 shows the years 2003 to 2004 with 3-day mean transports. Here, the seasonal cycle is not detectable due to the superimposed high frequency variability. The DFT gives high spectral energy at 55, 80, 103 and 48 days (figure 4.9). None of these frequencies produced a harmonic function with significant amplitude; the 2-year time series consists of too many components. Some of these frequencies correspond to the NBC ring shedding frequency (periods of 70-40 days), other can be produced as a result of the rings interacting with the island topography. Since

the NBC rings probably have much impact on the inflow signal during the observations as well, it is not surprising that the observed data shows varying situations in the different years and the seasonal cycle was found to be undetectable yet.

The analysis of the time series for Grenada Passage in FLAME_CLIM demonstrated very well, that the influences of the seasonal cycle can only be detected on long time series. The inability to detect a seasonal cycle in the observations can hence be easily attributed to the inadequate quantity of data (see above). A DFT applied to the FLAME_INTER inflow time series of the other passages reveal no distinct maximum in spectral energy, even at the seasonal frequency. A seasonal cycle in Anegada Passage is absent, in contrast to the indication from FLAME_CLIM. A relevant seasonal cycle is evident only in Grenada Passage, no other passage shows this behavior.

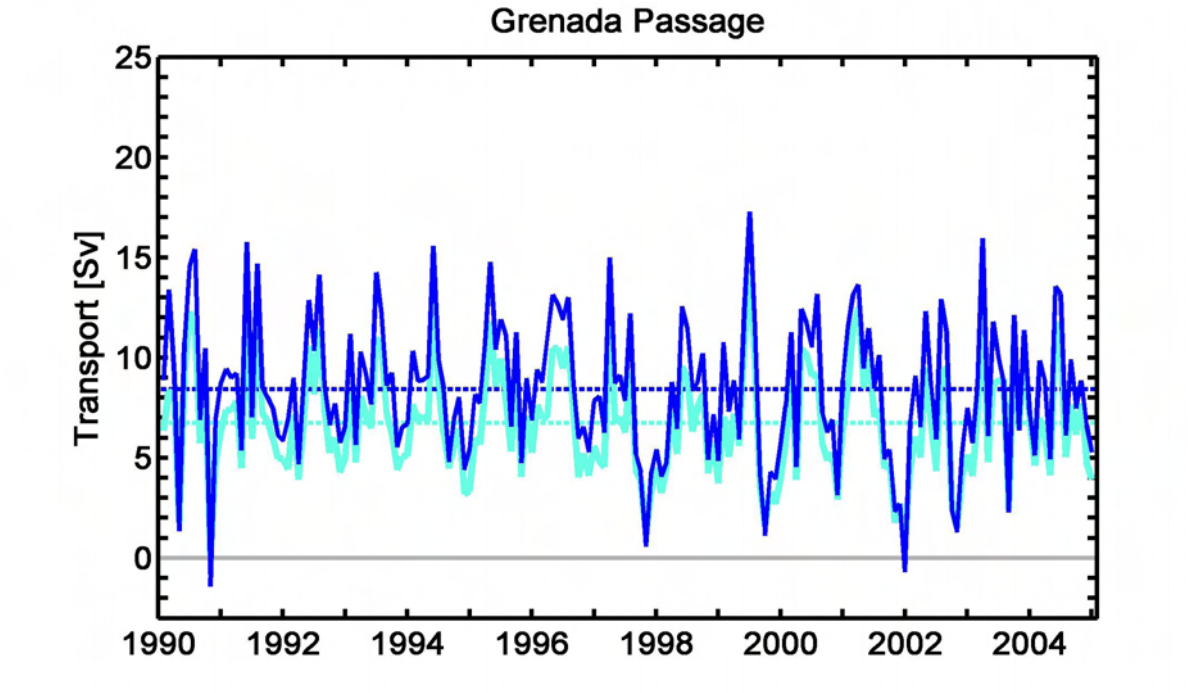

Figure 4.4: Transports (in Sv) in Grenada Passage for a 15-year timeseries from FLAME_INTER (1990-2005); monthly means. Dark blue: total transport; cyan: SAW transport; dashed: mean value

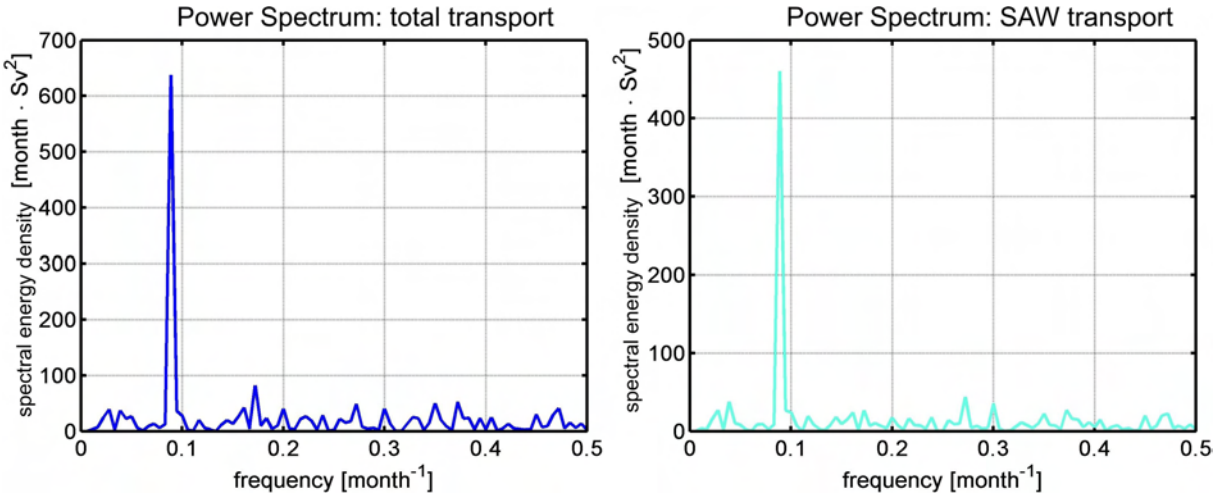

Figure 4.5: Power Spectra for the time series in Figure 4.4. left: spectrum for the total transport time series; right: spectrum for the SAW transport time series

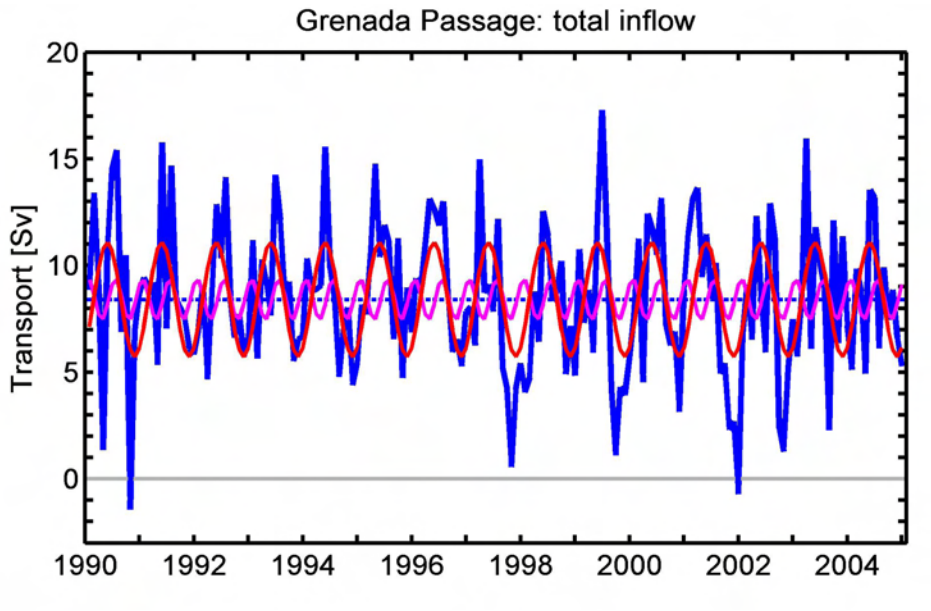

Figure 4.6: Transport timeseries (total inflow) from Fig. 4.4 with seasonal cycle in red and half-year cycle in magenta.

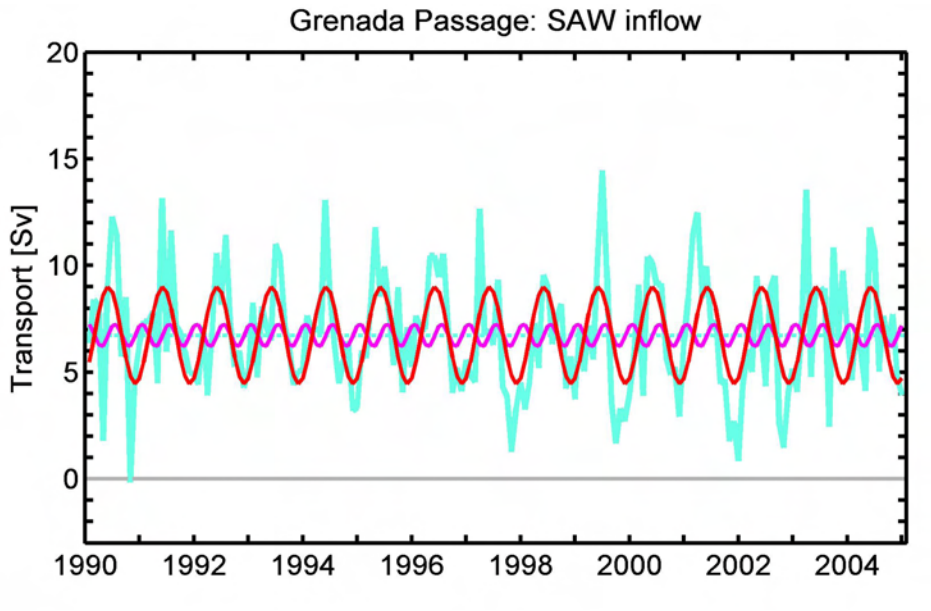

Figure 4.7: Transport timeseries (SAW inflow) from Fig. 4.4 with seasonal cycle in red and half-year cycle in magenta.

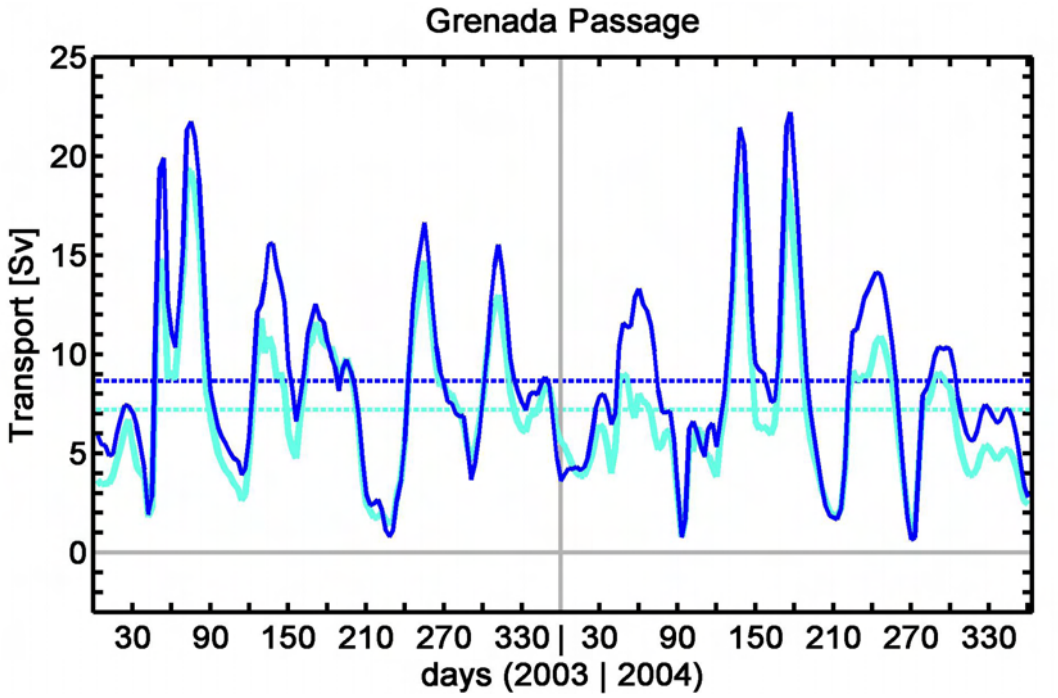

Figure 4.8: Transports (in Sv) in Grenada Passage for a 2-year timeseries from FLAME_INTER (2003-2004); 3-day means. Dark blue: total transport; cyan: SAW transport; dashed: mean value

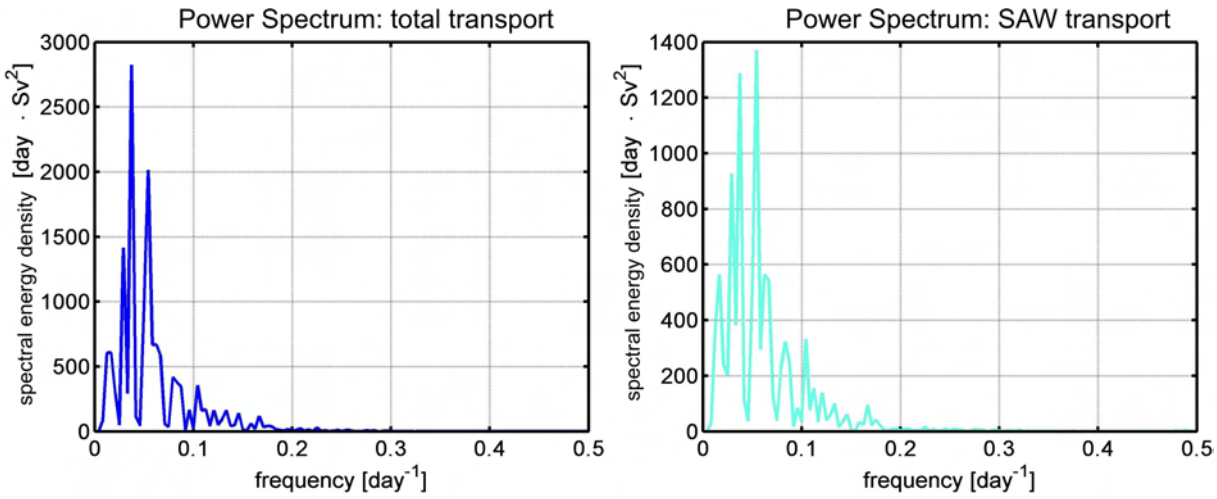

Figure 4.9: Power Spectra for the time series in Figure 4.8. left: spectrum for the total transport time series; right: spectrum for the SAW transport time series

5 South Atlantic Water transport by NBC rings

The transport of South Atlantic Water into the North Atlantic is not restricted to the Caribbean Passages, but also proceeds east of the Lesser Antilles in the Atlantic. During the ship cruises no permanent northward flow was found at 16°N, but pronounced NBC rings were observed (see Chapter 2). On all five surveys remarkably well structured rings were identified. These rings contribute substantially to the upper limb return flow of the MOC by carrying South Atlantic Water into the northern subtropical gyre. The FLAME model produces anticyclonic rings at the NBC retroflection, which propagate along the western boundary towards the Caribbean. When the rings reach the shallow topography of the Lesser Antilles, they are trapped by the island of Barbados and interact with the island chain. The ring transports, their shape and structure, and their interaction with the Lesser Antilles are discussed in this Chapter. The model is used to complement the understanding of the observed rings at 16°N.

5.1 Impact of NBC rings observed at 16°N

The SAW fractions and the transports across 16°N were found to be dominated by anticyclonic rings (Rhein et al., 2005). These rings are formed at the western boundary of the tropical North Atlantic, where the NBC retroflects into the North Equatorial Countercurrent. After separating from the retroflection region, the rings travel northwestward along the Brazilian coast (Johns et al., 1990). Their relevance for the northward transport of South Atlantic Water clearly depends on the frequency of their generation as well as on their horizontal and vertical structure.

The anticyclonic rings effect the layer-thickness of the water masses by thickening the density layers where the ring core is situated. This implies for surface intensified rings that they possess an accumulation of TSW in their center. As a result a positive sea surface height anomaly shows up, thus marking the rings in satellite altimetry measurements (Goni and Johns, 2003). In consequence, the layers below are depressed and the isopycnals show a downward slope. For subsurface rings, the behavior is similar below the core (depression in isopycnals), while the isopycnals above the core show a doming. Nevertheless, the effect on the sea level above a subsurface ring is rather small, and it cannot be traced by sea surface height measurements anymore. During the surveys the structure of the rings encountered varied in shape and distinctiveness, but on every cruise one ring could be identified and its transport calculated. The measurements at 16°N revealed surface as well as subsurface intensified rings, correlated with high SAW fractions especially in the LCW and IW layers, and are in detail examined for each cruise now.

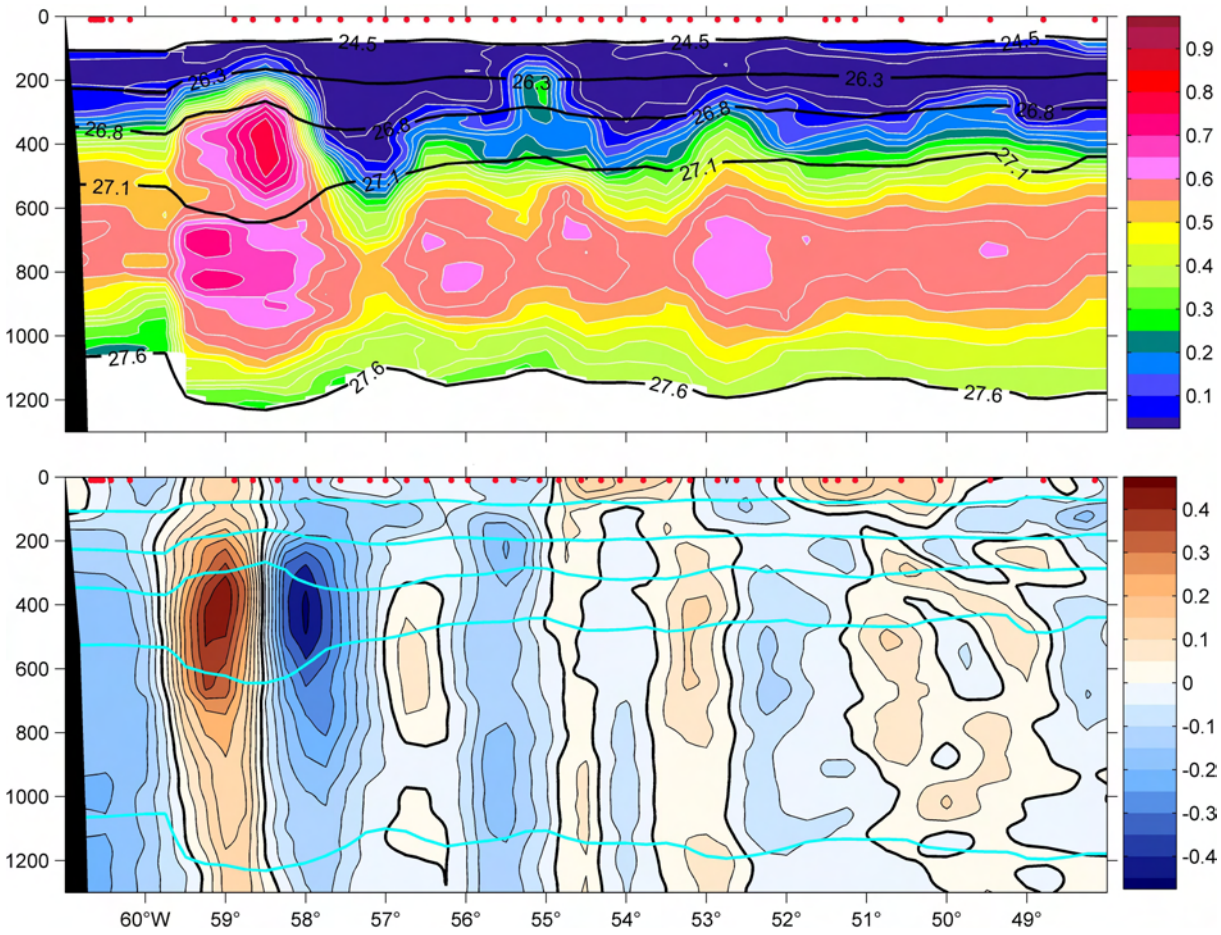

Figure 5.1: SAW fractions in % (top) and meridional current velocity in ms^{-1} (bottom) at 16°N, eastward off Guadeloupe in December 2000. The current velocities were obtained by ADCP measurements. Positive velocities (red) indicate northward flow, negative (blue) southward flow across the section. The isopycnals (black in the upper figure, cyan in the lower), separating the water masses, are 24.4 kgm^{-3}, 26.3 kgm^{-3}, 26.8 kgm^{-3}, 27.1 kgm^{-3} and 27.6 kgm^{-3}. The red dots on top of the figures mark the CTD stations, where measurements were performed.

Rings during S 152 (December 2000)

The SAW fractions and the meridional velocity field observed in December 2000 are presented in Figure 5.1. The SAW distribution and the velocity measurements indicate a subsurface ring centered at 58.5°W. The SAW distribution shows a sphere of high SAW fractions in LCW (>80%). The isopycnals shape around this core. In the velocity field the ring can be clearly identified as anticyclonic and subsurface intensified. The velocity maximum was found at 400 m depth, which fits well with the concentrated SAW sphere. The ring is restricted to 59.8°W and 57.3°W, which agrees best with the velocity structure of the ring, yielding a diameter of 267 km. The depth range covered by the ring is 200 m to 1150 m. The mean SAW fractions there are 14% in UCW, 39% in LCW and 34% in IW. Assuming a cylindrical shape, the ring volume is $5.3 \cdot 10^{13}$ m^3, of which $1.7 \cdot 10^{13}$ m^3 are SAW, resulting in a SAW transport of 0.5 Sv. East of 57°W, ring-like features re-appear. In the IW deformed spheres of high SAW fractions recur (>60%). The velocity behaves appropriately, alternating between weak positive and negative flow (< 15 cms^{-1}).

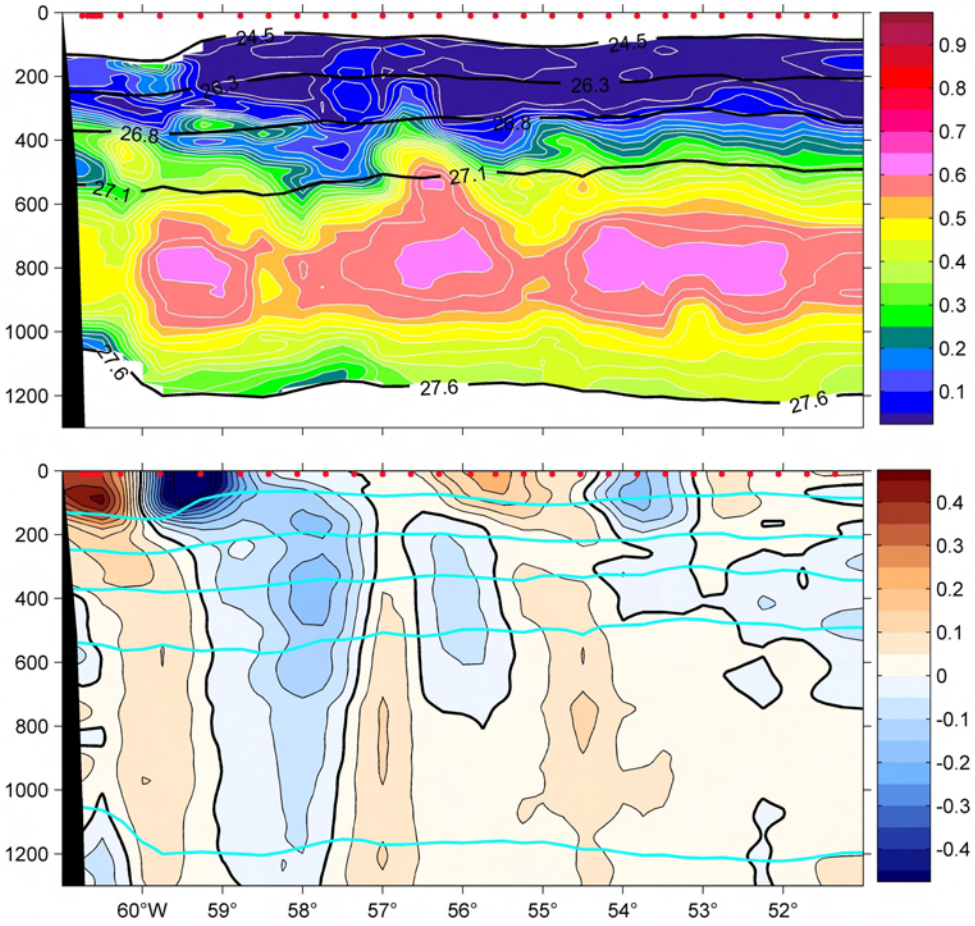

Figure 5.2: SAW fractions in % (top) and meridional current velocity in ms^{-1} (bottom) at 16°N, as in Figure 5.1, for June 2002. The scaling was adjusted to Figure 5.1 as well and the figure is aligned to the left, indicating the repeated part (the eastward extend) of the 16°N section during this cruise.

Rings observed during cruise M 53/3 (June 2002)

Measurements during June 2002 were implemented on a surface intensified ring close to the western boundary of the section. This time the ring is clearly detectable in the velocity field, and its imprint on the SAW distribution is only somewhat visible in the IW. The ring was located between the longitudes 60.5°W and 57.5°W, which yields a diameter of 320 km. The depth range covered by the ring is from the surface to 1150 m, with the strongest velocities occurring in the TSW and only weak currents in the deeper layers. Only the isopycnal 24.5 kgm^{-3} is thus noticeably depressed, the impact of the ring on the deeper density surfaces is small. The ring-center is situated at 60°W in the surface layer and at 59°W below 300 m depth. This points to a deformed ring. The mean SAW fractions are 6% in SMW, 8% in UCW, 22% in LCW and 36% in IW. The cylindrical ring volume is $9.2 \cdot 10^{13}$ m^3, of which $3.1 \cdot 10^{13}$ m^3 are SAW, which yields a SAW transport of 1 Sv. Further east, another shallow ring-shaped feature occurs near the surface (56°W-53°W) in the velocity distribution. The shape is confined to the upper layers (TSW and SMW). In the SAW fractions two other high SAW cores are noticeable in the IW, one of them extending into a high SAW event in the LCW (at 56.5°W).

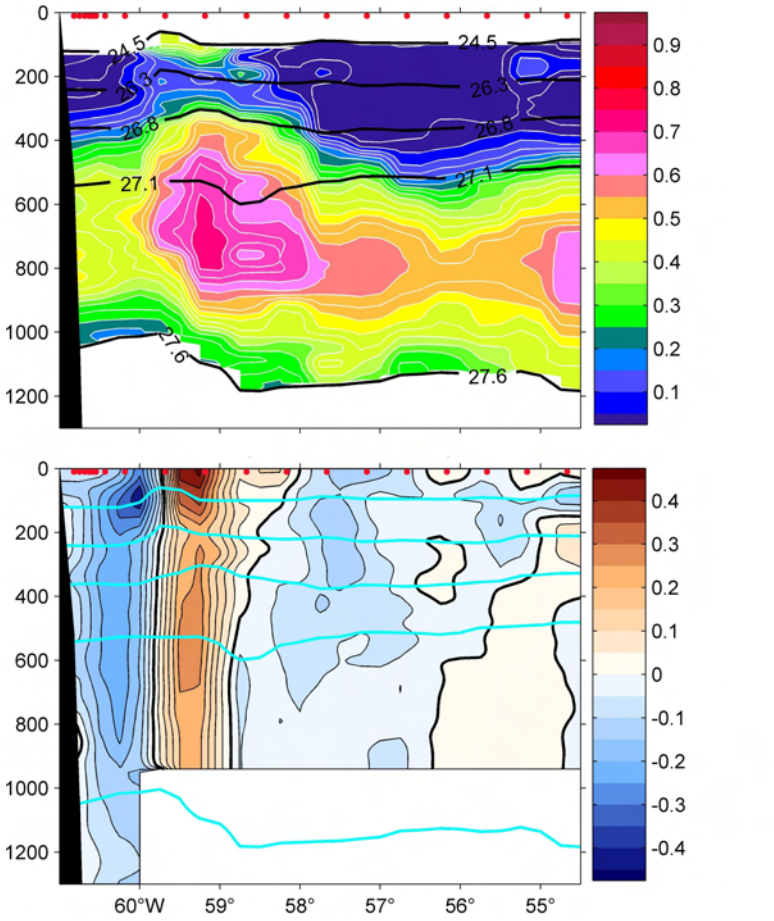

Figure 5.3: SAW fractions in % (top) and meridional current velocity in ms^{-1} (bottom) at 16°N, as in Figure 5.1, for June 2003. Aligned and scaled as Figure 5.2.

Rings observed during cruise S 171 (June 2003)

The interpretation of the data accomplished in June 2003 is somewhat challenging. Rhein et al. (2005) identified a surface intensified ring from 60°W to 58°W, which corresponds best to the SAW distribution. This ring has a diameter of 214 km and extends from the surface to 1100 m depth. The mean SAW fractions below the surface on this part of the section are 18% in SMW, 20% in UCW, 48% in LCW and 52% in IW. The cylindrical ring volume is $4 \cdot 10^{13}$ m^3, of which $1.7 \cdot 10^{13}$ m^3 are SAW, and yields a SAW transport of 0.5 Sv. This interpretation follows the 'normal' NBC ring rotation, which is anticlockwise, but contains weak southward flow. Nevertheless, the velocity field could as well indicate a cyclonic ring located further west, extending from the boundary to 58.5°W. When interpreted this way, a ring of $5 \cdot 10^{13}$ m^3 volume is obtained (diameter 240 km), which carries $2.1 \cdot 10^{13}$ m^3 SAW. The mean SAW fractions are slightly lower than further east: 15% in SMW, 20% in UCW, 47% in LCW and 48% in IW. The resulting ring transport is 0.7 Sv of SAW. The upward deflection of the isopycnals 24.5 kgm^{-3} and 26.3 kgm^{-3} support the assumption of an encountered cyclone, while the depression in the isopycnal 27.1 kgm^{-3} further east corresponds to the anticyclone. This possible existence of a cyclone will later be discussed in detail.

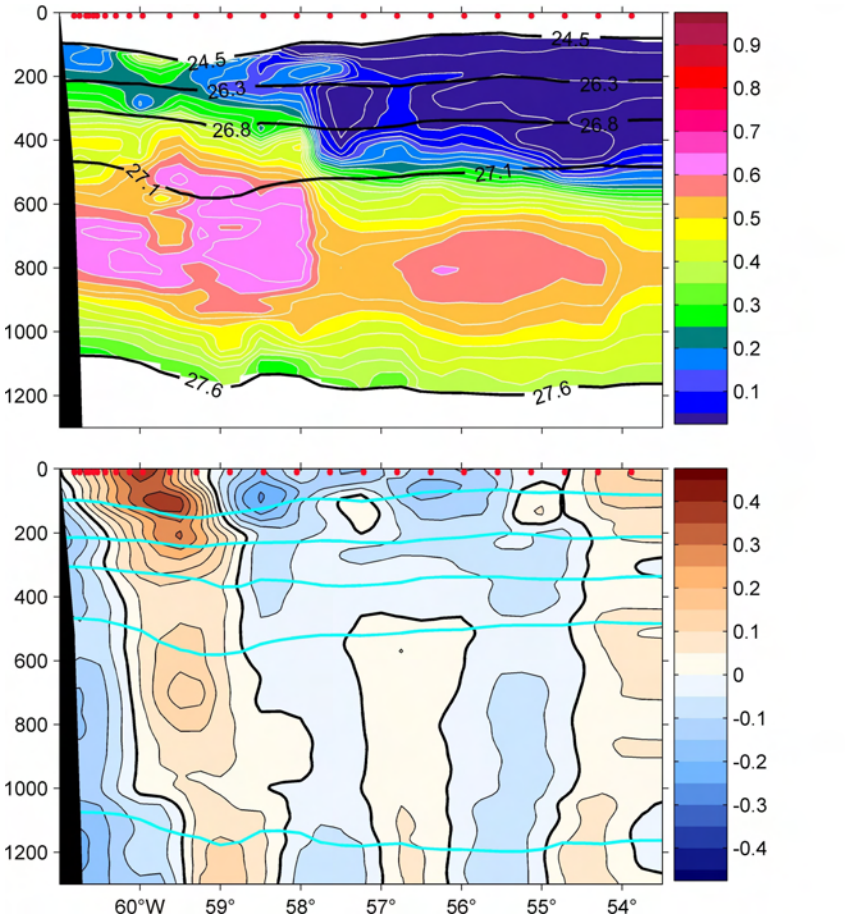

Figure 5.4: SAW fractions in % (top) and meridional current velocity in ms^{-1} (bottom) at 16°N, as in Figure 5.1, for July 2004. Aligned and scaled as Figure 5.2.

Rings observed during cruise M 62/1 (July 2004)

In July 2004 the currents at 16°N were weaker and less strongly shaped than during the other cruises. The southward velocities did not exceed 30 cms^{-1} and the northward velocities stayed below 40 cms^{-1}. The high velocity cores between 60.3°W and 58°W can nevertheless be interpreted as a ring, which corresponds to the SAW distribution. The cylindrical ring volume is $5 \cdot 10^{13}$ m^3 from the surface to 1100 m depth (a diameter of 240 km is obtained). The mean SAW fractions below the surface along this part of the section are 22% in SMW, 22% in UCW, 45% in LCW and 56% in IW, resulting in a SAW volume of $2.7 \cdot 10^{13}$ m^3. The resulting ring transport yields 0.9 Sv of SAW. Further east, the velocities are weak (< 15 cms^{-1}) and no more rings can be identified. The SAW fractions however show another high SAW core from 56.5°W to 54.5°W in the Intermediate Water.

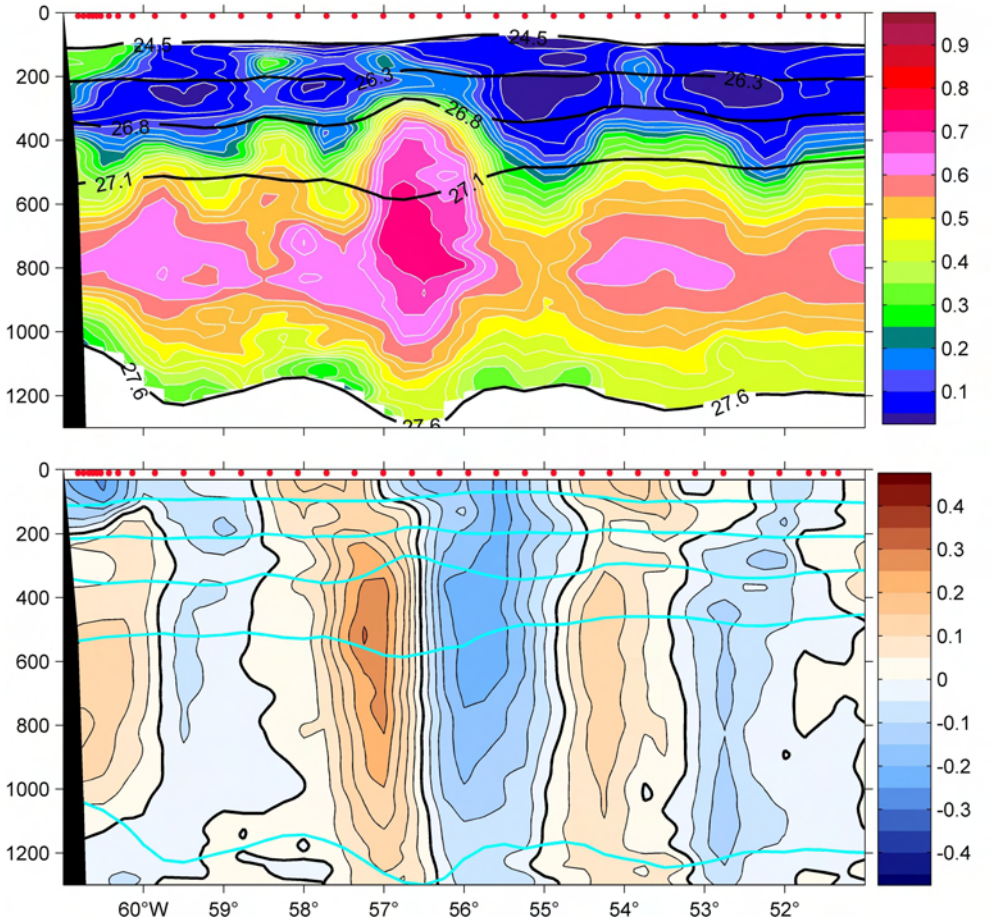

Figure 5.5: SAW fractions in % (top) and meridional current velocity in ms^{-1} (bottom) at 16°N, as in Figure 5.1, for September 2005. Aligned and scaled as Figure 5.2.

Rings observed during cruise M 66/1 (September 2005)

During the cruise carried out in September 2005 the measurements revealed another subsurface intensified ring. Off the western boundary, from 57.7°W to 55.2°W, the ring core was located in the LCW and IW layer. This ring is located farther east than all other rings identified before. However, the SAW fractions and velocities on the earlier cruises revealed ring-like features at this longitudes, e.g. on S 152 (December 2000). With a diameter of 265 km and a vertical range of 1050 m (200 m to 1250 m) the ring holds a volume of $5.8 \cdot 10^{13}\ m^3$. The SAW contribution to UCW is low, only 16%, but rapidly increases in the LCW layer with 50%. The IW layer even contains 56% SAW. The SAW volume sums up to $3 \cdot 10^{13}\ m^3$, resulting in a transport of 1.0 Sv. The ring core is indicated in the shaping of the isopycnals 26.8 kgm^{-3} and 27.1 kgm^{-3} and the maximum velocities between 400 m and 700 m depth. The density surface 27.6 kgm^{-3} exhibits a depression as well. The SMW and TSW layers are not effected, the ring has thus no imprint on the sea surface. East of the ring another anticyclonic feature appears in the IW velocity field (55°W-52°W), corresponding to a high SAW core.

5.2 Observed NBC ring properties

During all five cruises (Table 3.1) ring-like features were observed in both north-south velocity and SAW distribution, which was obtained from the hydrographic data as shown before (see Chapter 3). These features were found along the whole section, not only at the western boundary. When the features were pronounced and outstanding, they were identified as a NBC ring. One distinct ring was found on each survey. The existence of other ring-like features on the sections was noted repeatedly: the velocity distribution often shows alternating north and southward flow and cores of high SAW contributions (>60% SAW) appeared in the IW layer.

Since some of the observed rings revealed a near-surface velocity core, it is assumed that these rings transported SAW in the surface layer at least as far north as 16°N. The TSW trapped in these rings is thus considered to be of southern hemispheric origin entirely. The subsurface intensified rings had no imprint on the ocean's surface. The TSW above was therefore not influenced by the rings and consequently not included in the transport calculations.

cruise	date	diameter	volume	SAW volume	SAW trans.	type
S 152	Dec. 2000	267 km	$5.3 \cdot 10^{13}\ m^3$	$1.7 \cdot 10^{13}\ m^3$	0.5 Sv	subsurface
M 53/3	June 2002	320 km	$9.2 \cdot 10^{13}\ m^3$	$3.1 \cdot 10^{13}\ m^3$	1.0 Sv	surface
S 171	June 2003	214 km	$4.0 \cdot 10^{13}\ m^3$	$1.7 \cdot 10^{13}\ m^3$	0.5 Sv	surface
S 171*	June 2003	240 km	$5.0 \cdot 10^{13}\ m^3$	$2.1 \cdot 10^{13}\ m^3$	0.7 Sv	surface
M 62/1	July 2004	240 km	$5.0 \cdot 10^{13}\ m^3$	$2.7 \cdot 10^{13}\ m^3$	0.9 Sv	surface
M 66/1	Sept. 2005	265 km	$5.8 \cdot 10^{13}\ m^3$	$3.0 \cdot 10^{13}\ m^3$	1.0 Sv	subsurface

Table 5.1: Overview of the NBC-rings at 16°N, observed during the ship cruises. The row S 171* for June 2003 references to the possible interpretation of a cyclone (see text).

An overview of all rings observed during ship cruises and discussed previously is given in Table 5.1. The calculated ring transports depend obviously on the adopted ring volumes. It is not certain, that the cruise tracks always crossed the center of a ring. It is rather likely that measurements were taken along a ring secant, thus underestimating the ring volume. Garzoli et al. (2003) identified NBC rings off the Brazilian coast between 10°N and the equator and calculated a mean ring diameter of 392 km, which is larger than the ring diameters reported in Table 5.1. This indicates that the rings experience some volume loss along the way. Only the ring observed in June 2002 was of similar magnitude as the rings described in Garzoli et al. (2003). Goni and Johns (2003) identified surface intensified NBC rings using satellite altimetry. They reported a mean ring radius of 100 km, which agrees reasonably well with the mean ring radius of 129 km for the surface rings listed in Table 5.1. The large ring observed in June 2002 is probably an exception for the section at 16°N.

Table 5.1 provides a mean SAW transport of 0.8 Sv by NBC rings, which is independent of the interpretation of the ring from June 2003: whether the cyclone or the anticyclone is considered valid. The difference in the transport is small (0.2 Sv) and does not change the mean. The possibility of a cyclone will be addressed when the model results are discussed, as the model gives time series of the velocity fields and the development of rings can be investigated.

Goni and Johns (2003) analyzed ten years of altimeter data and estimated a mean ring shedding of 5-6 rings per year (of the surface intensified type, since noticed by sea height anomaly). They reported a high year to year variability with ring shedding any time of the year. However, the rings showed a weak tendency to form in the first half of the year. Johns et al. (2003) combined ship measurements in the region 6°N-10°N off the South American continental shelf with results from moored instruments (Garzoli et al., 2003). They identified 12 surface rings and 4 subsurface rings in a period of 22 month, which yields a mean ring shedding of 8.5 rings per year. These studies indicate a probable ring shedding of 6.5-8.5 rings per year (when 1-1.5 subsurface rings are added to the 5-6 rings obtained by Goni and Johns, 2003). Using the mean ring SAW transport of 0.8 Sv from Table 5.1, the total SAW transport by rings sums up to 5.2-6.8 Sv. On average, the SAW transport by rings amounts to 6 Sv, which occurs to 60% in the IW layer (3.6 Sv), to 25% in the Central Waters (1.5 Sv) and to 15% in the upper warm water (SMW and TSW, 0.9 Sv).

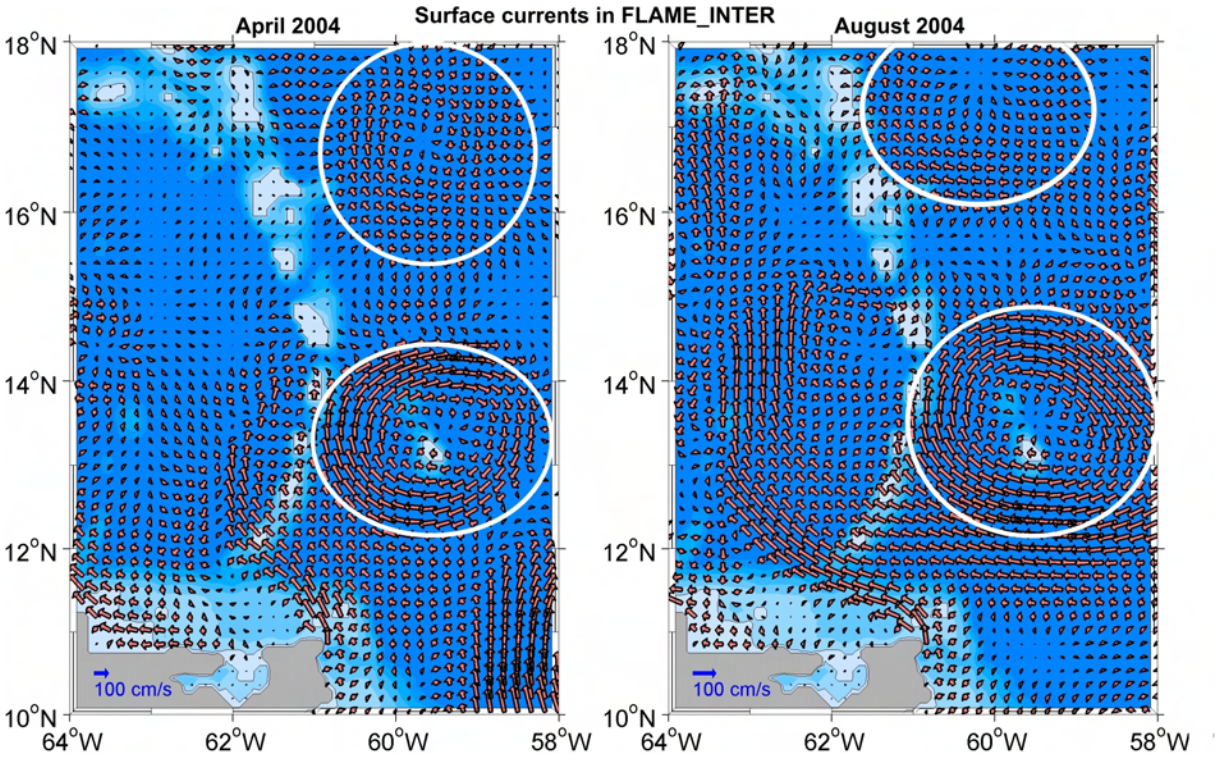

Figure 5.6: Surface currents in FLAME_INTER, illustrated are 3-day means in 2004. Every second velocity vector is shown. Examples of anticyclonic rings are framed by white circles. Left: April, 08-10; right: August, 17-19. The background indicates the model topography, land points are in grey.

5.3 NBC rings in FLAME_INTER

The NBC rings, propagating northward from the NBC retroflection, are short-living vortices and thus objects of high variability. For an examination of rings near the Lesser Antilles, the FLAME_INTER model run is used. Namely the period 2003-2004 is considered here, confined to the region shown in Figure 5.6, where examples for anticyclonic rings at the models sea surface are given. It is evident that anticyclonic rings occur in the model, which can easily be identified in the velocity field. For the purpose of clarity, only every other velocity vector is shown. Obviously the islands bordering the Caribbean are shallow ocean points in the model topography (cf. Chapter 3), since the pattern of the surface currents is not deformed by the presence of the islands. This circumstance reveals an important disagreement between the model and the actual ring propagation: the model probably fails in reproducing the surface ring pathways, as they can enter the Caribbean unhindered.

In Figure 5.6 two snapshots of the surface current fields near the Lesser Antilles are illustrated, each showing two anticyclonic rings. One is located around Barbados in both cases, while the other is near Guadeloupe/Antigua. The ring centering Barbados has a diameter of 325 km in April and of 346 km in August 2004. The northern ring is slightly smaller, a diameter of 287 km is obtained for April and of 308 km for August 2004. These diameters are well within the range of the observed rings reported in Table 5.1.

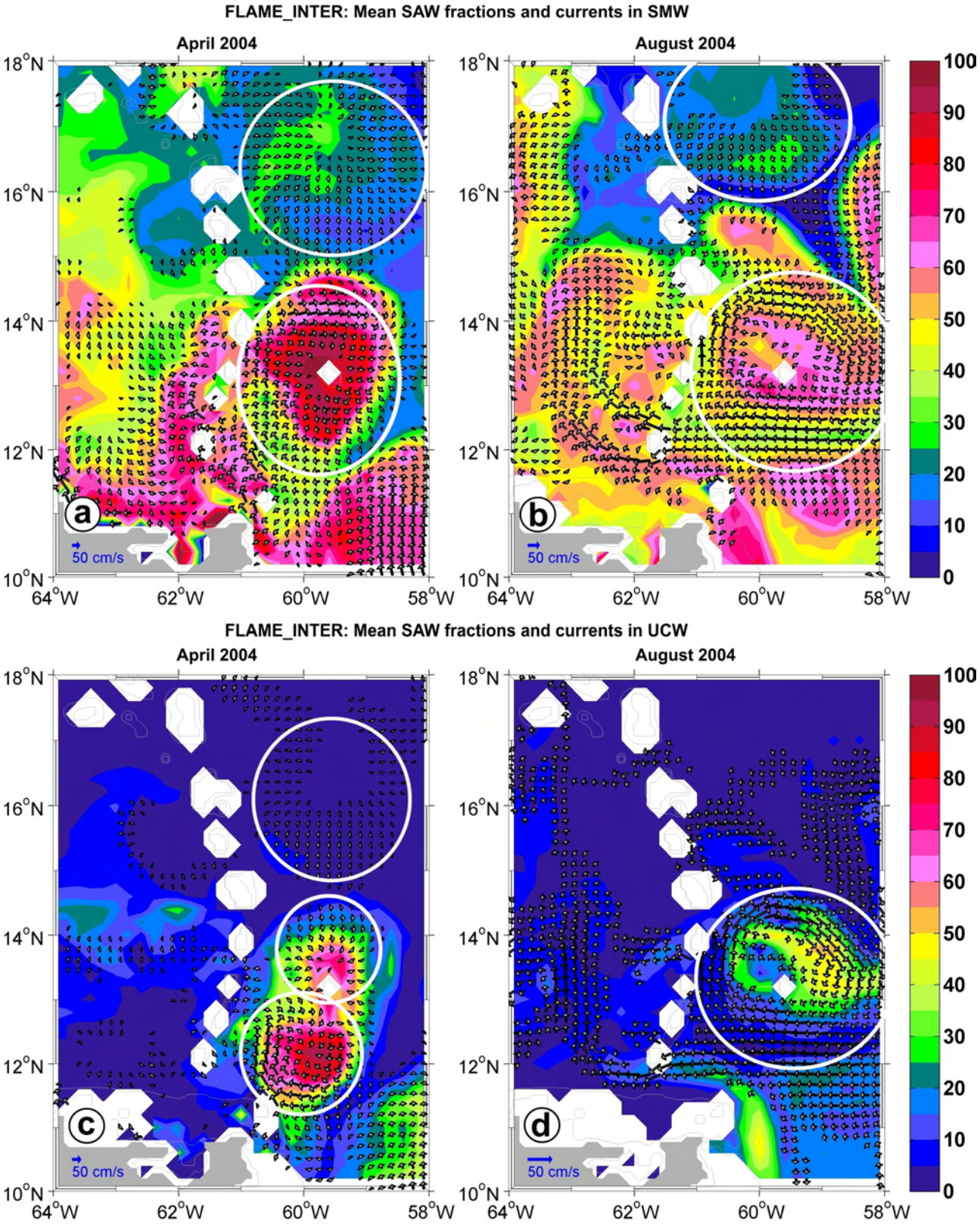

Figure 5.7: SAW distribution (in %) and currents in FLAME_INTER, illustrated are 3-day means in 2004. Every second velocity vector is shown, when a speed of 10 cms^{-1} is exceeded. Examples of anticyclonic rings are framed by white circles. a) SMW in April, 08-10; b) SMW in August, 17-19; c) UCW in April, 08-10; d) UCW in August, 17-19.

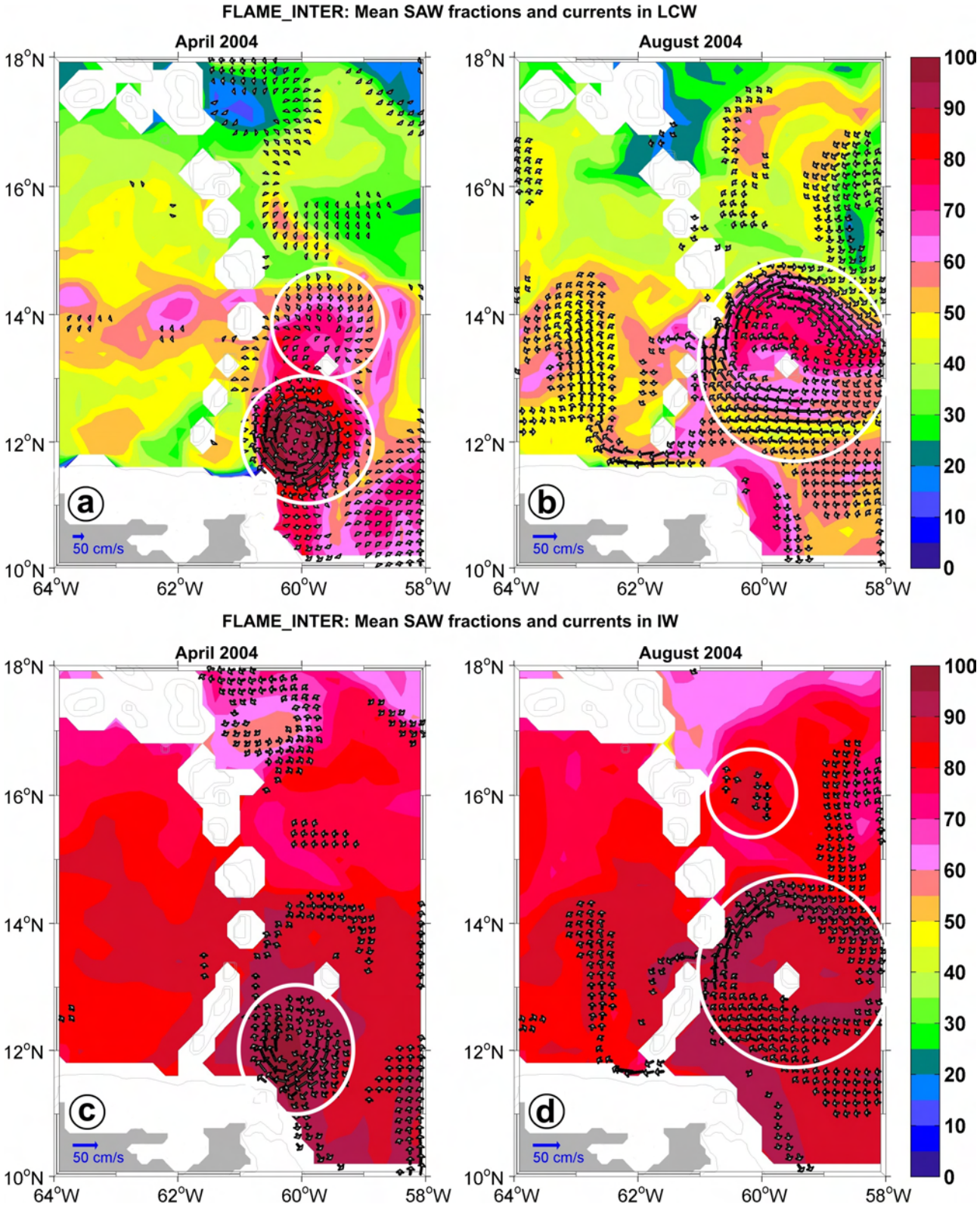

Figure 5.8: Same as Figure 5.7, but for the water masses LCW and IW. a) LCW in April, 08-10; b) LCW in August, 17-19; c) IW in April, 08-10; d) IW in August, 17-19.

To gain information on the SAW transport in the model, the subsurface layers are investigated, using the SAW analysis as before. The results of the water mass analysis are presented in Figures 5.7 and 5.8, for the same two snapshots as in Figure 5.6, which were discussed above. The figures not only give the SAW distribution for each density layer, but also all currents with speeds $> 10\ cms^{-1}$. In contrast to the surface currents in Figure 5.6, the influence of topography is evident in the subsurface layers, restricting the westward flow into the Caribbean. The island of Barbados represents an obstacle for the northward flow. The three islands Barbados, St. Vincent and Tobago form a topographic barrier in form of a triangle, which is capable of trapping the deeper parts of a ring. This is illustrated by the southern ring in Fig. 5.7 *a* and *c*: the SMW layer shows a large anticyclonic ring around Barbados (as in the TSW, see above), but in the UCW this ring is split into two vortices, one north of Barbados and another one located between Barbados and Tobago. The current speeds decrease with depth and in the two lowest layers (Fig. 5.8) only the rings are observable features in the velocity field, the currents outside of rings are weak. North of St. Lucia (approx. 15°N) the water masses below the SMW exhibit weak currents, and the northern rings from Fig. 5.6 are not identified in Figures 5.7 *d*, 5.8 *a, b, c*.

Rings approaching the Lesser Antilles

It is evident from Figures 5.6-5.8 that the water mass analysis provides a useful tool for tracking the NBC rings. The rings do not only show an anticyclonic sense of rotation but high SAW fractions in their center as well. Tracking is easiest done in the UCW layer, where the background SAW distribution is very small. An example for NBC rings approaching the Lesser Antilles from the southeast, along the South American coastline, is given in Figure 5.9. The ring core exhibits SAW fractions of more than 90%, which reveals the ring clearly against the background SAW distribution of below 20%. When propagating towards the Caribbean, the ring has a diameter of approx. 220 km (Fig. 5.9 *a*). The ring then moves around Tobago (Fig. 5.9 *b*) and gets trapped between St. Lucia and Barbados. Apparently, some ring volume is lost and enters the Caribbean Sea through Grenada and St. Lucia Passage, where traces of elevated SAW fractions appear (Fig. 5.9 *b* and *c*). The ring diameter decreases and finally the ring passes northward between the two islands St. Lucia and Barbados. The passage between these islands has a width of 160 km, which is identical to the ring diameter in Figure 5.9 *d*. The propagation of the ring center from 11°N (east of Trinidad) to 13.5°N (north of Barbados) has taken 40 days in the model. A week later, the ring is still attached to Barbados and a new NBC ring with a center built of SAW approaches the Lesser Antilles from the south (Fig. 5.9 *e*). The ring north of Barbados travels around the island, finally merging with the new ring, as illustrated in Figure 5.9 *f*.

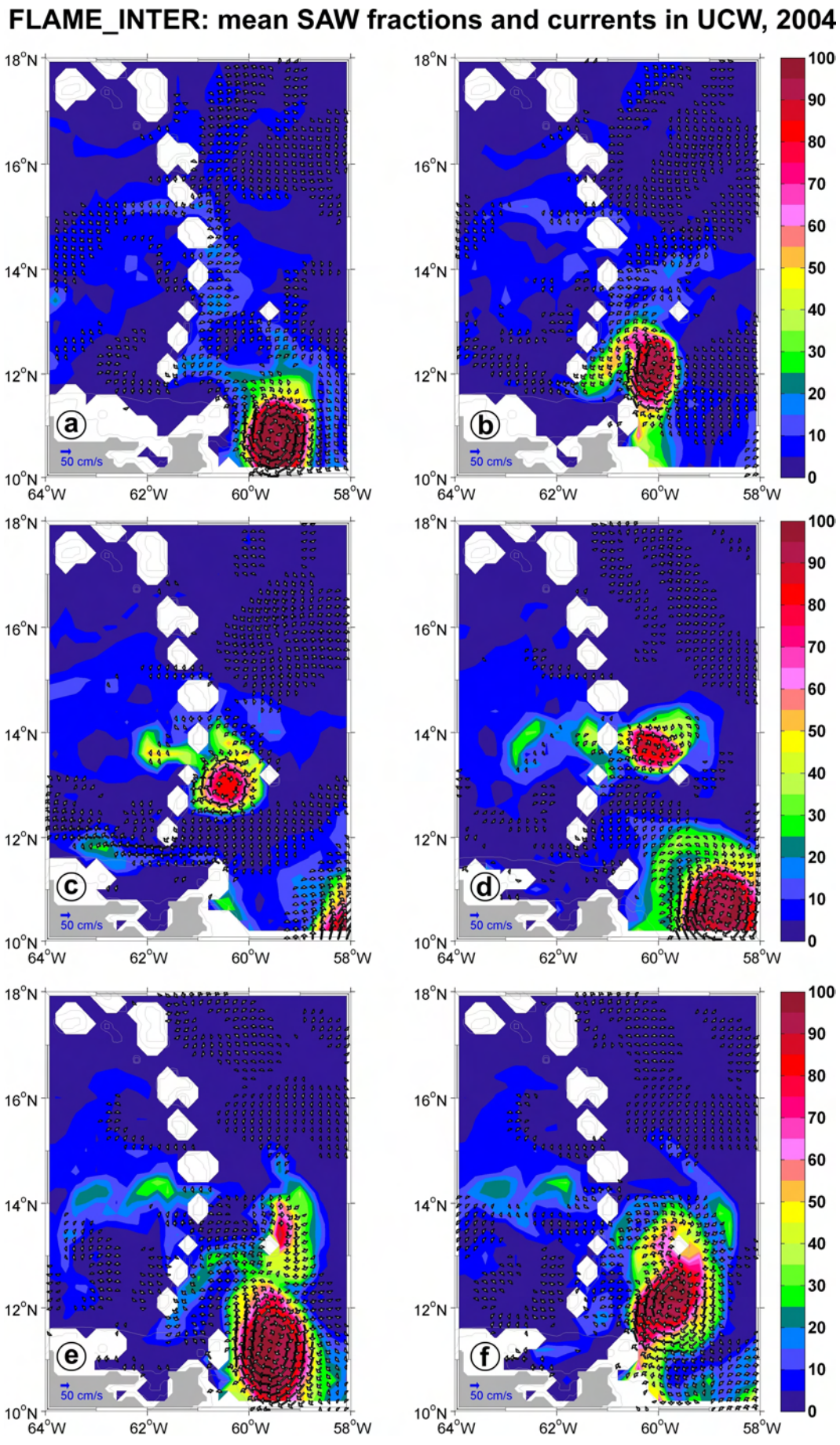

Figure 5.9: SAW fractions and current velocity in UCW in FLAME_INTER. The figure illustrates 3-day means in 2004. a) Feb., 01-03; b) Feb., 10-12; c) Feb., 25-27; d) Mar., 12-14; e) Mar., 24-26; f) Mar., 30-Apr., 01.

The example presented above is valid for all rings identified in the UCW, which approached the Caribbean along the South American coastline in FLAME_INTER during the period 2003-2004. Within the two years eight rings entered the region between 58°W and 61°W. They had a diameter of 220 km at minimum and 270 km at maximum. The mean diameter is 250 km at 11°N. The rings move northwestward around Tobago and get trapped ahead of the section St. Lucia-Barbados. Volume is lost to the Caribbean, and finally the rings are reduced to a diameter of 180 km, passing through the St. Lucia-Barbados gap. This behavior is adopted in the deeper layers of the LCW and IW. One of the rings is shallower than 500 m and not identified in the IW, but all other rings are deep-reaching. The SAW-imprint of the ring cores is slightly less extensive in the LCW, where the mean diameter of the rings is only 200 km. In the IW the ring cores appear weaker (in current strength), but with the same mean diameter of 250 km as in the UCW.

The water imported into the Caribbean Sea by the reduction of ring volume within the island triangle carries a strong SAW signature. The flow is very restricted and jet-like, since the Lesser Antilles Passages are much smaller than the 180 km width of the St. Lucia-Barbados section. The rings do not enter the Caribbean as vortices. Interaction with the islands nevertheless leads to the formation of new rings in the eastern Caribbean, when the currents in the passages are strong enough (Richardson, 2005, observed by drifter trajectories, Cenedese et al., 2005, observed by laboratory experiments).

For the water masses located above the UCW (SMW and TSW), the interpretation of the velocity field is more ambiguous, since strong currents appear beyond the rings and interact with the ring structures. Nevertheless, in the SMW nine rings could be identified by the SAW distribution and the current field, indicating at least one surface intensified shallow ring with high SAW contribution. In the surface currents twelve anticyclonic vortices have been identified at 11°N, which entered the region from the southeast. Some weak rings might have been missed, since wind induced transports interact with the sea surface. The rings in the upper layers are larger, they are at minimum 220 km and at maximum 380 km wide, with a mean diameter of 300 km. Due to the model topography the surface currents are not influenced by the presence of the Lesser Antilles. Thus the TSW layer will not reproduce the real ring propagation. The large surface rings are not reduced by the St. Lucia-Barbados section due to the deficits in the topography and conserve their volume at this position.

In summary, the two-year analysis of the FLAME_INTER model water masses and currents revealed eleven NBC rings, approaching the Caribbean from the southeast. Three of these rings were confined to the surface layers above 200 m depth and one included the Central Water, but not the IW. Seven rings reached down to 1100 m. The mean diameter of the rings before interaction with the Lesser Antilles modifies the rings was found to be 200-250 km below 200 m depth. No exclusive subsurface intensified rings were found at 11°N in the FLAME_INTER model run. For periods of no NBC ring activity south of Barbados, the boundary currents along Trinidad remained generally northwestward. Outflow through Grenada Passage occurred during the two-year period of investigation, but was a rare feature.

Modifications by island interaction

When the rings have passed the section from St. Lucia to Barbados, they are attached to Barbados and move around the island. The island of Barbados is maintained on the right side of ring propagation, and the rings eventually move southeastward again, later merging with subsequent rings, as was illustrated in Figure 5.12 *d*. Some of the rings do not "survive" the passage through the St. Lucia-Barbados section and disintegrate in the island triangle. Streams separate from these rings, and parts of the streams continue northward along the island arc, contributing to the transport through Dominica and Guadeloupe Passage. Other parts of the streams shape clockwise around Barbados. Large rings as shown in Figures 5.7 and 5.8 are formed with Barbados in the center. Eventually new rings are formed by the streams north of 14°N. The newly formed rings carry a less significant SAW structure than the original NBC rings (described at 11°N above). Their diameters do not exceed 200 km.

Results from laboratory experiments correspond nicely to the behavior of NBC rings near Barbados in FLAME. Cenedese et al. (2005) describe several experiments in a rotating tank. They produced a cyclonic vortex and examined the interaction of the westward moving vortex with two cylindric obstacles. When a large vortex encounters the smaller gap between two cylinders, the original vortex is unable to move undisturbed through the gap. The authors report the vortex to either lose most of its fluid (into a streamer through the gap) until it can move through the gap, or totally disappear upstream of the gap (or move around the cylinders). In the wake of the cylinders, the streamer is able to form a new cyclonic vortex, which is undisturbed by the movement of the original vortex. It can therefore move on as a new independent structure. Since the results are not generally limited by the use of cyclonic vortices, one can extend their findings to an anticyclonic vortex by changing the sign of swirl velocity. The authors predict a clockwise movement of anticyclonic vortices around an obstacle, corresponding to the case of a ring circling around Barbados, as in Figure 5.12.

In the UCW layer, noticeable SAW transport is restricted to latitudes south of 15°N. In the other layers, the flow through the St. Lucia-Barbados section partly continues northward and contributes to the transport through Dominica and Guadeloupe Passage. Anticyclonic flow around Barbados occurs in all layers down to 1100 m.

While the northward propagation of the rings in FLAME_INTER described so far is strongly hindered by the Lesser Antilles (especially Barbados, see below) and a loss of volume occurs, rings with diameters well above 250 km occur at 16°N. The rings approach the Lesser Antilles from the east, moving strictly westward at 16°N. During May 2003, a large anticyclone appeared at 58-59°W, which reached the western boundary (that is Guadeloupe) in Mid-June. The ring had a diameter of 270 km with current speeds of $30-40\ cms^{-1}$ and a distinct core of SAW (65% in the LCW layer). The ring characteristics were similar in the IW layer. A pronounced SAW core was absent in the layers above the LCW and the current speeds decreased as well. The ring can thus be considered to be

of the subsurface intensified type. It stayed off Guadeloupe, slowly dissipating, until the first of August 2003, when it finally was no longer identifiable.

Development of cyclones north of Barbados

North of Barbados cyclonic rings are produced occasionally in the FLAME_INTER model run. One example is presented in Figure 5.10 for March 2003. The ring is indicated by a white circle in the figure. A distinct ring core, containing a noticeable amount of SAW, is visible in each layer, as well as the cyclonic currents in the velocity field. The ring has a diameter of approx. 280 km.

Again, the observed cyclonic ring corresponds to the results obtained by the tank experiments in Cenedese et al. (2005). They produced a westward moving vortex, which upon interaction with the two "islands" (cylinders) formed a jet passing through the gap between them. Part of the original vortex fluid formed a stream around one cylinder, which formed a new cyclonic vortex in the wake of the cylinder. Meanwhile, the fluid from the jet moved through the gap and started forming a dipole structure downstream of it, with one cyclone and one anticyclone. The new anticyclonic vortex was stable and visible downstream of the islands, when the jet through the gap had sufficiently high velocity. Elevated velocities in the gap and high Reynolds numbers were found to be necessary for the dipole production.

A direct comparison between the laboratory model and observations of drifter trajectories (Fratantoni and Richardson, 2006) is provided by Cenedese et al. (2005) and adopted here in Figure 5.11. The tank experiment in Figure 5.11 *b* illustrates the interaction of a cyclonic vortex with a gap between two islands: a stream is formed anticlockwise around the right cylinder (thin line), and a dipole with one cyclone and one anticyclone develops downstream of the islands (thick line, dashed line). As the NBC rings are anticyclonic vortices, the directions of the resulting currents after interaction with Barbados and St. Lucia is reversed: a stream would enter the gap and move around the right cylinder in clockwise direction (as described in FLAME, see above) and no northward flow occurs to the east of the islands. The cyclone would develop as the right side of the dipole. This is consistent with the observations described by Fratantoni and Richardson (2006). Figure 5.11 *a* illustrates drifter trajectories from Fratantoni and Richardson (2006). One of the drifters started a cyclonic looping approximately 300 km downstream of Barbados, which is near the latitude of Guadeloupe. The location of the cyclone thus agrees at least in latitude with the observation of a cyclonic feature during the cruise S 171 in June 2003 (see Table 5.1, Figure 5.3 and text). The observed cyclone on S 171 had its center at 60°W, while the drifter looped further east, at approx. 58-59°W.

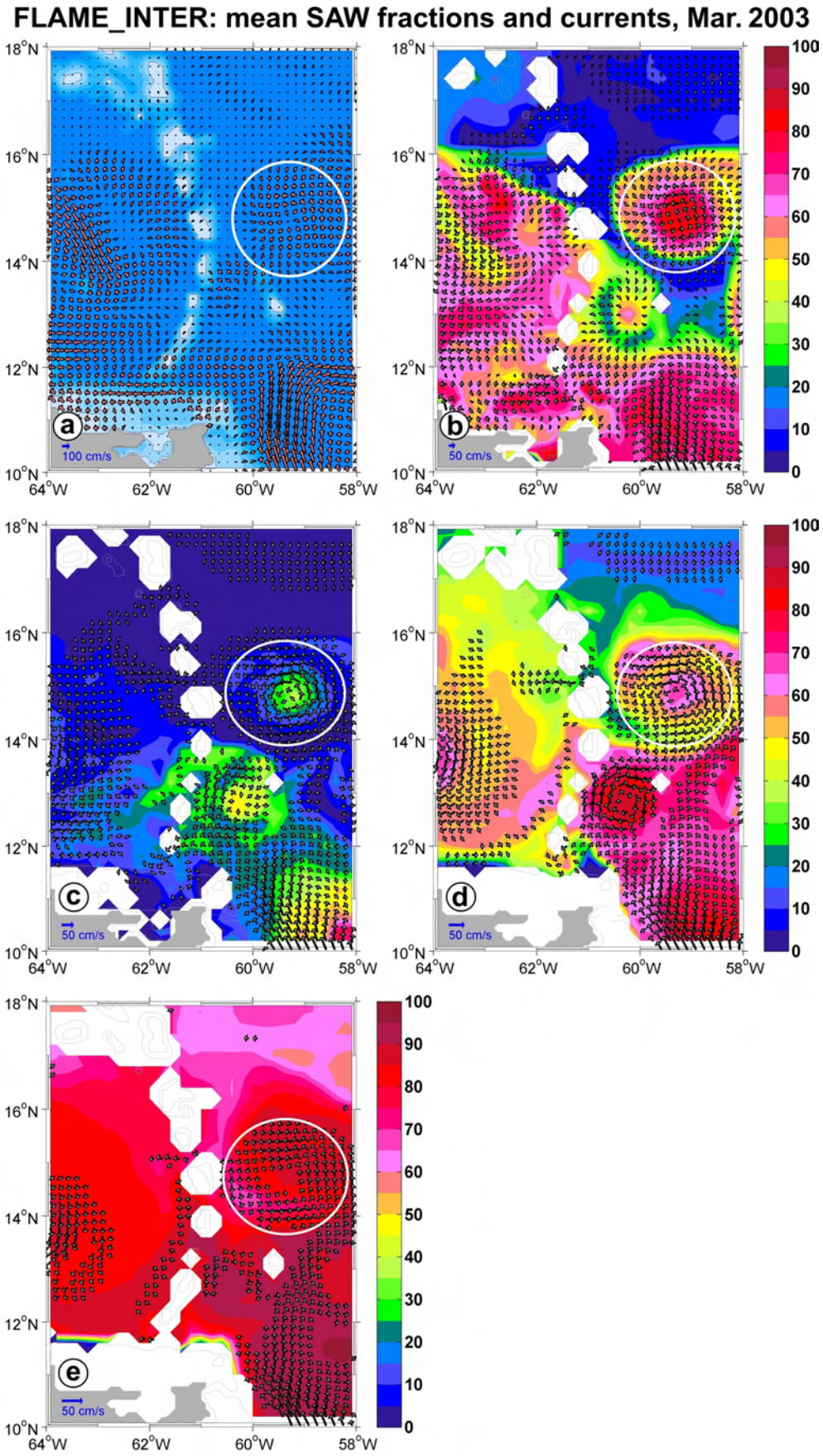

Figure 5.10: SAW fractions (in %) and current velocity in FLAME_INTER. The figure illustrates 3-day means from 2003: March, 11-13. a) TSW; b) SMW; c) UCW d) LCW e) IW. The cyclone is indicated by the white circle. Note that the TSW layer in a) is not part of the water mass analysis, the background indicates the model topography only.

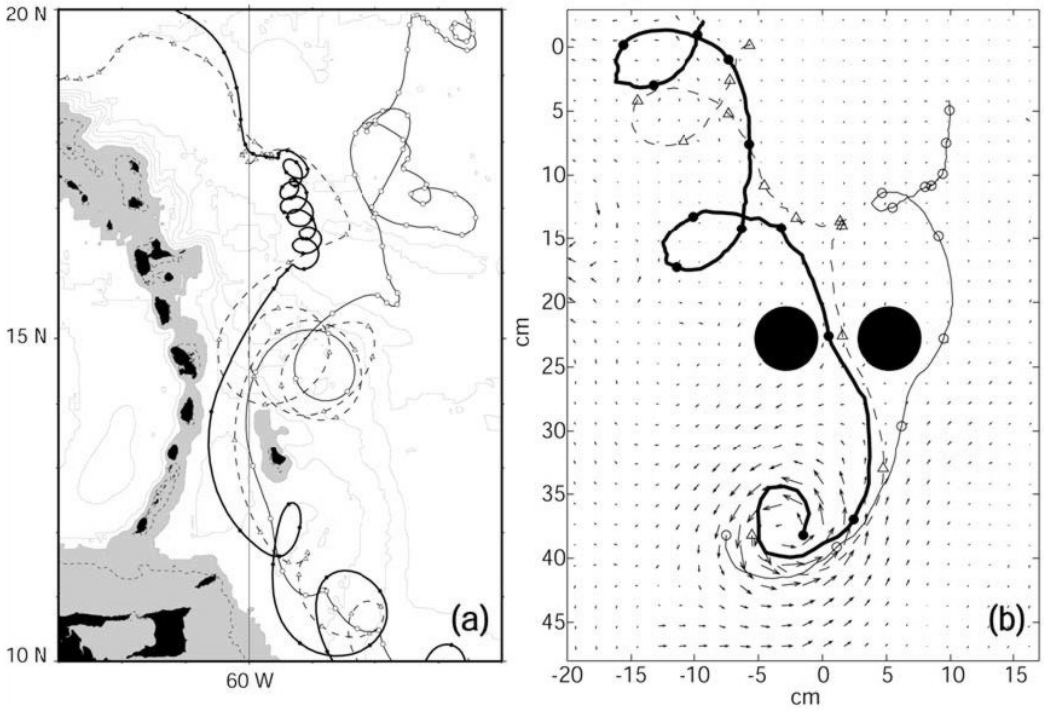

Figure 5.11: Examples of trajectories near the Lesser Antilles, from Cenedese et al. (2005), their Figure 14. Comparison of (a) observations and (b) laboratory model for a case in which a dipole was observed downstream of the island passage. Shown are trajectories of three satellite-tracked surface drifters in ring 3 (Fratantoni and Richardson, 2006) launched in an NBC ring in February 1999, compared with three synthetic drifters deployed in the velocity field of the laboratory model. Areas shallower than 1000 m are shaded. As described in the text, the sense of rotation for the laboratory eddies is reversed (cyclonic) relative to the observed anticyclonic NBC rings.

The results from FLAME_INTER match the conclusions of the studies discussed above and complement to the understanding of NBC ring interaction with the Lesser Antilles. In Figure 5.12 an example of the propagation and modification of NBC rings in the LCW layer are presented. In Fig. 5.12 *a* a ring arrives at the triangle of Tobago, St. Lucia and Barbados. Only a few days later, the diameter of the ring is reduced noticeably and a second ring approaches the region from the southeast (Fig. 5.12 *b*). A stream evolved six days later, moving clockwise around Barbados, and the second ring finally interacts with the first ring (Fig. 5.12 *c*). In Figure 5.12 *d* the core of the first ring passes through the gap between St. Lucia and Barbados, but the currents are modified to an anticyclonic structure around Barbados, integrating parts of the second ring. The two rings are merged completely in Figures 5.12 *e* and *f*, and a new cyclonic feature is formed north of the anticyclone around Barbados, at 14.7°N. The model does not reproduce the dipole structure of the laboratory experiments, but of course the velocity field in FLAME_INTER is much more complex than the tank vortex. The interaction of the second ring with the small first ring and the stream results in the formation of the large anticyclone around Barbados.

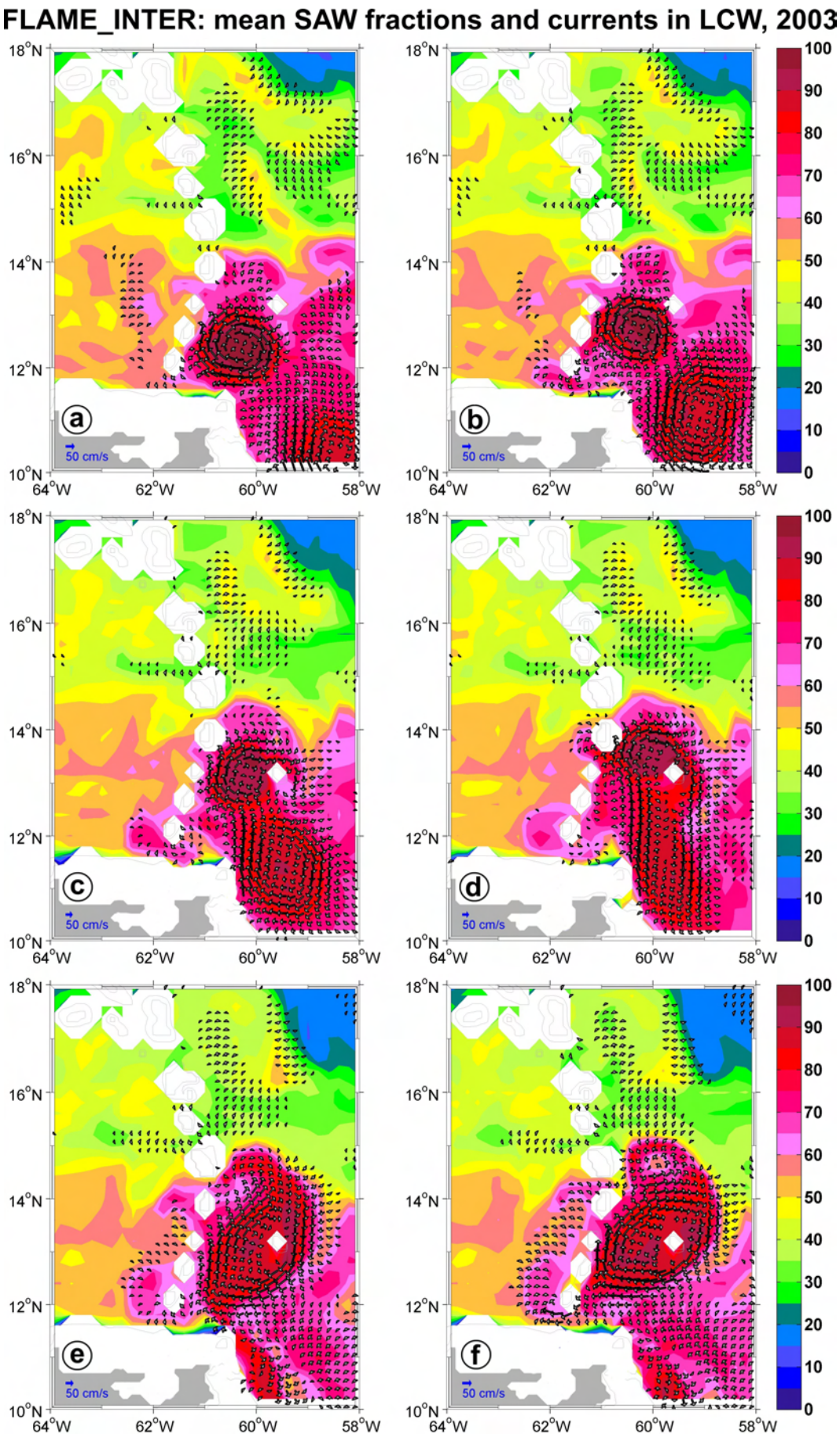

Figure 5.12: SAW fractions and current velocity in LCW in FLAME_INTER. The figure illustrates 3-day means in January and February 2003. a) Jan., 25-27; b) Jan., 31-Feb., 02; c) Feb., 06-08; d) Feb., 09-12; e) Feb., 16-18; f) Feb., 19-21.

6 Spreading of South Atlantic Water in the western tropical North Atlantic

In this Chapter the spreading of South Atlantic Water is investigated in the region from 30°W to 75°W and from the equator to 25°N. Hydrographic ship measurements are combined with profiles from Argo floats in this area to one database. This is used to calculate SAW fractions (see Chapter 3). The area of interest is divided into several sub-domains, where the mean SAW fractions are calculated. The analysis reveals the mean SAW propagation into the North Atlantic and identifies the regions of largest variability. The drifting buoys from Argo are used to obtain trajectories of the floats as well, revealing pathways into the Caribbean. The results from the equatorial Atlantic SAW distribution can be used to estimate the impact of the western South Atlantic SMW source, which is missing in the water mass analysis (see Chapter 2 and 3). An experiment with artificial floats in the FLAME model is used to validate the results from the water mass analysis and to give an estimate of the western South Atlantic SMW source in the model as well.

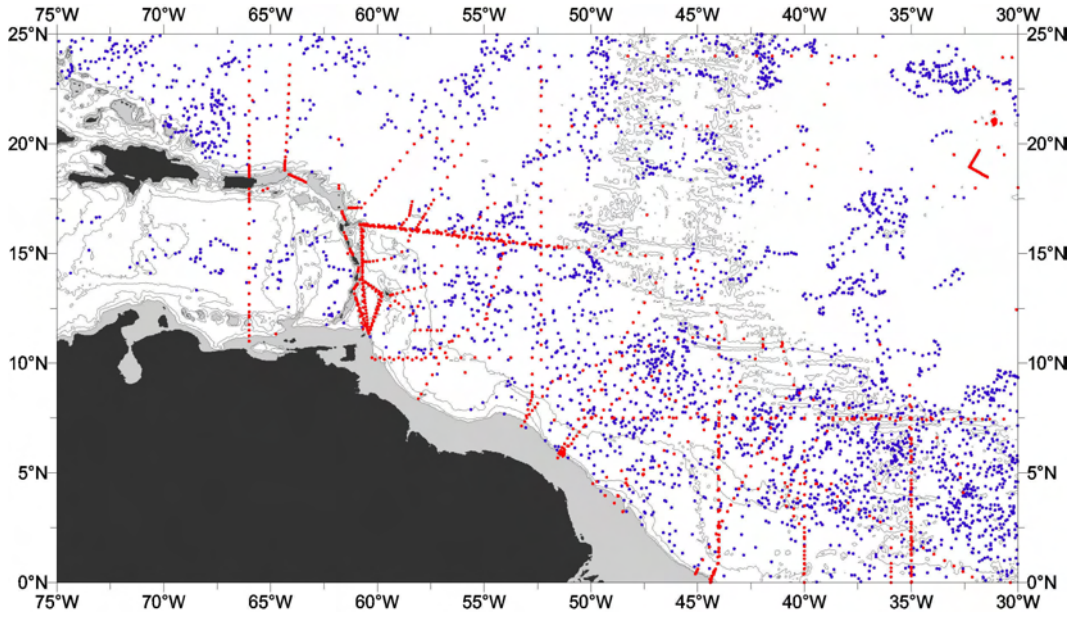

Figure 6.1: Locations of quality-checked profiles, obtained by Argo floats (blue) and ship measurements (red) from 1993 to 2007. The shelf shallower than 500 m is shaded in gray, the 1000 m, 2000 m and 4000 m isobaths are indicated.

6.1 Data set of Argo profiles and CTD data

The area of investigation was restricted to 30°W-75°W and 0°N-25°N, since the spreading of SAW in the western North Atlantic is addressed. The restriction of the area matches the limits of the water mass analysis as well: the defined source waters border the area of investigation to the north and south. Only the northern SMW source at 16°N lies within this area, since the SMW subducts south of 25°N (cf. Chapter 3). To the east, the influence of the STCs (see Chapter 2) prohibits a hydrographic tracking of the SAW.

Ship cruises carried out by the University of Bremen (Table 3.1) and data provided by HydroBase (Curry, 2001) for the western tropical North Atlantic yield together 1833 temperature and salinity profiles in the period from 1993 to 2005. Argo profiles are available on the websites of the Argo Data Centers (e.g. ftp://usgodae2.usgodae.org/pub/outgoing/argo/geo/). For the defined domain Argo provides more than 10,000 profiles in the period 01/2000-06/2007. However, many of them do not contain information on salinity and thus can not be used for the water mass analysis. The overall number of profiles, which provide salinity data and successfully pass through all quality checks (the checks are listed in Chapter 3), is only 3171. In combination with the ship derived data the western tropical North Atlantic is investigated by a data set consisting of 5004 temperature and salinity profiles. These are used to obtain the distribution of South Atlantic Water in the area of investigation, as at each profile location the respective SAW fractions in the water column are determined. As can be seen in Figure 6.1 the distribution of the profiles is scattered as expected. The data does not allow a separation into seasons or month, since some regions show a poor data coverage already on the annual basis (cf. Fig. 6.2).

The data set is divided geographically into several sub-domains. In these boxes the mean SAW portion and its standard deviation (STD in the following) are calculated for the four water masses: SMW, UCW, LCW and IW. Initially, the area was divided into regular 5° x 5° boxes. After evaluating the STD for each box, the extent and orientation of boxes with high STD was altered. The aim was to find an array of sub-domains with as low STDs as possible. Since the STD is a measure of the variation of the values within a box, the remaining areas of high STD indicate high variability in the water masses or a transition between different regimes (eg. the northern Subtropical Gyre and the Equatorial Gyre). The diversity of the profiles within any box should be as low as possible, in order to determine the mean spreading of SAW. The alignment of the boxes implies an orientation of the sub-domains with the propagation pathways of the water masses. As a result, the sub-domains are occasionally oblong and not in squares. The choice of boxes and the number of profiles available in each box are illustrated in Figure 6.2. In the area 10°N to 20°N nearly all boxes are arranged horizontally, with a 10° elongation in longitude and 5° in latitude. Besides, in the western boundary region south of 10°N a horizontal arrangement of boxes is preferred as well. The boxes reflect the mainly zonal circulation off the boundaries. Almost every box contains more than 50 quality-proved profiles, only five exhibit a lower accumulation of 30-50 profiles (shaded

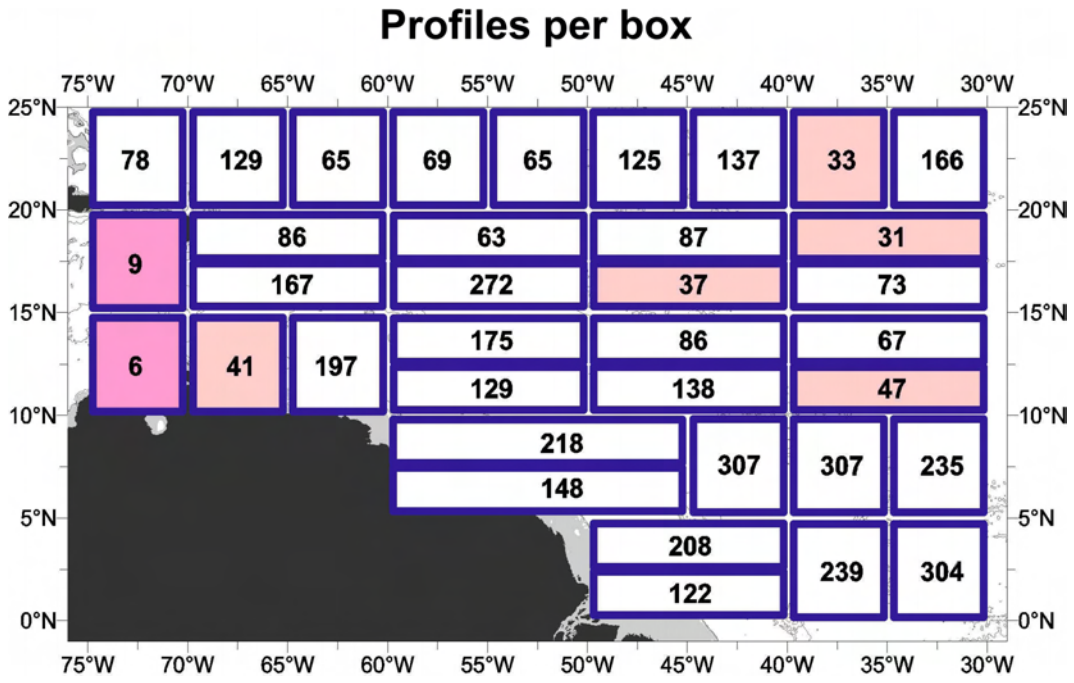

Figure 6.2: Choice of sub-domains with number of quality-proved profiles available in each box. Boxes with less than 50 and 10 profiles are shaded light and dark pink respectively.

boxes in the figure). The western Caribbean is badly sampled with less than 10 profiles. Results based on data from these boxes should be handled with caution.

6.2 Large-scale SAW distribution from observations

The mean SAW fractions for each box and the corresponding standard deviations are depicted in Figures 6.3 and 6.4. Obviously, SAW dominates the region east of 50°W and south of 10°N, where the fractions reach 60%-100% in all density layers. The percentage of SAW in the water masses is highest in the Central Water; both UCW and LCW contain 90%-100% SAW off the Brazilian shelf near the equator. The figures highlight the strong South Atlantic contribution to the water masses of the equatorial North Atlantic (e.g. Stramma and Schott, 1999). The dominance of the SAW between the equator and 10°N, revealed by this analysis, restricts the contribution of the North Atlantic Water to the EUC, NECC and NEUC to 0%-30%. These currents are to 70%-100% formed of South Atlantic origin waters.

The transition region from southern hemispheric water to North Atlantic Water (NAW) is found to be displaced in the different density layers. The upper two layers (SMW and UCW, Fig. 6.3 *a* and *c*) both exhibit a strong decrease in SAW fractions at a bordering line from near Trinidad to 15°N, 30°W. This is indicated by the black lines in Figures 6.3 *a* and *c*. South of this zonally inclined border the SAW fractions are 50% and more. North of this border percentages above 20% are present only in the southeastern Caribbean. An exception is the box 20°N-25°N, 70°W-75°W with a higher mean SAW fraction in

SMW (Fig. 6.3 *a*), but this is considered an artefact of the water mass analysis. The source for the northern SMW was positioned at 16°N east of Guadeloupe (cf. Chapter 3), which limits the confidence in the results of the analysis at latitudes >20°N. Since the SAW contribution southeast of the peculiar box is small, the increased SAW fractions are assumably generated by NAW originating further north, spreading southward into the box. Of course, this restriction does not hold for the water mass analysis of the deeper layers, where the assigned sources are located further north.

In Figure 6.3 *b* and *d* the standard deviation for the upper two layers is illustrated. The STD is elevated along the encountered boundary of SAW influence, which is caused by the crossover from high SAW fractions to low SAW fractions across this line. The changes occur on a narrow spatial scale (max. 5°), especially east of 50°W, and thus lead to high variability within the affected boxes. The other regions of high STD are grouped at the South American coast and the Windward Islands. The rings propagating from the NBC retroflection, which itself alters its position between 5°N and 10°N (Johns et al., 1990), generate varying conditions along the western boundary and therefore high STDs.

The SAW factions in the two lower layers (LCW and IW) reach noticeably higher latitudes. As is apparent in Figure 6.4 *a* and *c* the transition region from SAW to NAW stretches from 12°N to 18°N in the LCW and is not declined. While the SAW fractions in the equatorial North Atlantic (south of 7°N) are similarly high in UCW and LCW, the propagation of UCW is clearly inhibited compared to LCW. The SAW distribution in the IW layer is not much different from the LCW, but SAW influence is evident up to 20°N and even north of this latitude between 70°W and 55°W. The distribution is smooth and the SAW influence gradually decreases, not as abrupt as in the upper layers. North of 20°N the SAW presumably encounters the NEC, which is part of the North Atlantic subtropical gyre. The salinity at 25°N on the $\sigma_\theta = 27.4$ surface decreases from east to west (not shown), indicating an influence of less-saline South Atlantic Intermediate Water from 58°W westward in the NEC.

The standard deviation for the two lower layers is given in Figure 6.4 *b* and *d*. The STD for the two lower layers is generally smaller than the STD for the upper layers (cf. Fig. 6.3 *b* and *d* with Fig. 6.4 *b* and *d*). The LCW exhibits high variability off the Lesser Antilles, at 60°W to 50°W. The NBC rings, which do not enter the Caribbean Sea, possibly pass within this corridor.

The Caribbean Sea exhibits the strongest SAW influence in the southeast. The box contains the Windward Islands and thus the passages, which were found to be of major importance for the SAW inflow into the Caribbean (Chapter 4). From south to north, the SAW fractions in the LCW and IW decrease inside the Caribbean Sea. The islands form a barrier, the transport into the Caribbean occurs mainly in the southern passages. West of 70°W, the IW layer still consists of more than 40% SAW.

More data is needed to improve seasonal coverage to allow to examine the interannual variability.

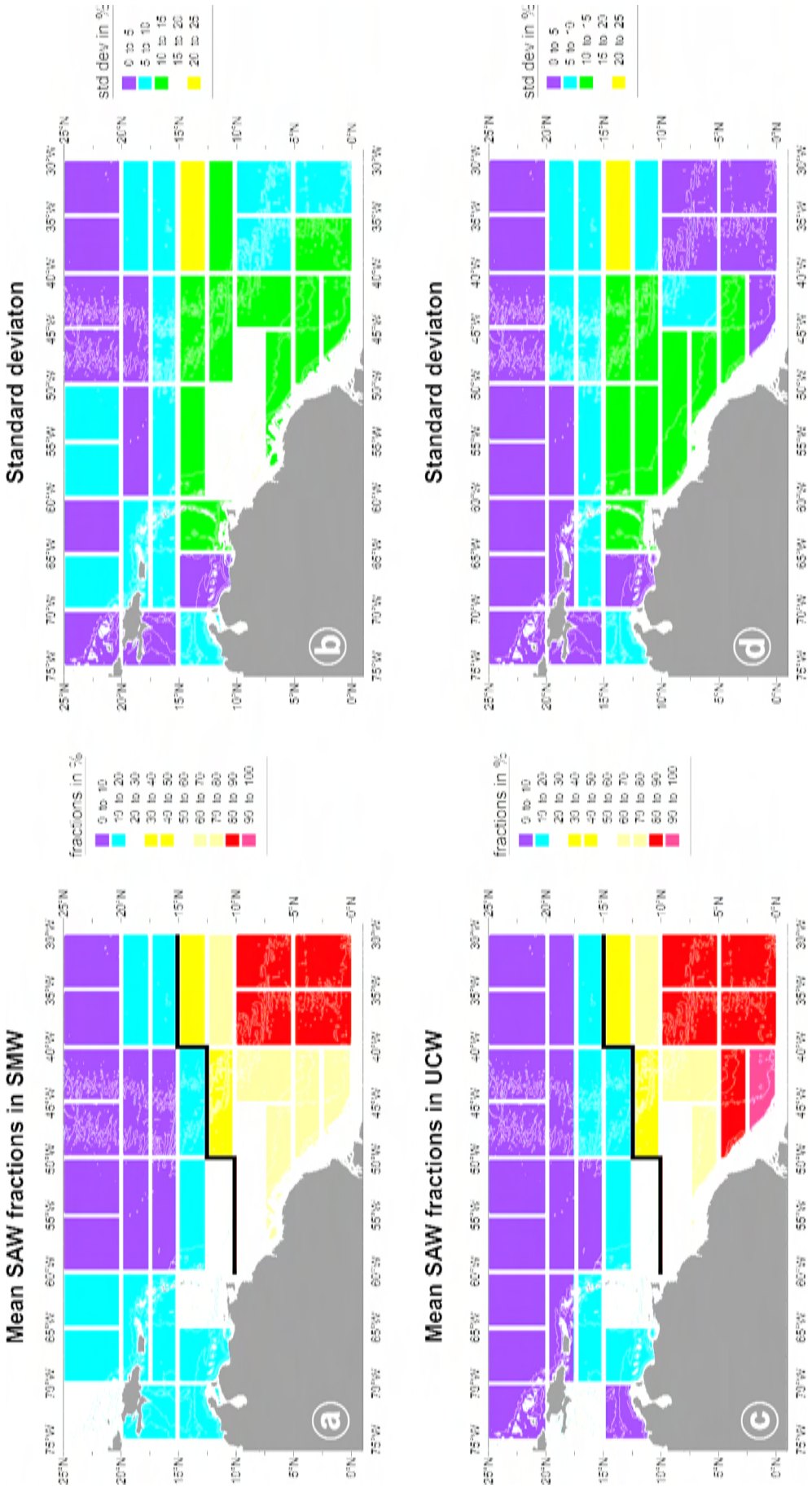

Figure 6.3: Mean South Atlantic Water distribution (in %) in the western tropical North Atlantic. (a): SAW distribution in SMW; (b): corresponding standard deviation; (c): SAW distribution in UCW; (d): corresponding standard deviation. The shelf shallower than 100 m is shaded in gray (a) and (b) and shallower than 200 m in (c) and (d). The black lines in (a) and (c) indicate the rapid decrease of SAW at the transition region from SAW to NAW. Note: the color scale for the SAW distribution here is different from the other figures in this work.

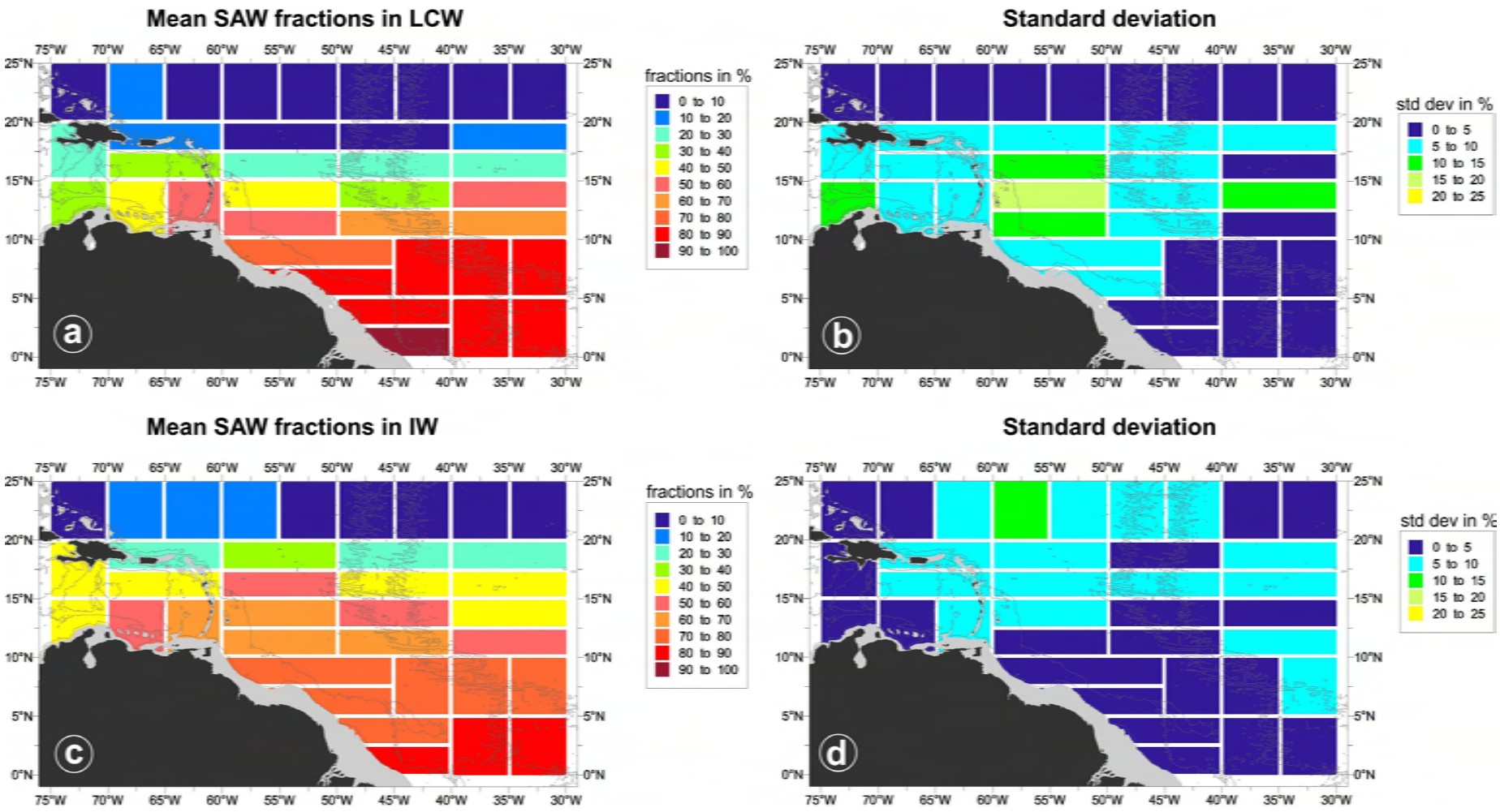

Figure 6.4: Mean South Atlantic Water distribution (in %) in the western tropical North Atlantic. (a): SAW distribution in LCW; (b): corresponding standard deviation; (c): SAW distribution in IW; (d): corresponding standard deviation. The shelf shallower than 200 m is shaded in gray (a) and (b) and shallower than 500 m in (c) and (d). The transition region from SAW to NAW is broader and zonal in this density layers and thus not indicated in this layers (contrary to Fig. 6.3). Note: the color scale for the SAW distribution here is different from the other figures in this work.

6.3 Large-scale SAW distribution in the FLAME model

The large-scale water mass distribution in FLAME was investigated as well. The monthly mean fields of temperature and salinity from FLAME_CLIM, used in Chapter 4 for obtaining the SAW transports into the Caribbean, were utilized in a larger area. The model analysis covers the area from 5°N to 24°N and from 50°W to 70°W. This region is slightly smaller than the region investigated by hydrographic float and CTD data above. In the chosen area more than 46,000 model grid points are situated, and thus the handling of the data sets was still challenging. Since the western boundary is the most important region for the spreading of SAW, the analysis was constrained to the smaller area.

For every climatological month, the SAW distribution was calculated. The resulting SAW fields were averaged and subsampled for better data handling. The produced mean annual SAW fractions and STDs are illustrated in Figures 6.5 and 6.6 for all four water masses. The transition region from southern hemispheric waters to North Atlantic Water is different in each layer. In the SMW layer high South Atlantic contributions are found south of 12°N ($> 50\%$) and near the Lesser Antilles south of St. Lucia. The southern SMW enters the Caribbean Sea and is still noticeable at 70°W throughout the Caribbean. The elevated fractions at the northwest corner of Figure 6.5 *a* is considered an artefact of the analysis, since SAW does not enter the North Atlantic Subtropical Gyre north of 16°N east of the Caribbean, as already noticed for the observational analysis (see the discussion there). The standard deviation shows high variability of mainly 6-14% for the SMW (Fig. 6.5 *b*), indicating true variability in the whole area except in the northeastern corner. The Central Waters (Figures 6.5 *c* and 6.6 *a*) exhibit a reduced spreading of SAW, strong South Atlantic influence is only evident south of 10°N. North of 20°N the SAW fractions are below 5% in this layer. While the southern origin LCW contributes slightly to the Caribbean inflow, the SAW fractions in the UCW do not indicate a transport into the Caribbean. Elevated standard deviation in this layers follow the SAW distribution, but extend the area of noticeable SAW influence. The standard deviation of the UCW (Fig. 6.5 *d*) indicates high variability up to 15°N and at the Lesser Antilles south of Martinique. As was shown in Chapter 5, NBC ring occasionally carry high amounts of SAW in the UCW layer to the Lesser Antilles. Since the modeled transport is too small to increase the mean SAW fractions at Barbados above 20%, only the high standard deviation denotes the ring propagation. This interpretation holds as well for the LCW layer in Figure 6.6 *a* and *b*. The SAW spreading in the LCW layer exhibits variability east of the Lesser Antilles. Incidental transport along the island arc north of Antigua is indicated by the STD. The most extensive spreading of SAW is evident in the IW layer, shown in Figure 6.6 *c*. In the intermediate depth, the transition region from SAW to NAW is at 17°-18°N. The southern IW does not only spread into the Caribbean, but also along the island arc on the Atlantic side of the Lesser Antilles. The IW layer exhibits small variability, only at the transition region north of 18°N elevated STDs are present (Fig. 6.6 *d*).

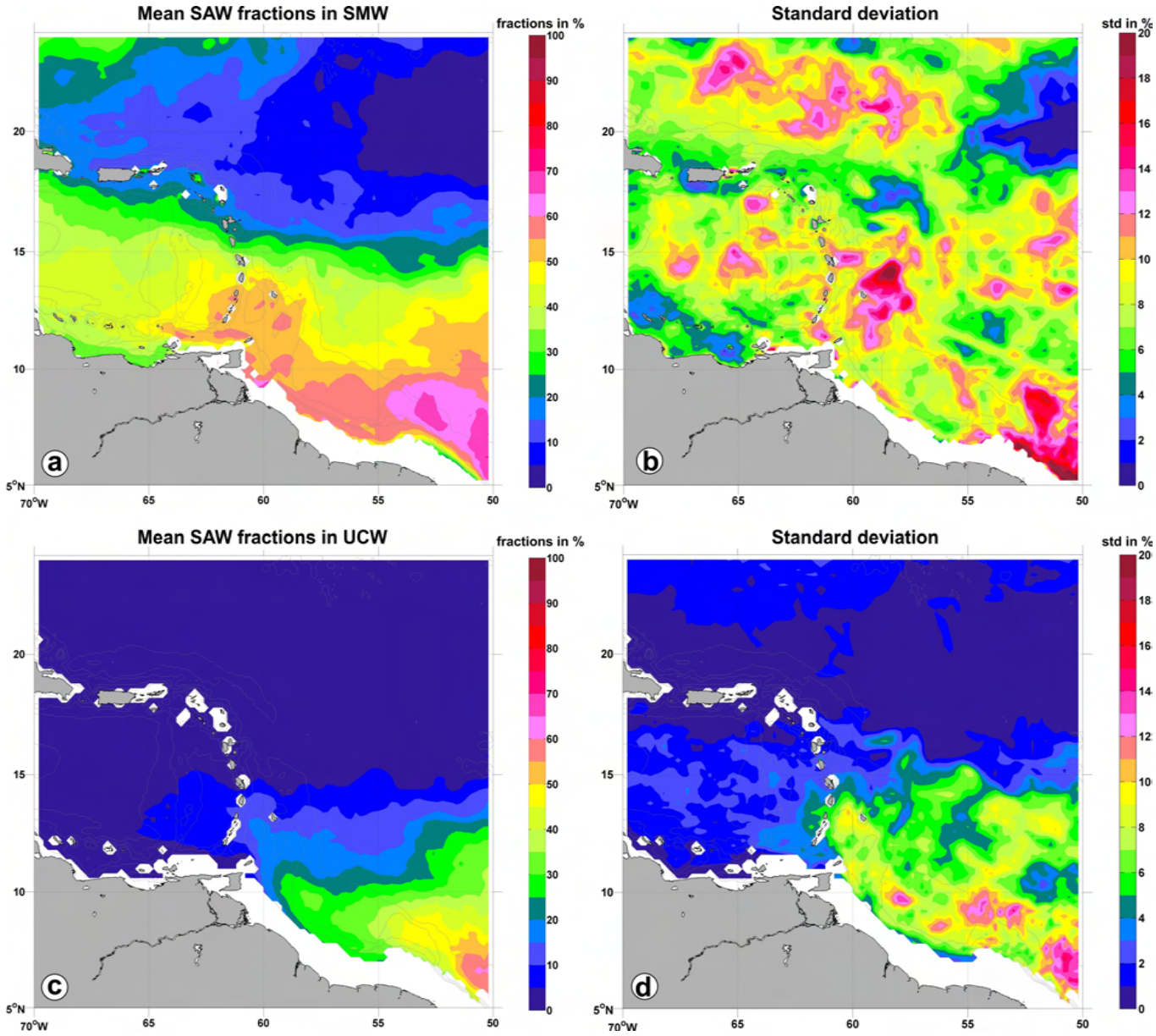

Figure 6.5: Mean South Atlantic Water distribution (in %) in the western tropical North Atlantic in FLAME_CLIM. (a): SAW distribution in SMW; (b): corresponding standard deviation; (c): Annual mean SAW distribution in UCW; (d): corresponding standard deviation. The topography is the same as in Figures 6.3 and6.4. Note the different scales for the mean fractions and standard deviations.

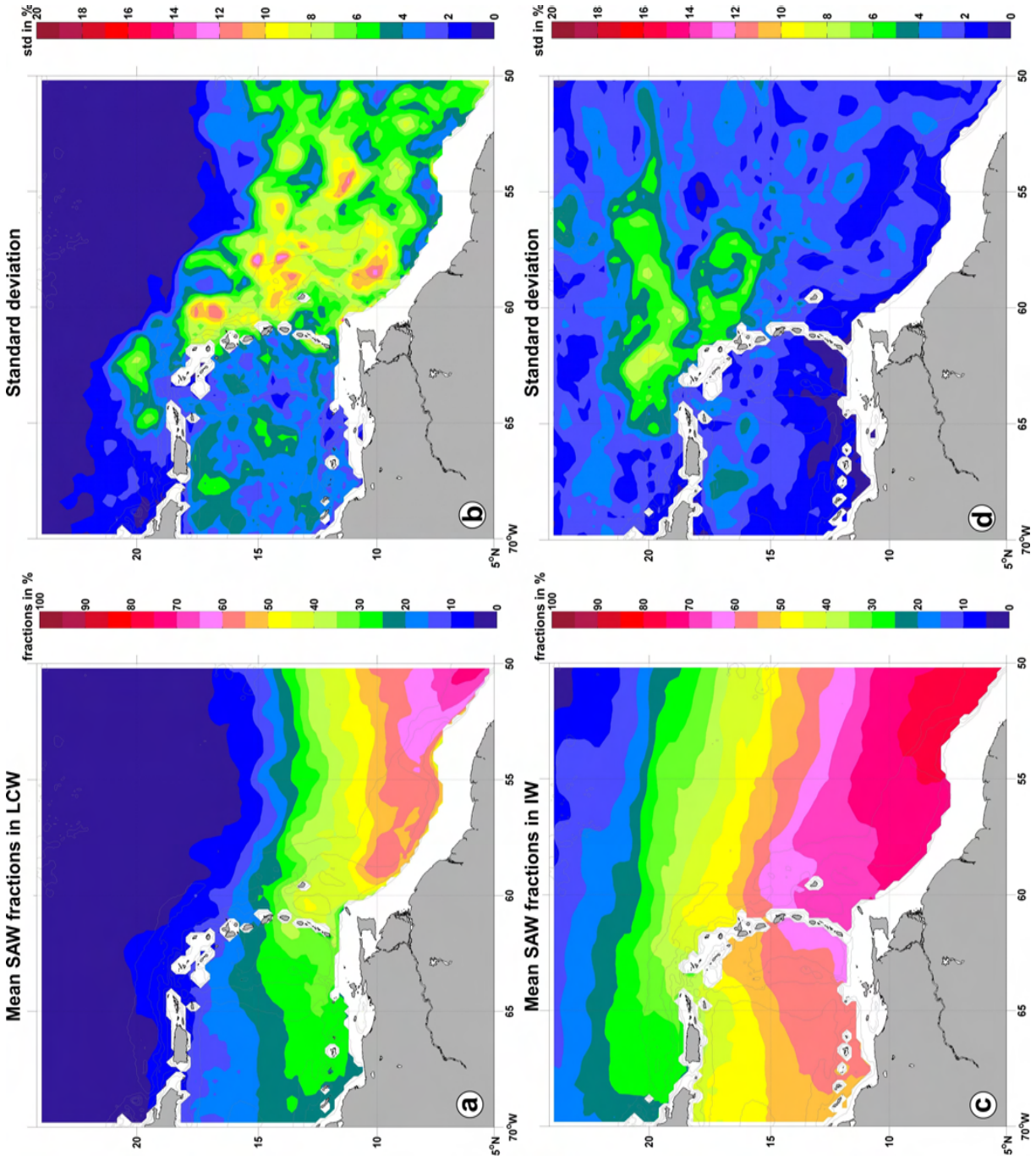

Figure 6.6: Mean South Atlantic Water distribution (in %) in the western tropical North Atlantic in FLAME_CLIM. (a): SAW distribution in LCW; (b): corresponding standard deviation; (c): Annual mean SAW distribution in IW; (d): corresponding standard deviation. The topography is the same as in Figures 6.3 and6.4. Note the different scales for the mean fractions and standard deviations.

The agreement between the SAW distribution obtained by Argo floats and ship measurements and the distribution in the FLAME model is best in the IW layer. Both results suggest a wide spreading of the southern IW into the North Atlantic. For the Central Water, observations and model agree on a low impact of UCW, but the model indicates generally less SAW fractions in both CW layers than the observations. The spreading of South Atlantic SMW is slightly enhanced in the model, compared to the observations. Both investigations denote high SAW fractions south of 10°N, confirming the high impact of the South Atlantic water masses to the equatorial current system. The observations and the model agree in decreasing variability with depth. The standard deviations are highest in the SMW layer in both cases and are very pronounced in the whole model area. The variability in the deeper layers (CW and IW) is less in FLAME_CLIM than in the observations.

6.4 Estimates for the saline South Atlantic SMW source

As already mentioned in Chapter 2, the SMW consists of three sources: a saline northern source, a saline southwestern source and a fresh southeastern source. With the T/S analysis applied, only the contributions of the northern and the southeastern source was calculated, the southwestern source is not covered by the approach. However, based on the geostrophic flow maps from Zhang et al. (2003), Rhein et al. (2005) estimated a SAW contribution from the saline southwestern source of 1.9 Sv to the Caribbean inflow.

With the analysis presented above a new approach for estimates of the southwestern source is attempted. The distribution of the fresh eastern South Atlantic SMW source near the equator from Figure 6.3 *a* shows fractions exceeding 70% at the western boundary region (2.5°N-5°N). East of this area the water is mainly composed of this fresh source: fractions of 80%-90% occur (40°W-30°W). These high fractions east of the boundary region indicate the flow direction of the fresh southeastern SMW: as noted in Chapter 2, it is brought to the western boundary with the equatorial branch of the SEC. The high contribution of the southeastern SMW source to the equatorial water masses has a fundamental effect on the spreading of the salty southwestern SMW source: its spreading is restricted, since the fresher eastern type dominates the equatorial region. Thus, at maximum 30% from the salty southwestern SMW source can contribute to the SMW layer near the equator at the western side of the basin. The contribution of the salty source to the NECC is less, only 20%-10% at maximum.

In Chapter 4 the SAW inflow into the Caribbean was calculated. In Table 4.3 the estimated SAW transports are summarized, based on the water mass analysis. The salty southwestern source of SMW was not included in this calculations. Since the transport of southern SMW to the Caribbean occurs assumably along the western boundary, the contribution of the southwestern source to the Caribbean inflow is somewhat blocked by the dominance of the southeastern source near the equator. An upper estimate of the SAW transport from the missing source is obtained, when considering that it can

at maximum increase the SAW flow in the SMW layer by 30% (as at maximum 30% of the equatorial waters are from this source). Applying this 30% supplement to the inflow of southeastern SMW (which is 1.0 Sv) results in an inflow from the southwestern SAW source of roughly 0.4 Sv. The observed mean SAW inflow into the Caribbean is increased by this approach to 8.8 Sv.

6.5 Float pathways to the Caribbean in FLAME

A float experiment in the FLAME_CLIM model marks water parcels in the passages and tracks the water back into their originating hemisphere. Artificial floats were introduced in the Caribbean inflow region at 11.5°N-16°N, 60.7°W (as indicated by the black line in Figure 6.7). 545 floats were placed in the SMW layer, distributed into the levels 76 m, 91 m, 108 m, 125 m and 145 m (at maximum/minimum 125/90 floats in one level, the exact number depending on topography). By a 3-year backward integration of the velocity field the origins of the floats were determined. In Figure 6.7 examples of the resulting float trajectories are given, separated by the originating hemisphere. The latitude 14.3°N separates the section into mainly northern and southern origin zones. At the shallower levels north of 14.3°N (76 m and 91 m) about half of the floats originate in the North Atlantic, indicating approx. 50% SAW contribution to this water. The deeper levels at 108 m, 125 m and 145 m showed a northern contribution of 85% (cf. Fig. 6.7 *a*); the deeper the floats are released, the higher the northern contribution is. South of 14.3°N the southern hemispheric floats dominate the upper SMW levels. At 76 m from 11.5°N to 12.5°N even 96% of the floats originate in the southern hemisphere (cf. Fig. 6.7 *b*). Nevertheless, the northern floats still dominate the deeper levels (108 m, 125 m, 145 m).

In the water masses below the SMW artificial floats were inserted as well. In the Central Water the separation of the northern and southern regimes at 14.3°N was evident as well: north of this latitude the floats are nearly totally of North Atlantic origin (90%), while south of 14.3°N the model provides 50% southern trajectories. A trend within the CW was apparent on the vertical scale as well: the contribution of southern floats increases at the deeper CW levels. This finding corresponds to the results of the water mass analysis applied in Chapter 4, where the contribution of SAW to the upper Central Water was found to be of minor importance. A float experiment in the IW layer showed, that the currents at depths below 580 m are too weak to track the floats backwards within three years. Even after 10 years of integration the origin of the majority of the floats was ambiguous.

The float experiments in the SMW layer of FLAME_CLIM are now used to obtain an estimate of the western South Atlantic source, which is missing in the water mass analysis (see Chapter 2 and the discussion in 6.4). The floats in the SMW, originating from the South Atlantic, are separated into eastern and western types. A ratio of 2:3, western:eastern source, is received by this approach.

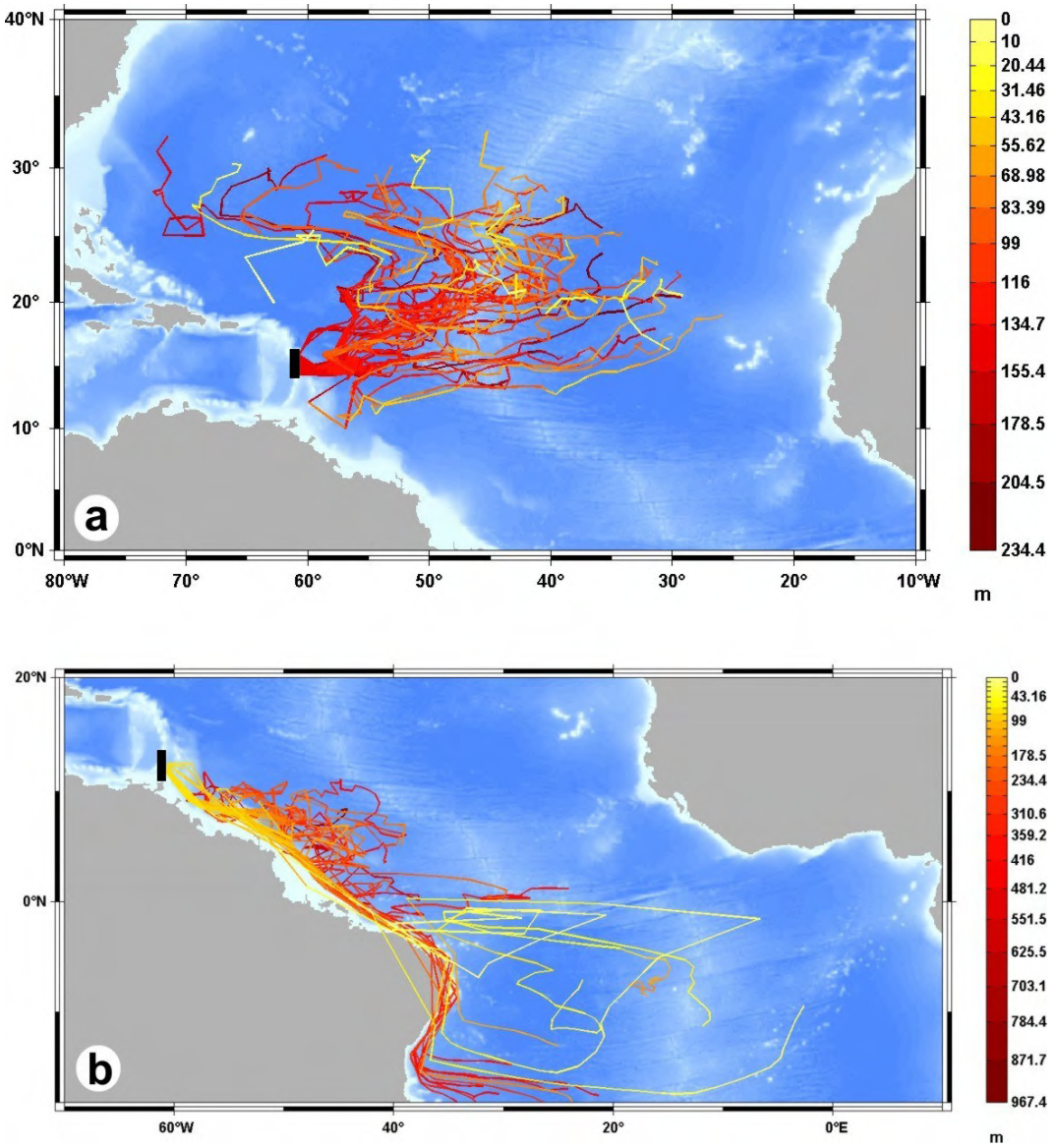

Figure 6.7: Examples for artificial float trajectories in FLAME. The positions are reported once in a month, the trajectories illustrated can thus cross over land. (a): examples of floats originating in the northern hemisphere, deployed on the 145 m level north of 14.3°N. (b): examples of floats originating in the southern hemisphere, deployed on the 76 m level south of 14.3°N. Note the different color scales.

In Chapter 4 the annual mean SAW inflow into the Caribbean south of Guadeloupe for FLAME_CLIM is specified (Table 4.4). For the shallow inflow a transport of 1.6 Sv occurs in the SMW layer from the southeastern source. This transport can be supplemented by 0.6 Sv from the southwestern source, increasing the SMW contribution to the inflow to 2.2 Sv. The model results acquired from the floats (1:3 source ratio) do not differ much from the obtained western South Atlantic contribution from Figure 6.3 *a* (max. 30% western contribution). The eastern South Atlantic source is more important than the western source in both cases.

6.6 Pathways revealed by Argo floats

Only a small number of Argo floats were deployed directly in the vicinity of the Caribbean Sea or into the boundary region off Brazil, north of the NBC retroflection. The profiles used in the analysis above are mainly obtained by floats entering the region from the north or by floats which were launched near the Mid-Atlantic Ridge. Nevertheless, some floats followed pathways from the equatorial Atlantic into the Caribbean or along the island arc up to 16°N. Their trajectories give hints on the SAW pathways and the velocities occurring and are discussed in the following.

In Figure 6.8 examples of Argo floats entering the Caribbean Sea are presented. The floats ascent every 10 days and their trajectories can be obtained by connecting the surface points. Of course, this method is not truly Lagrangian and biased by the surface flow and the currents in the layers during ascension. The movement of a float between two ascents is unknown, as it has no satellite connection when underwater. Thus the trajectories appear uncommonly straight and even cross over land (cf. Fig. 6.8 *a*). Unfortunately, some crucial information is lost for some floats deployed at the beginning of the Argo program, e.g. the depth in which the floats are assigned to drift (namely the parking depth). This is the case for all floats shown in Figure 6.8 *a*. The problem has been reported to the International Argo Information Center (AIC). The floats from Fig. 6.8 *b* are documented as requested.

float ID	launch date	last profile used	parking depth	mean speed	traj. in Fig.
49010	2000/01/12	2001/12/16	unknown	19 cms^{-1}	6.8 a: red
49022	2000/01/08	2002/11/10	unknown	17 cms^{-1}	6.8 a: black
31353	2000/01/23	2001/07/10	unknown	15 cms^{-1}	6.8 a: yellow
3900142	2000/11/13	2003/12/18	200 m	16 cms^{-1}	6.8 b: black
4900178	2002/02/23	2004/07/03	1000 m	7 cms^{-1}	6.8 b: red
4900754	2006/05/29	2007/08/02	1000 m	6 cms^{-1}	6.8 b: green
4900369	2003/06/04	2007/07/26	1000 m	4 cms^{-1}	6.8 b: yellow
49060	2001/03/24	2005/05/11	1100 m	6 cms^{-1}	6.8 b: magenta
49027	2000/01/10	2001/05/18	unknown	12 cms^{-1}	6.9 black
6900117	2004/11/30	2006/03/26	1000 m	9 cms^{-1}	6.9 red

Table 6.1: Deployment dates, dates of the last profile used and parking depths for all floats adopted in Figures 6.8 and 6.9.

Information accessible on the floats used in the figures are summarized in Table 6.1. The mean propagation speed was obtained by calculating the sum of the distances between the ascends and then dividing by the time difference between launch and the last profile. One can only speculate that the fast propagation of floats in Fig. 6.8 indicates a surface-near parking depth. The trajectories of unknown parking depth floats are presented here anyway, since the floats illustrate appealingly the inflow through the Lesser Antilles

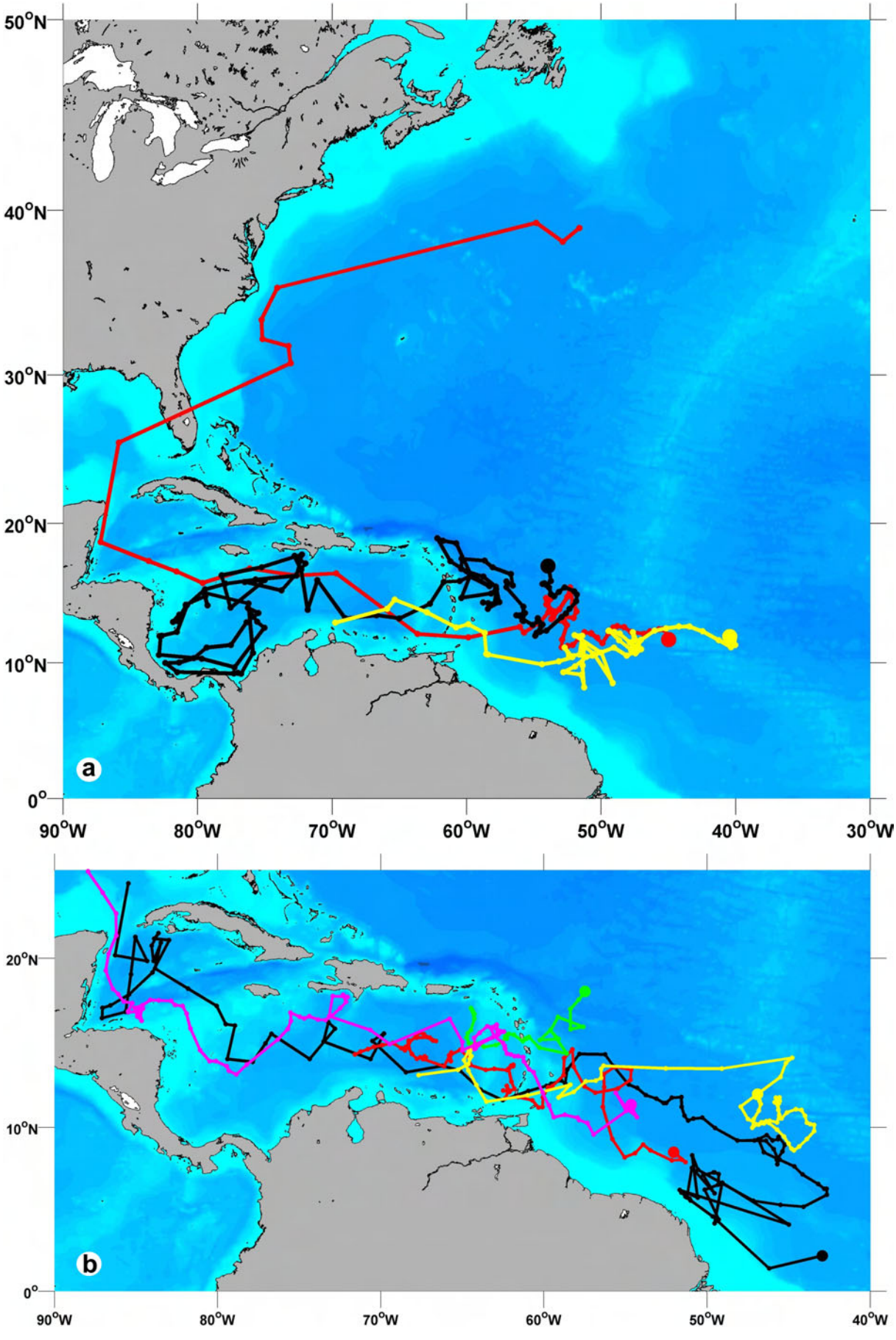

Figure 6.8: Trajectories of Argo floats. Large dots mark the locations of deployment. Float IDs are (a): 49010 (red), 49022 (black), 31353 (yellow) ; (b): 3900142 (black, parking depth: 200 m), 4900178 (red, parking depth: 1000 m), 4900754 (green, parking depth: 1000 m), 4900369 (yellow, parking depth: 1000 m), 49060 (magenta, parking depth: 1100 m)

Island arc. Float ID 49010 (Figure 6.8 *a*, red) continues its route directly into the Gulf of Mexico and the Gulf Stream and illustrates perfectly the pathway trough the Caribbean Sea into the Gulf Stream. All three trajectories in Figure 6.8 *a* demonstrate the turbulent, eddy-dominated velocity field east of the Lesser Antilles.

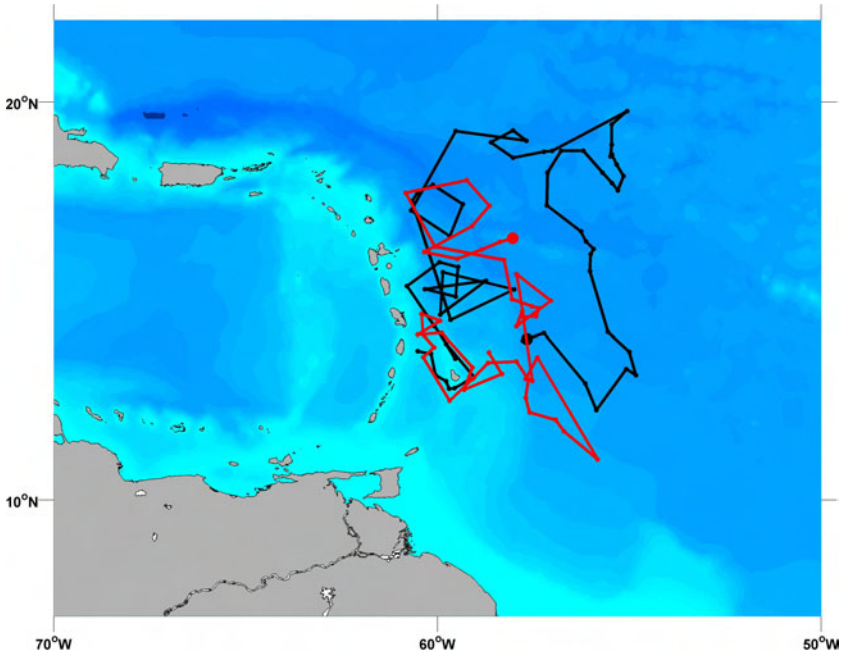

Figure 6.9: Trajectories of Argo floats. The larger dots mark the locations of deployment. Float IDs are 49027 (black) and 6900117 (red, parking depth: 1000 m).

The floats in Fig. 6.8 *b* move at a parking depth located within the deep part of the Intermediate Water, except for float 3900142 (black), which moves at a parking depth of 200 m. This float joins the NBC retroflection and makes a southeastward detour before propagating towards the Caribbean. The whole pathway from deployment to the Gulf of Mexico lasted three years. Float 49060 (magenta, 1100 m) took a similar route, but started further north. It was located 900 m deeper than float 3900142 and needed more than four years for its shorter journey. The currents at the 1100 m level were thus noticeably weaker than on the 200 m level. The other float trajectories presented in Figure 6.8 *b* are shorter and all on the 1000 m level. They indicate weak currents as well, since float 4900369 (yellow) needed more than four years for its trajectory. Slow currents in the IW are as well indicated by the trajectories of artificial floats in FLAME, see above.

In Figure 6.9 the circling of two floats east of the Caribbean is illustrated. Float 6900117 (red) is parked at 1000 m and the depth of float 49027 (black) is unknown as well. The similarity in its propagation suggests a similar parking depth, while the increased drifting speed hints to a parking in mid-depth (between 200 m and 1000 m). The float 49027 moves southeastward after deployment, but is then at 55°W carried northward, crossing even 20°N. It is advected westward and near 60°W turns southward again. The float trajectory indicates some cyclonic loops and ends near St. Lucia, after a clockwise movement around Barbados. Float 6900117 (red) moves with a slower speed and explores a smaller area

during its lifetime. The float shows similar looping movements and travels clockwise around Barbados as well. Both trajectories in Fig. 6.9 indicate interaction with rings east of the Lesser Antilles (cf. Chapter 5).

7 Discussion and Outlook

The Lesser Antilles Islands arc and the region north of the retroflection of the North Brazil Current were chosen to investigate the northward flow of South Atlantic Water into the northern hemisphere. This kind of flow represents the warm upper branch of the Meridional Overturning Circulation (MOC). This component of the MOC is difficult to observe since the wind driven subtropical gyres and the complex equatorial current system interact with the SAW flow. The area near the Lesser Antilles is one of the sparse locations suitable to directly observe the principal part of the net SAW flow. Here, most of the water masses from the North and South Atlantic can be distinguished by their different temperature and salinity features (Schmitz and Richardson, 1991, Poole and Tomczak, 1999, Rhein et al., 2005). This approach has been applied in this work to observational and modeled data. The inflow into the Caribbean through the Lesser Antilles Passages has been investigated closely in both the model data and the observations in Chapter 4. Since NBC rings contribute significantly to the northward transport of SAW, the ring transports and pathways have been examined in Chapter 5. All available hydrographic data have been used for a large scale analysis of the SAW distribution in the western tropical North Atlantic in Chapter 6. A comparison with the model was performed. In the following a short summary of the results is given and discussed, and the open questions remaining for further investigations are pointed out.

7.1 Caribbean inflow

Mean transports through the Lesser Antilles Passages into the Caribbean were calculated from shipboard ADCP measurements. Data from several ship surveys carried out by the University of Bremen have been used. Respective transport estimates inferred from these data were compared to estimates derived by Johns et al. (2002). In addition, two different model runs (FLAME_INTER and FLAME_CLIM) were analyzed, and respective transports were compared to the observed inflow. The mean inflow from observations was found to be 17.3 $\pm$ 4.8 Sv. Results from both model runs exceeded this inflow (FLAME_CLIM: 19.4 Sv $\pm$ 4.9 Sv; FLAME_INTER: 19.6 Sv $\pm$ 4.8 Sv). The somewhat simplified model bathymetry might be the cause of that difference. The FLAME results were closer to the observations than a previous model study by Johns et al. (2002). The FLAME model was able to reproduce general inflow features satisfyingly, but differences were noted within the details. The number of transport estimates derived from observations was sufficient to infer mean passage transports, but data were lacking to identify a seasonal cycle. Concerning the model analysis a seasonal cycle was only found in Grenada Passage in FLAME_INTER and in Anegada Passage in FLAME_CLIM.

The SAW calculations were restricted to the four cruises carried out by the University of Bremen, since hydrographic data is needed for the water mass analysis, which were not available for the other cruises. The distribution of SAW along the Lesser Antilles island arc indicates that the fractions of SAW in the passages are highest in the south (Grenada Passage) and decrease continuously when going further north. The deeper layers (IW and LCW) carry high SAW fractions, while low fractions are present in the UCW. For the SMW high variability in the SAW contributions are noted in the observational data, but the mean fractions were still lower than in UCW. The model analysis revealed that SAW fractions in FLAME_CLIM stayed below the observed fractions in all passages, while FLAME_INTER produced stronger SAW influence.

The mean SAW inflow into the Caribbean south of Guadeloupe was estimated to be 8.4 $\pm$ 2.4 Sv for the observations. This result was obtained by data from only four surveys and is thus less reliable than the estimates of the total inflow, especially when considering the errors of the water mass analysis as well. Nevertheless, the result agrees with the roughly 7 Sv of SAW flow entering the Caribbean presented by Wilson and Johns (1997). In comparison, model-derived estimates for these passages yield 7.6 $\pm$ 2.3 Sv SAW inflow in the FLAME_CLIM run (annual mean) and 10.2 $\pm$ 1.6 Sv in the FLAME_INTER run (15-year mean).

Differences between model results and observations with respect to SAW inflow result from the following disagreements: at first, the modeled total inflow does exceed the observed inflow. Since SAW transports were then obtained by relating the passage transports to calculated SAW fractions, the SAW transports reflect the differences in the SAW distribution along the island arc. The SAW fractions in FLAME_INTER were noticeably higher than the observed fractions which are again higher than the FLAME_CLIM fractions. The results from both model runs lie within the standard deviation of the observed inflow.

The most important difference between the observations and the model is found at the SAW inflow through St. Vincent and Grenada Passages. They are of similar relevance in the observations, but only a small proportion of the inflow occurs through St. Vincent passage in the model and Grenada Passage dominates the SAW inflow.

Johns et al. (1999) proposed a significant inflow through Anegada Passage. This could not be validated during the ship survey carried out in September 2005. The transport observed in this passage at this time was zero (yielding zero SAW transport as well). Nevertheless, FLAME indicated considerable variability in Anegada Passage, and during other cruises some inflow was detected (3-4 Sv). Further ship observations are needed to evaluate this topic since existing data is currently not extensive enough to solve related questions satisfactorily. Flow through Antigua Passage was noticeable during the cruise in September 2005 and 0.6 Sv of SAW inflow were calculated. The transport through Antigua Passage was less in the model, as the topographic representation prevents transports in the IW layer into the Caribbean. The sum of transports through Antigua and Anegada Passages is 0.5 Sv in FLAME_CLIM and 0.9 Sv in FLAME_INTER. The contribution of

the northern passages to the SAW inflow into the Caribbean is thus small.

The absence of a distinct seasonal signal in the observations near the Caribbean is somewhat surprising at first view. Seasonal variability in the equatorial currents is known from ship (Brandt et al., 2006) and model data (Giarolla et al., 2005). A strong connection between upper layer current variability and wind forcing is developed especially in the NECC, whose position shows a semiannual cycle as well (Fonseca et al., 2004). To investigate more closely the seasonal variability of Grenada Passage in the model, a time series covering 15 years at monthly resolution was analyzed in more detail (from FLAME_INTER). A period of 1 year was found to be the only important period for the inflow through Grenada Passage in the 15-year time series with monthly resolution. The maximum inflow occurred in May and the minimum in November. The amplitude of the 1 yr oscillation was 2.3 Sv for the SAW portion and 2.7 Sv for the total inflow. The latter agrees well with the model study by Johns et al. (2002). A further model time series covering two years at 3-day-resolution was found to be too short to reveal the impact of the seasonal cycle on the transport through Grenada Passage. This result agrees with the suggestion of Wilson and Johns (1997) that processes on other time scales may be of great importance to the transport variability at the southern Lesser Antilles. Assumably, the influence of North Brazil current rings passing east of Grenada Passage masks the seasonal signal on short time series. It is thus not surprising that the few observations in the passages are not sufficient to resolve the seasonal cycle.

7.2 NBC ring propagation

The SAW flow across 16°N results from the northward propagation of anticyclonic rings produced in the NBC retroflection region. These rings carry high amounts of south Atlantic origin water, especially in the intermediate layer. The observations at 16°N revealed the existence of NBC rings along the section, which could be identified in the SAW distributions and velocity field. All rings were found to be deep reaching, and both surface and subsurface intensified types were found. A peculiar feature was present in the velocity field of one particular survey and could be interpreted as an cyclonic eddy. This is not consistent with rings produced in the NBC retroflection region having an anticyclonic sense of rotation. The maxima in the corresponding SAW distribution nevertheless were displaced to the center of this cyclone, rather indicating an anticyclone. Both interpretations are possible and the data is not sufficient to exclude either the cyclonic or the anticyclonic case.

Although shallow, surface intensified rings are frequently encountered south of 10°N in the ring translation corridor along the South American coast (see Wilson et al., 2002 or Johns et al., 2003), these shallow types seem to disintegrate before reaching 16°N. Identified rings showed a mean diameter of 260 km and a mean ring volume of $5.7 \cdot 10^{13}\ m^3$. These values are of the same magnitude as are obtained from deep reaching rings (Johns

et al., 2003) as well as from the analysis of drifter trajectories (Fratantoni and Richardson, 2006).

Results from the water mass analysis and ring properties were combined to infer the SAW flow within the rings. The mean SAW transport estimated from ship measurements was 0.8 Sv per ring. Assuming that the observed rings are typical and that 6.5-8.5 rings per year reach 16°N (assuming the ring production rate presented by Goni and Johns, 2003 and Johns et al., 2003), the annual mean SAW ring transport across 16°N amounts to 6 Sv.

In the FLAME model NBC rings are produced as well, they approach the Lesser Antilles from the southeast. The region 10°N-18°N, 58°W-64°W was analyzed for the modeled years 2003-2004. The water mass analysis was again found to be a useful tool, as the tracking of NBC rings was easy when combining the SAW distribution with the velocity field. Especially in the UCW layer rings are outstanding features in the SAW distribution. Current speeds are low outside of rings in the subsurface layers. The rings represent high velocity events with an anticyclonic sense of rotation in the current field. The surface currents are not influenced by the presence of the Lesser Antilles in FLAME. Thus the TSW layer will not reproduce the real ring propagation.

Within the two modeled years eight rings were identified in the subsurface layers, entering the region between 58°W and 61°W. The mean diameter was 200-250 km below 200 m depth. No exclusive subsurface intensified rings were found at 11°N in the FLAME INTER model run. The rings moved northwestward around Tobago and were trapped in the topographic triangle of Tobago, St. Lucia and Barbados. The rings were reduced to a diameter of 180 km by volume export to the Caribbean, finally passing through the St. Lucia-Barbados gap. Some of the rings did not continue their path northward, but were disintegrated totally at this topographic trap. Streamers were separated from the trapped rings, which either migrated clockwise around Barbados (sometimes forming new vortices with subsequent NBC rings) or formed new anticyclonic and sometimes cyclonic rings north of Barbados. Although the influence of the Lesser Antilles on the NBC rings was found to be complex, the presented consequences of interaction with the islands corresponded well to the results of laboratory experiments from Cenedese et al. (2005). A clockwise movement around Barbados was described by Fratantoni and Richardson (2006) for drifter pathways. The import into the Caribbean from the reduction of the ring volume at the Lesser Antilles probably follows the same mechanisms. The streams passing through the Windward Island Passages eventually induce new ring formation, since both anticyclones and cyclones have been observed in the eastern Caribbean Sea as well (Richardson, 2005). High eddy activity in the Caribbean Sea is equally indicated by Argo trajectories.

When considering the model results, the cyclone found in the observations becomes a possible feature, formed as a result of NBC ring interaction with the St. Lucia-Barbados gap. Since the cyclones in the model are formed out of streams leaking northwards through the gap, the displaced SAW distribution of the cyclone is consistent with this interpreta-

tion. Richardson (2005) and Fratantoni and Richardson (2006) described cyclones north and east of the Leeward Islands from drifter trajectories. Fratantoni and Richardson (2006) even connected the apparent cyclone north of Barbados with the accelerated flow through the St. Vincent-Barbados gap. The observed cyclonic vortex drifted northward along the island arc.

Another ring pathway was revealed by the model. One anticyclone was found to approach Guadeloupe from the east, by a strictly westward movement along 16°N. This ring had a diameter of 270 km and was subsurface intensified. A distinct core of SAW was found in the LCW layer (65% SAW). The rings discussed before were strongly reduced by the presence of the Lesser Antilles and could not yield diameters of more than 180 km north of Barbados, unless they were newly-formed by the streams. The observed rings at 16°N nevertheless provided a mean ring diameter of 260 km, thus indicating that at least one other pathway for NBC rings exists, where the original diameter is virtually preserved. Richardson (2005) found drifter moving southwestward within an anticyclone east of Guadeloupe, matching the ring pathway in FLAME. Argo float trajectories indicated anticyclonic vortices in the IW layer off Guadeloupe as well. This pathway outside of the influence of the topography at the Lesser Antilles will be the topic of further investigations, as well as the fate of the rings north of Guadeloupe.

The investigation of rings in FLAME has thus provided three mechanisms for rings reaching 16°N off Guadeloupe: firstly, NBC rings can approach the Lesser Antilles from the southeast, interact with the islands and be reduced to small vortices (approx. 180 km in diameter) when reaching 16°N. Secondly, rings may take the same pathway, but disintegrate totally at the islands and new eddies (anticyclonic and cyclonic) are formed out of streams north of Barbados which propagate to 16°N. This newly-formed rings probably have a deformed SAW core and a less pronounced maximum in SAW due to mixing with the waters north of Barbados. At last, one model ring was found to propagate along 16°N westward, carrying a distinct SAW core, indicating unhindered propagation from the formation region. The model analysis was restricted to 58°W and the history of this ring before reaching 16°N is unknown yet. The last pathway was of low importance in the model, only one ring was found during the two year period investigated.

Fratantoni and Richardson (2006) suggested a separation of rings at 200-400 m, in an upper and a lower part, at the latitude of Tobago. The shallow part was found to propagate further northwestward, while the deeper part remained near Tobago, interacting with subsequent rings. Ring-ring interactions were found to be commonplace by Fratantoni and Richardson (2006). The model exhibits ring-ring interaction as well, but the separation of rings in two parts could not be validated in the model analysis.

7.3 Spreading of SAW

The large-scale distribution of SAW was investigated by hydrographic ship measurements and profiles from Argo floats. The analysis revealed the mean SAW propagation into

the North Atlantic and identified the ring translation corridor along the South American coast as the region of largest variability. SAW was found to dominate the region east of 50°W and south of 10°N, here mean SAW fractions reached 60%-100% in all density layers. Thus, water masses transported by the equatorial currents including the EUC, NECC and the NEUC essentially comprise SAW. The transition region from SAW to NAW was zonally inclined in the upper two layers (SMW and UCW), extending from Trinidad to 15°N, 30°W. In the lower layers (LCW and IW), the transition region was stretched from 12°N to 18°N for the LCW and to 20°N for the IW and not declined. The SAW distribution was smooth and the SAW influence gradually decreased from south to north. On the locations of the transition regions elevated standard deviations were found. They indicated existent variability in the position of the transition zones: they may migrate northward and southward. IW originating from the South Atlantic was found to spread the farthest into the North Atlantic. The southern UCW was most restricted to the equatorial region. Currently, the spatial and temporal data resolution is not extensive enough to allow for analyzing seasonal changes or interannual variability. The Argo program shows promise in providing these data in the future. One aim will be to improve the resolution of the observational analysis and identify the areas of water mass variability in more detail and to validate the mean values in the regions with low data resolution. A separation into seasons would be the next step, when sufficient data coverage is available for all seasons. While FLAME confirms a seasonal cycle in Grenada Passage, this question is still unanswered from the ship derived data.

The salty SMW source was not included in the water mass analysis. However, the analysis of the large-scale SAW distribution was suitable to obtain an estimate for the SMW contribution to the Caribbean inflow. The spreading of SMW from this source is restricted, since the fresher eastern type dominates the equatorial region. Thus, at maximum 30% of salty southwestern SMW can contribute to the SMW layer near the equator and consequently to the Caribbean inflow as well. If this contribution is taken into account the observed mean SAW inflow into the Caribbean is increased to 8.8 Sv (compared to 8.4 Sv without the SMW contribution).

The FLAME_CLIM model run was used to investigate the SAW distribution in the model. The model results point to a wide spreading of southern IW into the North Atlantic as well. Observations and model agreed on a low impact of UCW to the SAW transports, but the model indicated generally less SAW fractions in both CW layers than the observations. The spreading of South Atlantic SMW is slightly enhanced in the model, compared to the observations. The SMW is the layer of largest variability in the model. Artificial floats were released in the model velocity field near the Lesser Antilles, and an estimate for the missing southwestern SMW source was obtained by analyzing their trajectories. The floats in the SMW, originating from the South Atlantic, were separated into eastern and western types. A ratio of 1:3, western:eastern source, was received by this approach. For the shallow inflow a transport of 1.6 Sv occurs in the SMW layer from the southeastern source in FLAME_CLIM. This transport can be supplemented by 0.6 Sv from the southwestern source, increasing the SMW contribution to the inflow to 2.2 Sv.

7.4 Total SAW transport and implications for the MOC flow

In Figure 7.1 the resulting SAW transport through the Lesser Antilles islands arc is illustrated. Transports presented there are derived from calculations presented in Chapter 4 (Tables 4.3-4.5). They include the flow through Anegada and Antigua Passage, complemented with the estimate for the missing SMW source introduced in Chapter 6. In the upper two layers (TSW+SMW), 6.6 Sv are obtained from the observations and the FLAME_INTER results. The FLAME_CLIM run exhibits less inflow in this layers, 5.8 Sv in the mean. The Central Water flow is 2.0 Sv in the observations. The model shows less inflow in the climatological run in this layer (1.1 Sv) and stronger inflow in the FLAME_INTER run (2.4 Sv). A clear disagreement between the observations and the model is found in the intermediate layer. While the observed transport is only 0.7 Sv, the model results are 1.7 Sv and 2.7 Sv in this layer. The reasons for this discrepancy were discussed before: the modeled SAW transport in this layer is increased by higher SAW fractions in the IW (which is especially the case in FLAME_INTER.).

The total SAW inflow into the Caribbean through the Lesser Antilles islands arc is thus estimated to be 9.3 Sv inferred from observations. A similar annual mean transport of 8.6 Sv was obtained from the climatological run of FLAME, while FLAME_INTER exhibits slightly stronger mean inflow (10.7 Sv for a time series of 15 years). When considering the errors of this approach and the assumptions made, the agreement between the results from the observations and both model runs is reasonable.

From hydrographic data and studies with an inverse model Ganachaud and Wunsch (2000) estimated 16-18 Sv of upper layer MOC transport crossing the equator and thus balancing the net deep water export. When adding the Caribbean SAW inflow and the ring transport estimates for SAW (6 Sv, Chapter 5), the total SAW transport investigated in this work is 15.3 Sv for the observations. 7.5 Sv (50%) occur within the upper layers (TSW+SMW), the Central Water contribution is 3.5 Sv (22%), and the Intermediate Water transport sums up to 4.3 Sv (28%). While most of the upper layer and CW flow takes the Caribbean pathway through the Lesser Antilles (78%), the IW transport mostly occurs at 16°N in the NBC rings (84%). The MOC return flow, which takes the interior pathway through the Atlantic via the STCs (Chapter 1), must thus be rather small, as only 1-3 Sv were missing at the western boundary.

The overturning stream function in FLAME amounts to 16 Sv of deep water transported southward in the tropical region (Hüttl and Böning, 2006). Subtracting 1 Sv of northward bottom water flow, the warm northward MOC transport is in the order of 15 Sv in the model. Of this 15 Sv, 11 Sv occur in the surface and central water layers, only 4 Sv remain in the intermediate layer (cf. Hüttl and Böning (2006), their Figure 1 c). The annual mean SAW inflow into the Caribbean was 8.6 Sv in FLAME_INTER, whereof 1.7 Sv pass in the IW. Hence, the MOC flow which does not take the Caribbean route in FLAME_CLIM is 2.3 Sv in the IW and 4.1 Sv in the layers above. The relevance of the Caribbean pathway in FLAME_INTER is even more pronounced: only 1.3 Sv in the IW

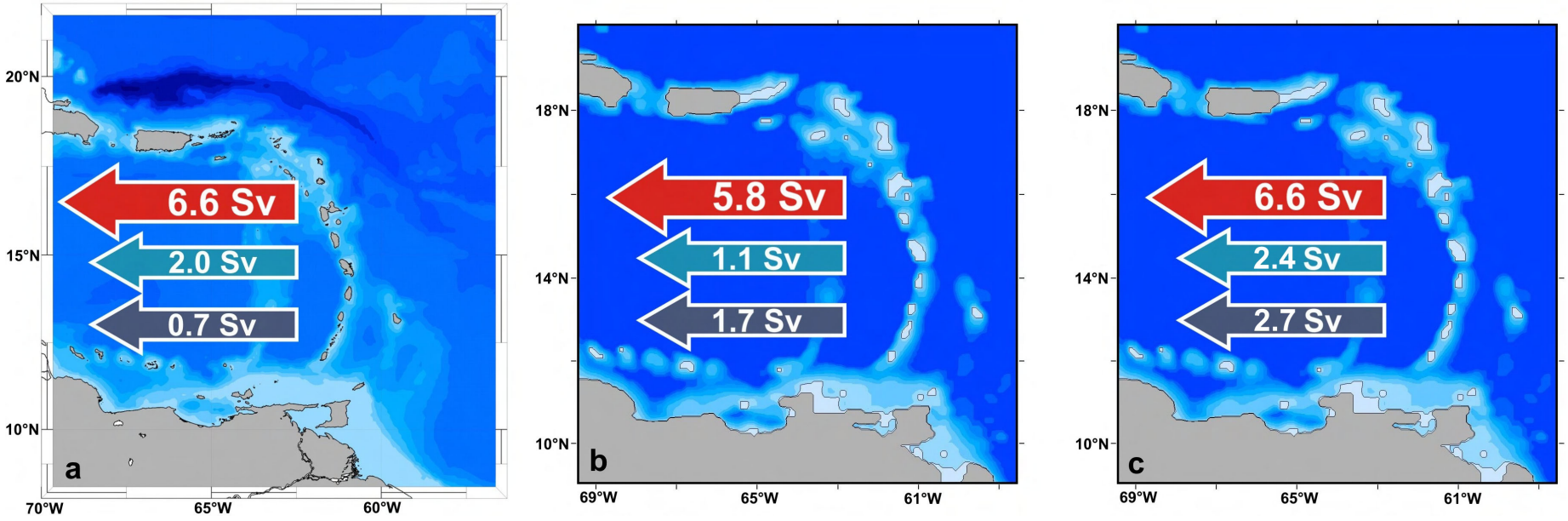

Figure 7.1: Mean South Atlantic Water inflow into the Caribbean Sea. Red arrows indicate the upper warm water flow (TSW+SMW), blue arrows the CW and dark blue arrows the IW. Transports are derived from (a) observations, (b) the FLAME_CLIM model run, and (c) the FLAME_INTER model run.

layer and 2 Sv in the layers located above take the Atlantic route. Assuming the interior Atlantic pathways are of minor importance in the model as well, the northward transport by NBC rings into the northern subtropical gyre is 3.3 Sv. This estimate indicates a lower ring transport independent from the Caribbean as observed (that was 6 Sv). The rapid disintegration of modeled NBC rings at the Lesser Antilles, which were described in the model analysis of Chapter 5, might thus exceed the real ring decomposition. Of course, the effect of the model bathymetry, lacking the small islands of the Lesser Antilles at the the surface, increases the modeled transport into the Caribbean as well.

The combination of observational data and model results as presented in this study has shed light on important aspects of the subtropical circulation in the North Atlantic. Its relevance for the MOC was investigated and the composition of water masses and the import of SAW into the northern hemisphere of the Atlantic Ocean analyzed. Comparing the model output with observations helps to identify model-dependent deficits and similarities to the "real" ocean. As was pointed out earlier several question yet remain open and are left for future work. For example, the Atlantic pathways and the fate of NBC rings in the FLAME model north of Barbados deserve further investigations.

References

M. Arhan, A. Colin de Verdière, and L. Mémery. The eastern boundary of the subtropical North Atlantic. *Journal of Physical Oceanography*, 24:1295–1316, 1994.

M. Baklouti, J.-L. Devenon, A. Bourret, J.-M. Froidefond, J.-F. Ternon, and J.-L. Fuda. New insights in the French Guiana continental shelf circulation and its relation to the North Brazil Current retroflection. *Journal of Geophysical Research*, 112(C02023): doi:10.1029/2006JC003520, 2007.

W.H. Berger and G. Wefer. Expeditions into the Past: Paleoceanographic Studies in the South Atlantic. In G. Wefer, W.H. Berger, G. Siedler, and D.J. Webb, editors, *The South Atlantic: Present and past circulation*, pages 363–410. Springer-Verlag Berlin Heidelberg, 1996.

C.W. Böning, F.O. Bryan, W.R. Holland, and R. Döscher. Deep-water formation and meridional overturning in a high-resolution model of the North Atlantic. *Journal of Physical Oceanography*, 26:1142–1164, 1996.

C.W. Böning, M. Scheinert, J. Dengg, A. Biastoch, and A. Funk. Decadal variability of subpolar gyre transport and its reverberation in the North Atlantic overturning. *Geophysical Research Letters*, 33(LS21S01):doi:10.1029/2006GL026906, 2006.

B. Bourles, R.L. Molinari, E. Johns, W.D. Wilson, and K.D. Leaman. Upper layer currents in the western tropical North Atlantic (1989-1991). *Journal of Geophysical Research*, 104:1361–1375, 1999.

P. Brandt, F.A. Schott, C. Provost, A. Kartavtseff, V. Hormann, B. Bourles, and J. Fischer. Circulation in the central equatorial Atlantic: Mean and intraseasonal to seasonal variability. *Geophysical Research Letters*, 33(L07609):doi:10.1029/2005GL025498, 2006.

W.S. Broecker. The great ocean conveyor. *Oceanography*, 4, No. 37:79–89, 1991.

C. Cenedese, C. Adduce, and D.M. Fratantoni. Laboratory experiments on mesoscale vortices interacting with two islands. *Journal of Geophysical Research*, 101(C09023): doi:10.1029/2004JC002734, 2005.

P.U. Clark, N.G. Pisias, T.F. Stocker, and A.J. Weaver. The role of the thermohaline circulation in abrupt climate change. *Nature*, 415:863–869, 2002.

R. Curry. HydroBase 2: a database of hydrographic profiles and tools for climatological analysis. Technical report, Technical Reference, 2001.

J. Dengg, C.W. Böning, U. Ernst, R. Redler, and A. Beckmann. Effects of an improved model representation of overflow water on the subpolar North Atlantic. *International WOCE Newsletter*, No. 37, WOCE International Project Office, Southampton, United Kingdom:10–15, 1999.

A. Dessier and J.R. Donguy. The sea surface salinity in the tropical Atlantic between 10°S and 30°N - seasonal and interannual variations (1977-1989). *Deep-Sea Research I*, 41:81–100, 1994.

R.R. Dickson and J. Brown. The production of North Atlantic Deep Water: Sources, rates, and pathways. *Journal of Geophysical Research*, 99(C6):12319–12341, 1994.

N. Didden and F. Schott. Eddies in the North Brazil Current retroflection region observed by Geosat altimetry. *Journal of Geophysical Research*, 98:20121–20131, 1993.

J.-C. Duplessy. Climate and the Gulf Stream. *Nature*, 402:593–595, 1999.

C. Eden and C.W. Böning. Sources of eddy kinetic energy in the Labrador Sea. *Journal of Physical Oceanography*, 32:3346–3363, 2002.

C.A. Fonseca, G.J. Goni, W.E. Johns, and E.J.D. Campos. Investigation of the North Brazil Current retroflection and North Equatorial Countercurrent variability. *Geophysical Research Letters*, 31(L21304):doi:10.1029/2004GL20054, 2004.

D. Fratantoni and D. Glickson. North Brazil Current Ring generation and evolution observed with SeaWiFS. *Journal of Physical Oceanography*, 32:1058–1074, 2002.

D. Fratantoni and P.L. Richardson. The Evolution and Demise of North Brazil Current Rings. *Journal of Physical Oceanography*, 36:1241–1264, 2006.

D.M. Fratantoni, W.E. Johns, T.L. Townsend, and H.E. Hurlburt. Low-Latitude Circulation and Mass Transport Pathways in a Model of the Tropical Atlantic Ocean. *Journal of Physical Oceanography*, 30:1944–1966, 2000.

A. Ganachaud and C. Wunsch. Improved estimates of global ocean circulation, heat transport and mixing from hydrographic data. *Nature*, 408:453–457, 2000.

Z.D. Garraffo, W.E. Johns, E.P. Chassignet, and G.J. Goni. North Brazil Current rings and transport of southern waters in a high resolution numerical simulation of the North Atlantic. In G.J. Goni and P. Malanotte-Rizzoli, editors, *Interhemispheric Water Exchange in the Atlantic Ocean*, chapter 15, pages 375–410. Elsevier Oceanography Series, 2003.

S.L. Garzoli, A. Ffield, and Q. Yao. North Brazil Current rings and the variability in the latitude of retroflection. In G.J. Goni and P. Malanotte-Rizzoli, editors, *Interhemispheric Water Exchange in the Atlantic Ocean*, chapter 14, pages 357–374. Elsevier Oceanography Series, 2003.

S.L. Garzoli, A. Ffield, W.E. Johns, and Q. Yao. North Brazil Current retroflection and transports. *Journal of Geophysical Research*, 109(C01013):doi:10.1029/2003JC001775, 2004.

E. Giarolla, P. Nobre, M. Malagutti, and L.P. Pezzi. The Atlantic Equatorial Undercurrent: PIRATA observations and simulations with GFDL Modular Ocean Model at CPTEC. *Geophysical Research Letters*, 32(L10617):doi:10.1029/2004GL022206, 2005.

C.F. Giulivi and A.L. Gordon. Isopycnal displacements within the Cape Basin thermocline as revealed by the hydrographic data archive. *Deep Sea Research I*, 53: doi:10.1016/j.dsr.2006.05.011, 2006.

G.J. Goni and W.E. Johns. Synoptic study of warm rings in the North Brazil Current retroflection region using satellite altimetry. In G.J. Goni and P. Malanotte-Rizzoli, editors, *Interhemispheric Water Exchange in the Atlantic Ocean*, chapter 13, pages 335–356. Elsevier Oceanography Series, 2003.

G.R. Halliwell, Jr., R.H. Weisberg, and D.A. Mayer. A synthetic float analysis of upper-limb meridional overturning circulation interior ocean pathways in the tropical/subtropical Atlantic. In G.J. Goni and P. Malanotte-Rizzoli, editors, *Interhemispheric Water Exchange in the Atlantic Ocean*, chapter 11, pages 287–312. Elsevier Oceanography Series, 2003.

F.L. Hellweger and A.L. Gordon. Tracing Amazon River water into the Caribbean Sea. *Journal of Marine Research*, 60:537–549, 2002.

C. Hu, E.T. Montgomery, R.W. Schmitt, and F.E. Muller-Karger. The dispersal of the Amazon and Orinoco River water in the tropical Atlantic and Caribbean Sea: Observation from space and S-PALACE floats. *Deep-Sea Research II*, 51:1151–1171, 2004.

S. Hüttl and C.W. Böning. Mechanisms of decadal variability in the shallow subtropical-tropical circulation of the Atlantic Ocean: A model study. *Journal of Geophysical Research*, 111(C07011):doi:10.1029/2005JC003414, 2006.

W.E. Johns, T.N. Lee, F. Schott, R.J. Zantopp, and R.H. Evans. The North Brazil Current retroflection: seasonal structure and eddy variability. *Journal of Geophysical Research*, 95:22103–22120, 1990.

W.E. Johns, T.L. Townsend, D.M. Fratantoni, and W.D. Wilson. On the Atlantic inflow to the Caribbean Sea. *Deep Sea Research I*, 49:211–243, 2002.

W.E. Johns, R.J. Zantopp, and G.J. Goni. Cross-gyre transport by North Brazil Current rings. pages 411–441, 2003.

E. Kalnay, M. Kanamitsu, R. Kistler, W. Collins, D. Deaven, L. Gandin, M. Iredell, S. Saha, G. White, J. Woollen, Y. Zhu, M. Chelliah, W. Ebiszusaki, W. Higgins, J. Janowiak, K. Mo, C. Ropelewski, J. Wang, A. Leetma, R. Reynolds, R. Jenne, and

J. Joseph. The NCEP/NCAR 40-Year Reanalysis Projekt. *Bulletin of the American Meteorological Society*, 77(3):437–471, 1996.

P.S. Kelly, K.M.M. Lwiza, R.K. Cowen, and G.J. Goni. Low-salinity pools at Barbados, West Indies: Their origin, frequency, and variability. *Journal of Geophysical Research*, 105(C8):19699–19708, 2000.

D. Kieke. *Water mass circulation and variability in the subpolar North Atlantic*. PhD thesis, University of Bremen, 2005.

K. Kirchner, M. Rhein, C. Mertens, C.W. Böning, and S. Hüttl. Observed and modeled MOC related flow into the Caribbean. *Journal of Geophysical Research*, (in revision), 2007.

B. Klein and M. Tomczak. Identification of diapycnal mixing through optimum multiparameter analysis 2. Evidence for unidirectional diapycnal mixing in the front between North and South Atlantic Central Water. *Journal of Geophysical Research*, 99(C12): 25275–25280, 1994.

J.R.E. Lutjeharms. The exchange of water between the South Indian and South Atlantic Oceans. In G. Wefer, W.H. Berger, G. Siedler, and D.J. Webb, editors, *The South Atlantic: Present and past circulation*, pages 125–162. Springer-Verlag Berlin Heidelberg, 1996.

M. Lux, H. Mercier, and M. Arhan. Interhemispheric exchanges of mass and heat in the Atlantic Ocean in January-March 1993. *Deep Sea Research I*, 48:605–638, 2001.

J.F. McManus, R. Francois, J.-M. Gherardi, L.D. Keigwin, and S. Brown-Leger. Collapse and rapid resumption of Atlantic meridional circulation linked to deglacial climate changes. *Nature*, 428:834–837, 2004.

L. Mémery, M. Arhan, X.A. Alvarez-Salgado, M.-J. Messias, H. Mercier, C.G Castro, and A.F. Rios. The water masses along the western boundary of the south and equatorial Atlantic. *Progress in Oceanography*, 47:69–98, 2000.

E. Oka and K. Ando. Stability of temperature and conductivity sensors of Argo profiling floats. *Journal of Oceanography*, 60:253–258, 2004.

R. Pacanowski. MOM2 documentation, users guide and reference manual. Technical report, GFDL Ocean Group, Geophysical Fluid Dynamics Laboratory, Princeton, NJ, 329 pp., 1995.

R. Poole and M. Tomczak. Optimum multiparameter analysis of the water mass structure in the Atlantic Ocean thermocline. *Deep Sea Research I*, 46:1895–1921, 1999.

S. Rahmstorf. Thermohaline ocean circulation. In S.A. Elias, editor, *Encyclopedia of Quaternary Sciences*. Elsevier Oceanography Series, 2006.

M. Rhein, K. Kirchner, C. Mertens, R. Steinfeldt, M. Walter, and U. Fleischmann-Wischnath. Transport of South Atlantic Water through the passages south of Guadeloupe and across 16°N, 2000-2004. *Deep Sea Research I*, 52:2234–2249, 2005.

P.L. Richardson. Caribbean Current and eddies as observed by surface drifters. *Deep Sea Research II*, 52:429–463, 2005.

Q. Schiermeier. Artefacts in ocean data hide rising temperatures. *Nature*, 447:8–9, 2007.

W.J. Schmitz, Jr. and P.L. Richardson. On the sources of the Florida Current. *Deep Sea Research (Suppl. 1)*, 38:S379–S409, 1991.

F.A. Schott, J. Fischer, and L. Stramma. Transports and pathways of upper layer circulation in the western tropical Atlantic. *Journal of Physical Oceanography*, 28(10): 1904–1928, 1998.

S.R. Signorini, R.G. Murtugudde, C.R. McClain, J.R. Christian, J. Picaut, and A.J. Busalacchi. Biological and physical signatures in the tropical and subtropical Atlantic. *Journal of Geophysical Research*, 104(C8):18367–18382, 1999.

D. Snowden and R. Molinari. Subtropical cells in the Atlantic Ocean: An observational summary. In G.J. Goni and P. Malanotte-Rizzoli, editors, *Interhemispheric Water Exchange in the Atlantic Ocean*, chapter 11, pages 287–312. Elsevier Oceanography Series, 2003.

H. Stommel. Asymmetry of interoceanic fresh-water and heat fluxes. *Proc. Natl. Acad. Sci. USA*, 77(5):2377–2381, 1980.

L. Stramma and M. England. On the water masses and mean circulation of the South Atlantic Ocean. *Journal of Geophysical Research*, 104(C9):20863–20883, 1999.

L. Stramma and F.A. Schott. The mean flow field of the tropical Atlantic Ocean. *Deep-Sea Research II*, 46:279–303, 1999.

L. Stramma, M. Rhein, P. Brandt, M. Dengler, C.W. Böning, and M. Walter. Upper ocean circulation in the western tropical Atlantic in boreal fall 2000. *Deep-Sea Research I*, 52:221–240, 2005.

L.D. Talley. Antarctic Intermediate Water in the South Atlantic. In G. Wefer, W.H. Berger, G. Siedler, and D.J. Webb, editors, *The South Atlantic: Present and past circulation*, pages 363–238. Springer-Verlag Berlin Heidelberg, 1996.

M. Tsuchiya. Cirulation of the Antarctic Intermediate Water in the North Atlantic. *Journal of Marine Research*, 47:747–755, 1989.

J. Willebrand, B. Barnier, C.W. Böning, C. Dieterich, P.D. Killworth, C. Le Provost, Y. Jia, J.-M. Molines, and A.L. New. Circulation characteristics in three eddy-permitting models of the North Atlantic. *Progress in Oceanography*, 48:123–161, 2001.

W.D. Wilson and W.E. Johns. Velocity structure and transport in the Windward Island Passages. *Deep-Sea Research I*, 44(3):487–520, 1997.

W.D. Wilson, E. Johns, and R.L. Molinari. Upper layer circulation in the western tropical North Atlantic Ocean during August 1989. *Journal of Geophysical Research*, 99(C1): 22513–22523, 1994.

W.D. Wilson, W.E. Johns, and S.L. Garzoli. Velocity structure of North Brazil Current rings. *Geophysical Research Letters*, 29(8):doi:10.1029/2001GL013869, 2002.

C. Wunsch. What is the thermohaline circulation? *Science*, 298:1179–1180, 2002.

D. Zhang, M.J. McPhaden, and W.E. Johns. Observational evidence for flow between the subtropical and tropical Atlantic: The Atlantic subtropical cells. *Journal of Physical Oceanography*, 33:1783–1797, 2003.

I presented preliminary results of this work on the following international conferences and workshops as first author:

April 2005	Poster presentation on the General Assembly of the European Geosciences Union in Vienna (Austria)
October 2005	Oral presentation on the Tropical Atlantic Variability Workshop in Venice (Italy)
April 2006	Poster presentation on the General Assembly of the European Geosciences Union in Vienna (Austria)
October 2005	Oral presentation on the Tropical Atlantic Variability Workshop in Paris (France)
April 2007	Oral presentation on the General Assembly of the European Geosciences Union in Vienna (Austria)

Parts of the results were already published in international journals

M. Rhein, K. Kirchner, C. Mertens, R. Steinfeldt, M. Walter, and U. Fleischmann-Wischnath. Transport of South Atlantic Water through the passages south of Guadeloupe and across 16°N, 2000-2004. *Deep Sea Research I*, 52:2234–2249, **2005**.

K. Kirchner, M. Rhein, C. Mertens, C.W. Böning, and S. Hüttl. Observed and modeled MOC related flow into the Caribbean. *Journal of Geophysical Research* (in revision), **2007**.

Acknowledgments

Now, I finally would like to thank all my colleges from *the Department of Oceanography at the University of Bremen*. They gave me the opportunity to start and continue with this work. In times of low motivation or when my work seemed to be stuck in a dead end, there was always someone with an open office door and time for a talk. The discussions prior to a conference meeting during the talk preparation-phase were always helpful and well-reasoned.

Special thanks go to Monika Rhein, who supervised this work. She was always available for discussions and encouraged me to find my own path in research and the scientific work. Oliver Huhn and Dagmar Kieke went to the exhausting work of improving my language and grammar in this work. They raised a lot of important questions and their proof-reading very much improved this thesis.

Many thanks are addressed to the FLAME group of the *Leibniz-Institut für Meereswissenschaften der Universität Kiel (IFM-GEOMAR)*, since they provided the model data. Sabine Hüttl (now at the *University of Bremen* as well) prepared the model data for me and never complained about the additional work I charged her with. I further thank Claus Böning for the co-evaluation of this thesis.

I thank very much my husband-to-be Per Jochumsen for continuous encouragement and an always existent plan for relaxing from work. My friends and family might have felt a bit neglected during the last weeks of my work on this thesis and I want to apologize for occasional inattention. Nevertheless you all made me believe that I will make it to the end. Eventually. ☺